UNIVERSITY OF CALIFORNIA

Los Angeles

Mechanisms of Chemically-Induced Diffuse Pulmonary Hemorrhage

A dissertation submitted in partial satisfaction of the

requirements for the degree Doctor of Philosophy

in Molecular Toxicology

by

Priti Prasad

2017

ABSTRACT OF THE DISSERTATION

Mechanisms of Chemically-Induced Diffuse Pulmonary Hemorrhage

by

Priti Prasad

Doctor of Philosophy in Molecular Toxicology

University of California, Los Angeles, 2017

Professor Ram Raj Singh, Chair

Hydrocarbon oils, such as 2,6,10,14-tetramethylpentadecane (TMPD) and Hexadecane, are alkanes present in crude oil, food and in mineral oils used in cosmetics, laxatives, and food-coatings. Individuals exposed to TMPD have increased inflammatory diseases. To understand the pathogenesis of TMPD-induced inflammation, investigators have administered TMPD intraperitoneally (ip) to animals that develop autoantibodies, nephritis, arthritis, pneumonitis, and diffuse pulmonary hemorrhage (DPH) depending on animals' genetic background. We established disease assessment methods, dose response, routes of exposure, and evaluated immune cells' role in pathogenesis of TMPD-induced inflammation. Compared to none of controls, 73% of C57Bl/6 mice given TMPD (500 µl, ip) exhibited weight-loss, and pneumonitis, vasculitis and/or DPH. We established clinical (20% weight-loss), semi-quantitative, and quantitative assessments

of TMPD-DPH. DPH/pneumonitis rates were much decreased at lower doses (250-125 µl, ip) of TMPD. However, oropharyngeal aspiration of as low as 6 µl TMPD caused rapid morbidity/mortality, with increased serum creatinine kinase, aspartate aminotransferase, and pneumonitis; 75% animals survived 4 µl-dose and exhibited pneumonitis/DPH. All immune cells tested were abnormal in diseased lungs at 2-weeks post-TMPD (500 µl, ip). At Day 7, prior to histopathological changes, while both Hexadecane and TMPD caused myeloid cell abnormalities, only TMPD caused lung-infiltration with B-cells that expressed B1 subset markers: $CD19^{+}CD11b^{+}$/$CD19^{+}CD5^{+}$. Such B1-cells were simultaneously reduced in their usual location (peritoneal cavity). $CD19^{-/-}$ mice that have less B1-cells have less DPH with ip TMPD than wildtype mice. Adoptive transfer of $CD45.1^{+}$ wildtype peritoneal-fluid cells into the peritoneum of $CD45.2^{+}CD19^{-/-}$ recipients led to lung-infiltration with $CD45.1^{+}$ B-cells and more DPH/pneumonitis than $CD19^{-/-}$ recipients reconstituted with $CD19^{-/-}$ B-cells. Furthermore, ip TMPD induced in the lungs a differential expression of a set of immune/inflammatory genes including chemokine *Cxcl13* that is known to drive B1 B- cells' migration. However, pneumonitis/DPH development was independent of B-cells, when the lungs were directly exposed to TMPD via oropharyngeal aspiration. Thus, a systemic (ip) exposure to TMPD induces B1 B-cells to traffic from the peritoneum to the lungs and cause pneumonitis/DPH. Our observations have implications for chemically-induced inflammation, and DPH that is often a fatal complication in humans with inflammatory diseases and upon exposure to pesticides/cocaine.

The dissertation of Priti Prasad is approved.

John A. Belperio

Michael D. Roth

Oliver Hankinson

Ram Raj Singh, Committee Chair

University of California, Los Angeles

2017

“My parents Dr. Usha and Dr. Sarat Prasad inspired me from a very young age to pursue science as a career. I respect and admire their contribution to society as physicians. I am grateful to be their daughter, and fortunate to fulfill their dream of becoming Dr. Priti Prasad. My mother introduced me to the field of toxicology and I have pursued it with a passion for the past twenty years. Sasha has been a source of unconditional love and joy at home, and I could not imagine my life without her. My best friend Aarti, has been my pillar of strength through all of life’s challenges. Thanks to my brother Subir, sister Sonia, all family members, and close friends for being highly supportive of my academic endeavors.”

TABLE OF CONTENTS

LIST OF FIGURES

LIST OF ABBREVIATIONS

DPH	Diffuse pulmonary hemorrhage
TMPD	2,6,10,14-tetramethylpentadecane or Pristane
TMPD-DPH	2,6,10,14-tetramethylpentadecane induced diffuse pulmonary hemorrhage
Hex	Hexadecane
PBS	Phosphate buffered saline
ip	Intraperitoneal
WT	Wild type
B6	C57BL/6
B10	C57BL/10
$CD19^{-/-}$	CD19-deficient
hCD19Tg	Transgenic mice overexpressing CD19
MZB	Marginal zone B
BCR	B cell receptor
IL	Interleukin
BAL	Bronchoalveolar lavage
PF	Peritoneal fluid
DPBS	Dulbecco's Phosphate Buffered Saline
UCLA	University of California, Los Angeles
WAH	Warren Hall, mouse vivarium at UCLA
TPCL	Translational Pathology Core Laboratory at UCLA
DLAM	Division of Laboratory Animal Medicine

LIST OF ABBREVIATIONS (continued)

H&E	Hematoxylin and Eosin
RBCs	Red blood cells
CoA	Coenzyme A
3H	Tritium, a radioactive isotope of hydrogen
TLR	Toll-like receptors
NF-KB	Nuclear factor kappa-light-chain-enhancer of activated B cells
TNF	Tumor necrosis factor
Th1	Type 1 T helper
Th2	Type 2 T helper
TGF-β1	Transforming growth factor-β1
P13K	Phosphoinositide 3-kinase
Ccl5	Chemokine (C-C motif) ligand 5 (*Ccl5)*
Ly96	Lymphocyte antigen 96
CXCL13	Chemokine (C-X-C motif) ligand 13
miR-155	MicroRNA-155
BCL6	B-cell lymphoma 6 protein
SOCS1	Suppressor of cytokine signaling 1
PPARα	Peroxisome proliferator-activated receptor α
β-CyD	beta cyclodextrin
DCs	Dendritic cells
DNase	Deoxyribonuclease I from bovine pancreas
EDTA	Ethylenediaminetetraacetic acid

LIST OF ABBREVIATIONS (continued)

BSA	Bovine serum albumin
BM	Bone marrow
mAb	Monoclonal antibody
DAVID	Database for Annotation, Visualization and Integrated Discovery Bioinformatics Resources
SEM	Standard error of the mean
IFN	Interferon
pDC	plasmacytoid Dendritic Cell
mDC	myeloid Dendritic Cell
OA	Oropharyngeal aspiration
MOSH	Mineral oil saturated hydrocarbons
USP	United States Pharmacopeia
LPS	Lipopolysaccharide
CNS	Central nervous system

ACKNOWLEDGEMENTS

The main person who has enabled my lifelong dream of attaining a PhD to come true is my mentor, Dr. Ram Raj Singh. It has been a privilege working with an esteemed physician-scientist during my doctoral degree. I am deeply grateful to Dr. Singh for giving me the opportunity to work in his laboratory, and all the guidance he has provided towards building my academic career. During the last few years Dr. Singh has given me fatherly wisdom and kind support when I had any major personal problem. The best aspect of Dr. Singh's mentorship is his ability to assign a task, provide basic guidance and allow me to work on it in an independent manner. This enabled me to explore different aspects of science and develop skills to interact with experts in diverse scientific fields. Dr. Singh's faith in my scientific abilities has been a motivating factor for all my accomplishments during the doctoral degree.

I have been fortunate to learn from most of the 15 members at Dr. Singh's laboratory especially during the early stages of my doctoral training. I would like to thank all of them since I learned something from each one of them. Specifically, I am thankful to Dr. Julia Pinkhasov, who was the first person to train me in basic immunology techniques and flow cytometry. She took a keen interest in my project and was always there to provide valuable intellectual and technical support. Julia became one of my closest friends and I value her opinion in all aspects of my life. Dr. Ramesh Halder, an experienced immunologist, has provided guidance in enhancing my knowledge of immunology and improving my technical skills. I am thankful to Dr. Julia Pinkhasov and Dr. Ramesh Halder, who allowed me to assist them with experiments on their respective projects, and has resulted in me being coauthors on their manuscripts which were

submitted for publication recently. Guidance from Dr. Isela Valera, who works on a chemically-induced model of scleroderma lung disease, has been very useful in my studies related to lungs.

A very special thanks to Dr. Oliver Hankinson, Director of the Doctoral Program in Molecular Toxicology, for believing in my academic aspirations. He always provided guidance for any academic issue that has arisen during my graduate years, and has helped in successfully resolving it.

I am truly grateful to my committee members, Dr. Michael D. Roth, Dr. Hankinson, and Dr. John A. Belperio for providing critical scientific advice that enabled me to perform new experiments and build the research project in a positive direction.

This research work was supported by various funding sources including the National Research Service Award (NRSA) Predoctoral Fellowship NIH grant awarded by UCLA Molecular Toxicology Training Program Committee, Rheumatology Research Foundation, Lupus Foundation of America, and NIH R01 and R21 grants in Dr. Singh's laboratory. I am thankful for the funds provided by these organizations that supported this research project, and ensured the successful completion of my doctoral degree. I am grateful that my research work was recognized by many organizations, including the American College of Toxicology (ACT), Southern California Society of Toxicology (SCCSOT), Association of Scientists of Indian Origin (ASIO), Association of Rheumatology Health Professionals (ARHP), and Federation of Clinical Immunological Societies Centers of Excellence (FOCIS), who have awarded me travel awards to present my research work at international/national meetings. Each award inspired me to work harder, instilled a sense of self-confidence that my research work was valuable and

directly contributing to benefit human health, and gave me the opportunity to improve my presentation skills as a scientist.

When I joined my mentor's lab, Dr. Singh asked me to prepare a summary of the effect of environmental agents (including hydrocarbon oils) on autoimmune diseases, which became part of a published book chapter: Singh RR, Pinkhasov J, Prasad P, and Dubey S. Autoantigenesis and Antigen-based Therapy and Vaccination in SLE; Dubois' Lupus Erythematosus and Related Syndromes. 8th ed. Chapter 21. 286-303. Elsevier. 2013. I would like to acknowledge the contributions of the coauthors in the book chapter: Dr. Singh, Dr. Pinkhasov and Dr. Dubey.

Initially, when I started working on this project, I did not have any knowledge of pathology. My heartfelt thanks to Dr. Michael C. Fishbein, Professor of Pathology and Medicine, UCLA, who has trained me to read histology slides. Dr. Fishbein read, scored all the histology slides for this project, and took pictures for the tissues included in this thesis. He always made time to meet with me, and has been an excellent mentor.

I would like to acknowledge many investigators for their help in conducting global gene expression analysis in the lungs. Postdoctoral fellow Dr. Tristan Grogan at the UCLA Biostatistics Core and his supervisor/Director Dr. David Elashoff assisted with statistical analysis. My sincere thanks to Dr. Luz Orozco at the UCLA Bioinformatics Collaboratory and Director Dr. Matteo Pellegrini for bioinformatics analysis of the microarray data. Luz was the first person at UCLA to train me as a graduate student, and taught me several techniques including collection of mouse peritoneal fluid, cell culture, immunofluorescence staining, and utilizing the DAVID bioinformatics resources for data analysis. Luz has not only been a true friend over the years, but also a source of

inspiration, and I am very proud of all her scientific accomplishments.

I would like to acknowledge the contributions of UCLA Translational Pathology Core Laboratory (TPCL), specifically Ms. Yunfeng Li for optimizing and performing the immunofluorescence staining on lung samples, and Dr. Clara Magyar for scanning the lung slides and performing software analysis. Thanks to Ms. Gemalene Sunga at the UCLA Immune Assessment Core (IAC) who met with me several times and assisted in designing antibody panels for immunophenotyping, and acquiring flow cytometry data on the LSR Fortessa BV605.

My mentor assigned me many undergraduate students in the last few years, and it was a privilege to have worked with them and train them. I am thankful and acknowledge the contribution of all the UCLA undergraduate students including KimNgan Pham Nguyen who is now a medical student at UCLA, Shaun Shiv Singh, Ryu Sato, Kajal Bawa, Rohan Sharma, and Dhiraj Nallapothula, for assisting me with various aspects of this research project.

The principal investigator Dr. Ram Raj Singh, supervised the research work in this dissertation. After I prepared the first draft of the thesis, he reviewed each chapter and provided critical comments.

PRITI PRASAD, M.S.

Education

- **PhD, Molecular Toxicology, UCLA**. **GPA 3.7/4** Expected June 2017
- **Research Fellow**, All India Institute of Medical Sciences, New Delhi, India 1998-2000
- **M.S. (Toxicology),** Jamia Hamdard University, New Delhi, India 1996-1998
- **B.S. (Zoology),** University of Delhi, India 1993-1996

Honors & Awards

- Outstanding Student in Rheumatology Award by the Association of Rheumatology Health Professionals **(**ARHP), the American College of Rheumatology (ACR). **2017**
- Member of National Delta Omega Honorary Society in Public Health. **2017**
- Southern California Society of Toxicology (SCCSOT) Graduate Student Travel Award for poster presentation at Society of Toxicology (SOT) 55th Annual Meeting, New Orleans. **2016**
- Second place awarded for poster presentation at SCCSOT regional meeting, Carlsbad. **2015**
- Second place for ASIO Best Graduate Student Award by the Association of Scientists of Indian Origin (ASIO), SOT 54th Annual Meeting, San Diego. **2015**
- Student Travel Award to present a poster at the American College of Toxicology (ACT), 35th Annual Meeting, Orlando. **2014**
- National Research Service Award (NRSA) Predoctoral Fellowship NIH grant awarded by UCLA Molecular Toxicology Training Program Committee. **2014-2016**
- Gina Finzi Memorial Student Summer Fellowship by Lupus Foundation of America. **2014**
- Rheumatology Research Foundation Health Professional Research Preceptorship. **2012-2014**
- Student Representative, UCLA Molecular Toxicology Doctoral Program. **2012-2013**
- Trainee Satellite Symposium Travel Award, ranked in top ten abstracts for **oral** and poster presentation, Federation of Clinical Immunology Societies Centers of Excellence. **2013**
- Student Travel Award to present a poster at the ACT 33rd Annual Meeting, Orlando. **2012**
- NRSA Predoctoral Fellowship NIEHS grant awarded by UCLA Molecular Toxicology Training Grant Committee. **2011-2012**

Publications

• **Prasad P**, Halder RC, Valera I, Fishbein MC, Singh RR (2017). Investigating the Role of $CD19^{+}$ B1 B cells in the Pathogenesis of Hydrocarbon Oil-induced Diffuse Pulmonary Hemorrhage. Manuscript in preparation.

• Pinkhasov J, **Prasad P**, Singh RR (2017). Ubiquitination Mediated Via Cbl-b Regulates the Expression of T Cell Receptor Signal Fine-Tuning Molecules in Systemic Autoimmunity. Manuscript submitted for publication.

• Halder RC, **Prasad P**, Tran C, Singh RR (2017). A self-glycerophospholipid suppresses inflammation and immunity via mobilization and recruitment of $Ly6C^{+}$-myeloid cells. Manuscript submitted for publication.

• Singh RR, Pinkhasov J, **Prasad P**, and Dubey S. Autoantigenesis and Antigen-based Therapy and Vaccination in SLE; Dubois' Lupus Erythematosus and Related Syndromes. 8th ed. Chapter 21. 286-303. Elsevier. 2013

• **Prasad P**, Lall SB & Mathur M, “Effect of intra-tracheal instillation and inhalation of silicon dioxide on some biochemical variables in broncho-alveolar lavage fluid and lung histopathology in rats”; *Drug and Chemical Toxicology*. 2000; 23(3): 459-475; PMID:10959547

Published Poster Abstracts:

• **Prasad P**, Halder R, Valera I, Sato R, Bawa K, Fishbein M, and Singh RR. $CD19^+$ B1 B Cells in the Pathogenesis of Hydrocarbon Oil-Induced Diffuse Pulmonary Hemorrhage. *The Toxicologist*, Supplement to Toxicological Sciences. 156 (1), Abstract #2980, pp 466, 2017.

• Singh RR, **Prasad P**, Tran C, Halder RC. A self-glycerophospholipid suppresses immunity and inflammation via recruitment of $Ly6C^+$ myeloid cells. Presented at the American Association of Immunology annual meeting, Washington DC, 2017.

• Singh RR, Bui V, **Prasad P**, Ranganath V, Halder RC, Pinkhasov J. Dysregulation of TCR signal fine-tuning molecules due to increased ubiquitination in systemic autoimmune disease. J Immunology, 196 (1 Supplement) 48.9, 2016.

• Prasad P, Valera I, Fishbein MC, Singh RR. Investigating the Role of B Cells in the Pathogenesis of Hydrocarbon Oil-Induced Lung Hemorrhage. *The Toxicologist*, Supplement to Toxicological Sciences. 144 (1), Abstract #1363, pp291, 2015.

• **Prasad P**, Valera I, Fishbein MC, Singh RR. Investigating Cellular and Molecular Pathogenesis of Hydrocarbon Oil-Induced Lung Hemorrhage and Inflammation. *International Journal of Toxicology*. Poster Abstracts. 34(1). 77-1, 2015.

• Halder RC, Tran C, Okorogu R, Valera I, **Prasad P**, Kim P, and Singh RR. Phospholipid-reactive T cells negatively regulate the function and expansion of glycolipid-reactive T cells (P4012). The *Journal of Immunology*, (Meeting Abstract Supplement).190, 42.7, 2013.

• **Prasad P**, Valera I, Singh RR. P501 Hydrocarbon oil induced autoimmune diffuse alveolar hemorrhage. Poster Abstracts. *International Journal of Toxicology*. 32(1). 77, 2013.

Teaching Experience

• **Faculty (part-time), 2014 Spring semester, California State University, Northridge**
Health Science 391 - Computer Applications for Health Sciences: Introduction to computer technology, including legal, and ethical considerations, and its application to health education, health research, health administration, and clinical health practice. Upper division, required, 3 credit unit course for undergraduate students.

• **Teaching Assistant (TA) for 2013 Fall, 2014 Spring, and 2015 Spring quarters, UCLA**
Life Sciences 23L, "Introduction to Laboratory and Scientific Methodology**"**, an undergraduate required course where students performed laboratory experiments in the area physiology, molecular biology, cell biology, genotyping and bioinformatics. Weekly in-lab quizzes, class work sheets and report writing assignments. Laboratory, three hours; Letter grading.

Work Experience

• **Ph.D. Candidate**, **Molecular Toxicology IDP Program, UCLA** **September 2010-June 2017**
Dept. of Medicine, Div. of Rheumatology January 2012-June 2017
Dept. of Medicine, Div. of Environmental Cardiology & Vascular Biology April 2010-Dec 2011

• Research Associate, Dept. of Pathology & Lab Medicine, UCLA Oct 2009-March 2010

• Scientist, Safety Assessment, GlaxoSmithKline, North Carolina April 2007-Jan 2009

• Regulatory Specialist, Scientific & Regulatory Affairs July 2004-March 2006
The Wrigley Company, Chicago

• Scientist, Toxicology, Medical Affairs & Safety, Pfizer Inc, New Jersey Dec 2001-July 2004

• Research Fellow, Toxicology Division, Department of Pharmacology 1998-2000
All India Institute of Medical Sciences (AIIMS), New Delhi, India

CHAPTER 1

INTRODUCTION and BACKGROUND

Diffuse pulmonary hemorrhage (DPH) is a distinct clinicopathologic syndrome of lung hemorrhage, inflammation, vasculitis, and acute respiratory failure. It occurs in patients with inflammatory disorders such as lupus, exposure to toxic substances (isocyanates, trimellitic anhydrides, and certain pesticides), recreational drugs (crack cocaine), medications (chemotherapeutic agents, propylthiouracil, and diphenylhydantoin), and organ transplantation [1]. DPH is without any effective treatment and is associated with a high mortality [2]. Advances in the treatment of DPH have been hampered because of the heterogeneity of clinical findings and the lack of suitable model systems until recently when two laboratories reported the induction of DPH in C57BL/6 (B6) and C57BL/10 (B10) mice upon an intraperitoneal (ip) injection of 2,6,10,14-tetramethylpentadecane (TMPD), also known as pristane [3, 4]. Pathologically, TMPD-induced DPH (TMPD-DPH) mimics DPH in humans. Hence, investigations into mechanisms of TMPD-DPH may elucidate the pathogenesis of DPH caused by toxic substances and inflammatory diseases.

Hydrocarbon oils as candidate environmental agents in the etiology of DPH:

TMPD ($C_{19}H_{40}$) is an isoprenoid alkane present in crude oils and as a major component of mineral oil [5]. TMPD is a byproduct of the fractional distillation of petroleum [6]. Medicinal mineral oils are used as laxatives, protective coatings for foods, and in cosmetics. Canned sardines contain up to 370 mg/kg and white bread up to 550 mg/kg of mineral oil [7, 8]. TMPD is also found in many plants and marine organisms [9]. The concentration of TMPD in 55 common fruits and vegetables was assessed by quantitative gas-liquid chromatography. The highest content was observed in parsley which contained 124.0 μg per gram of fresh sample; TMPD levels within the remaining 54 foodstuffs

(included tomatoes, strawberries, avocado, mushrooms) analyzed ranged from 0.02 to 1.70 µg of TMPD per gram of fresh sample. The amounts of TMPD in average serving sizes of representative samples ranged from 1.5 to 107.0 µg [10].

Dietary exposure to mineral oil is estimated at 9−45 grams per year, some of which is absorbed through the intestine [11]. Thus, people can get exposed to fairly large amounts of TMPD through various sources. In fact, a community comparison study from New Mexico showed that people living near an oil field waste site with increased levels of TMPD in house dust, had an increased prevalence of immune inflammatory disorders as compared to unexposed population [12]. Therefore, animal observations showing that a single ip injection of TMPD induces autoantibodies in otherwise healthy strains of mice [13], exacerbates autoimmune disorder in genetically autoimmune-prone strains, and induces DPH in B6 and B10 mice, provides an important opportunity to investigate the role of environment and gene-environment interactions in the pathogenesis of inflammation associated DPH. Other researchers, and my mentor's laboratory has shown that TMPD induces a different type of inflammatory disorder in different mouse strains, thus providing a model system whereby the same inciting environmental agent induces a different clinical syndrome in different genetic backgrounds [14-18].

We used Hexadecane ($C_{16}H_{34,}$ hex) as a control oil, since like TMPD it is also a component of medicinal mineral oils. In a previous study, a single ip injection of 0.5 ml of Hex in BALB/cJ mice (3 months old, females) induced chronic peritoneal inflammation [19]. All hex-injected mice developed massive ascites within 2–2.5 months, but none of the TMPD-injected nor the untreated mice developed ascites. The number of peritoneal cells increased ~10-fold over controls. These cells were predominantly $CD11b^{+}Gr1^{+}$

mature neutrophils (~60%) and macrophages [19]. Thus, Hex induces a different type of immune/inflammatory response compared to TMPD. In our studies, none of the Hex exposed young B6 mice developed any lung hemorrhage.

Given the lack of understanding of pathogenesis of potentially fatal vasculitides and DPH, TMPD-DPH provides a unique opportunity to better understand the early pathogenetic events, since the exact timing of the inciting agent is known as compared to human studies where the exact timing of pathogenetic events cannot be determined.

Relevance and Implications of the Route of Administration and Dose of TMPD:

Humans are exposed to hydrocarbon oils via ingestion (foods, medications), inhalation (diesel exhaust, oil mists, aspiration of ingested mineral oil), skin absorption (cosmetics, skin contact with oils or fuels), or injection (immunization) [7-9, 11, 12]. It is not clear whether nonperitoneal exposure to hydrocarbons can induce immune dysregulation. However, such exposure has been shown to cause an intense inflammatory reaction (lipogranulomas) in the lungs, liver, and lymph nodes of individuals [20, 21]. Moreover, ingested mineral oil is absorbed through the intestine and becomes distributed throughout the body [20, 21].

Although, a single dose of 0.5 ml via ip route, given to mice is quite large, humans can be exposed to considerable quantities of hydrocarbon oils over the course of a lifetime. It has been estimated that an average person living in a developed country ingests 45 grams of mineral oil per year in food. Individuals using mineral oil chronically as a laxative have much greater exposure [11]. At the recommended dose of 1–3 tablespoons (15-45 ml) per day, exposure may be as high as 0.75 ml/kg/day for a 60-kg person, or the equivalent of 20µl/day in a mouse weighing 26.7 grams. On a kg-per-kg

basis, the ip dose given to the mice in these studies is comparable to that of a human ingesting mineral oil as a laxative for 25 days [22].

In rats, dose response studies indicated that a low dose of 30 μg of TMPD (administered as a single ip injection or via diet during 1 week) per gram of bodyweight elicits significant biological responses [23], [10].

There are no published studies, to the best of our knowledge, which show whether exposure TMPD or Hex via oral/tracheal routes causes lung disease in animals.

TMPD Metabolism and Adsorption:

In the environment TMPD a branched-chain alkane is hardly biodegradable compared to n-alkanes such as hex [24]. Although the fatty acid oxidation scheme works neatly for even-numbered chain lengths, it cannot work completely for fatty acids that contain an odd number of carbons, β-oxidation of these compounds leads to propionyl-CoA and acetyl-CoA, rather than to two acetyl-CoA at the final step, this may be a factor for the different biological responses to different hydrocarbon oils.

The fate of TMPD has been studied in rats after a single per os administration of 3H-labeled TMPD. The study showed an extensive fecal excretion (66%) mainly as unchanged hydrocarbon, whereas about 14% of ingested TMPD was excreted in urine as TMPD metabolites and tritiated water. After one week, 8.3% of the ingested 3H still was stored in the carcass, and radioactive distribution in tissues and organs showed a preferential incorporation into adipose tissue and liver. Over 75% of the radioactivity stored in the carcass was associated with TMPD/pristane metabolites and tritiated water. Tissue metabolites were characterized by thin layer chromatography, gas chromatography and mass spectrometric analyses. Four metabolites were identified:

pristan-1-ol, pristane-2-ol, pristanic acid and 4,8,12-trimethyltridecanoic acid. This study showed that TMPD undergoes subterminal hydroxylation or terminal oxidation followed by the classical beta-oxidation process [25].

In a recent study, tissue distribution of TMPD was examined by mass spectrometry and showed that TMPD (ip, 0.5 ml) migrated to the lungs and bone marrow in B6 mice [26]. Lung tissue and bone marrow was extracted 7 days after TMPD-injection and analyzed by mass spectrometry. A TMPD standard yielded the characteristic fragmentation pattern of four molecular ion peaks. The four characteristic peaks were seen in lung tissue of TMPD-injected B6 mice, but not untreated B6 mice. To confirm the presence of TMPD in the lung, cryosections of lung tissue from TMPD-injected mice were stained with oil red O, revealing numerous oil red O–positive droplets within the alveolar walls, and were absent in lungs from untreated mice, consistent with the mass spectrometry data. Peritoneal TMPD-injection also causes bone marrow inflammation in mice [27], and TMPD was detected by mass spectrometry in bone marrow of TMPD-injected B6 mice, but not in bone marrow of untreated B6 mice, which suggests that the oil was widely dispersed following an ip injection [26].

The excretion routes and tissue distribution of [3H] TMPD were measured in rainbow trout after a single intragastric dose (0.1 mg). This branched-alkane was quickly and largely absorbed. The study showed that the major routes of excretion were fecal (40.4% of the dose) and bronchial (39.6%). In feces radioactivity was exclusively due to [3H] TMPD, whereas 3H resulting from gill excretion was principally associated with tritiated water. Only 2.6% of the radioactivity was cleared via the kidneys and found in the urine as metabolites. After 48 hours, no hydrocarbon accumulation was observed in

gallbladder, while in liver and fat, respectively, 69 and 34% of the radioactivity originated from TMPD, the rest of the labeling being mostly associated with lipid components [28].

A previous study showed the normal tissue-associated levels of TMPD in Copenhagen rats during ontogeny and adult life to address whether dietary TMPD can be adsorbed from the gut and disseminated throughout the body. During this study, the possible effects of dietary TMPD on chromatin conformation of lymphoid cells were also examined by flow cytometry. The data indicated that 1) TMPD crossed the placenta and accumulated in fetal tissues, 2) neonates were exposed to TMPD via the colostrum, 3) there were significant increases in the amount of tissue-associated TMPD in young adults and subsequent redistribution of the TMPD to the muscle and adipose tissues in older rats and 4) after dietary exposure, significantly elevated levels of TMPD were associated with the tissues and concomitant changes in chromatin conformation were observed. Collectively, these results suggest that TMPD can be adsorbed from dietary sources and disseminated to the tissues, and can exert a transient, yet marked effect on lymphoid cells in rodents [29].

TMPD-DPH model to investigate the pathogenesis of DPH:

Pathogenesis of DPH is unclear. Advances in the pathogenesis of DPH have been hampered due to the heterogeneity of clinical findings, a paucity of access to clinical tissues from early stages of disease, and the lack of suitable animal models. Thus, the discovery of TMPD-DPH provides a model system to study DPH pathogenesis [3, 4]. Using this model, the prevalence of DPH was lower in $Rag1^{-/-}$ B6 mice than in wild-type (WT) B6 controls, although 50% of $Rag1^{-/-}$ mice did develop DPH. This suggests that DPH can develop in the absence of T and B cells, although they may play a role in promoting

DPH. Interestingly, B6 Ig$\mu^{-/-}$ mice that do not have any B cells had a strikingly reduced prevalence of DPH (7% vs 84% in WT B6), and reconstitution of B6 Ig$\mu^{-/-}$ mice with wild-type splenic B cells increased the DPH prevalence to 50%, thereby suggesting a possible role of B cells in development of DPH [4]. However, no immune complexes or complement deposition was detected in the DPH lungs. Furthermore, the transfer of serum from DPH mice to naive mice did not induce DPH, although the sample size was too small in this experiment [4].

A community study from New Mexico showed that people living near an oil field waste site with increased levels of TMPD in house dust had increased proportions of $CD19^{+}$ B cells in their peripheral blood compared to the control population [12]. Furthermore, my mentor's lab reported an increase in marginal zone B (MZB) cells, and immunoglobulin isotypes produced by these MZB cells in BALB/c mice injected with TMPD [30].

MZB cells and another B cell type, called, B1 B cells, provide an initial and prompt antibody response, mainly to T cell-independent antigens. Due to their anatomical location, these B cells are the first cell populations to encounter antigens acquired through the peritoneum and blood stream [31], [32]. B1 B cells are innate-like lymphocytes that generate natural antibodies with important functions in tissue homeostasis and immune defense. While B1 B cell frequencies in secondary lymphoid tissues are low, relative high frequencies are found within peritoneal and pleural cavities of mice [33]. Guided by our preliminary data, we focused on these cells in our studies.

B1b cells express Mac-1 (CD11b/CD18), a leukocyte adhesion molecule that is also expressed on many myeloid cell types. Mac-1 plays a role in inflammation by

regulating migration of leukocytes into injured tissue. A recent study showed that depletion of neutrophils and eosinophils or adoptive transfer of classically activated macrophages resulted in the exacerbation of TMPD-DPH in both WT and Mac-$1^{-/-}$ B6 mice. However, the peritoneal transfer of $F4/80^{hi}MMR^{+}$ (mannose receptor) alternatively activated macrophages reduced the prevalence of DPH in WT mice. Thus, Mac-1 can promote acute inflammatory responses in the peritoneal cavity and lungs by downregulating granulocyte migration and subsequent phenotypic conversion of macrophages in the TMPD-lupus model [34]. Relevant to our study, the Mac-1 effects attributed to myeloid cells in previous studies, could be owing, at least in part, to Mac-1 expression and function in B1 B cells.

Induction of DPH is independent of toll-like receptors, inflammasomes, and inducible nitric oxide. Mortality is increased in interleukin-10 (IL-10)-deficient mice, and TMPD treatment decreased IL-10 receptor expression in monocytes and STAT-3 phosphorylation in lung macrophages. In vivo neutrophil depletion was not protective, while treatment with clodronate liposomes prevented DPH, which suggests that macrophage activation plays a role in DPH pathogenesis [26].

B cell-deficient mice were resistant to induction of DPH, but susceptibility was restored by infusing IgM. $C3^{-/-}$ and $CD18^{-/-}$ mice were also resistant to DPH. A recent study suggested that the development of DPH involves opsonization of dead cells by natural IgM and complement followed by complement receptor-mediated lung inflammation [35].

Roles of B cells in vascular inflammation are not well defined. In atherosclerosis, a chronic inflammatory disease of the arterial wall, B1 cells are believed to secrete

protective IgM antibodies that act as scavenger of deleterious molecules whereas B2 lymphocytes probably worsen the disease by activating pro-inflammatory T lymphocytes [36]. In summary, little is known about the role of innate B cells in vascular inflammation, and their role is not known in DPH.

Role of CD19 in B Cells and CD19$^{-/-}$ Mice:

CD19 is a type I one-pass transmembrane protein with a highly conserved, 242 amino acid cytoplasmic domain that includes multiple tyrosine residues which are associated signaling kinases and molecules. CD19 is present on B cell surface and regulates signaling thresholds for B cell receptors that regulate B lymphocyte selection, activation, and differentiation [37]. CD19 is critically involved in establishing intrinsic B cell signaling thresholds through modulating both B cell receptor-dependent and independent signaling. Through studies of CD19 transgenic and knockout mouse models, it becomes clear that CD19 plays a critical role in maintaining the balance between humoral, antigen-induced response and tolerance induction [37].

CD19 potentiates signals from the B cell receptor (BCR), which results in phosphoinositide 3-kinase (P13K) activation, and subsequent serine/threonine kinase Akt phosphorylation [38, 39]. In the absence of CD19, Akt kinase activity is reduced and is transient. In addition, coligation of CD19 with surface immunoglobulin leads to augmented Akt activity in a dose-dependent manner. Thus, CD19 is a key regulator of Akt activity in B-cells; as such it may contribute to pre-BCR or BCR-mediated cell survival *in vivo* [39]. In addition, there is diminished Akt phosphorylation in CD19$^{-/-}$ B cells following low dose anti-IgM stimulation compared to WT B cells [38], [39].

CD19-deficient mice were generated to examine the role of CD19 in B cell growth regulation in vivo. Deletion of CD19 had no deleterious effects on the generation of B cells in the bone marrow, but there was a significant reduction in the number of B cells in peripheral lymphoid tissues. B cells from CD19-deficient mice exhibited markedly decreased proliferative responses to mitogens, and serum immunoglobulin levels were also significantly decreased [40]. In contrast, transgenic mice overexpressing CD19 (hCD19Tg) had significant defects in early B cell development in the bone marrow, augmented mitogenic responses, and increased serum immunoglobulin levels. These experiments indicate that CD19 functions to define signaling thresholds for cell surface receptors that regulate B lymphocyte selection, activation, and differentiation [40].

To selectively modify genes in B lymphocytes, Rickert et al. generated mice (designated $CD19^{-/-}$ (Cre); B6 background) which express cre under the transcriptional control of the B lineage-restricted CD19 gene. In a model system involving the cross of $CD19^{-/-}$ (Cre) mice with mice bearing a loxP-flanked substrate, they found a deletion efficiency of 75–80% in bone marrow-derived pre-B cells and 90–95% in splenic B cells [41]. We have used these $CD19^{-/-}$ (Cre) mice to study the pathogenesis of TMPD-DPH.

The B-1 subpopulation of B lymphocytes is particularly sensitive to CD19 regulation, since their development is severely decreased in $CD19^{-/-}$ mice. Specifically, development of $CD5^{+}$ B cells was severely decreased in $CD19^{-/-}$ mice [42]. The frequencies of peritoneal B-1a and B-1b cells were clearly different between $CD19^{-/-}$ B6, WT B6, and hCD19Tg mice when CD5 expression was used to differentiate peritoneal B1a ($CD5^{+}CD11b^{+}$) and B1b ($CD5^{-}CD11b^{+}$) cells. Although the peritoneal $CD11b^{+}$ B

cell population exhibited an IgM^{hi} phenotype in all mice, the vast majority of $CD11b^{+}B220^{+}$ cells were $CD5^{-}$ in $CD19^{-/-}$ mice [43].

The $CD19^{-/-}$ mouse model has been utilized to study atopic dermatitis, skin and lung fibrosis [44, 45]. Suppressed allergic skin inflammation in $CD19^{-/-}$ mice is likely due to the decreased B-cell numbers and/or impaired proliferation capacity of B cells, and reduced peritoneal B1a cells may decrease IL-17 secretion [44].

CD19 deficiency inhibited the development of skin and lung fibrosis, and autoantibody production by inhibiting TLR4 signals in a bleomycin-induced scleroderma model. B-cell activation contributes to downstream inflammatory infiltration of other immune cells. CD19 deficiency inhibited the production of Th1, Th2 cytokines and TGF-β1 (except TNF-α), suppressed mast cell and macrophage infiltration [45]. Thus, CD19-deficiency might affect the development of immune inflammatory diseases via its multiple roles in B cell development and phenotype and in its secondary effects on other immune cells.

TMPD-DPH model, Immune gene responses and Role of MicroRNAs:

When we started this research project, there was no published study on the immune response genes or microRNAs in the TMPD-DPH model. In 2014, we performed a microarray analysis on lungs from PBS/TMPD/Hex-injected mice, and identified a cohort of differentially expressed genes, two of which could be involved in the trafficking of B1 B cells to the lung. In 2016, a study reported that MicroRNA-155 (miR-155) expression was significantly increased during the development of DPH. Disease progression was reduced in miR- $155^{-/-}$ mice as well as by in vivo silencing of miR-155 using a miR-155 antagomir. In the process of TMPD-DPH, elevated miR-155

downregulated the expression of BCL6 (B-cell lymphoma 6 protein), SOCS1 (suppressor of cytokine signaling 1), and anti-inflammatory factor PPARα (peroxisome proliferator-activated receptor α), resulting in the ectopic activation of NF-KB (nuclear factor kappa-light-chain-enhancer of activated B cells) signaling pathway. Consequently, various inflammatory cytokines, such as IL-6 and TNF (tumor necrosis factor) are aberrantly overexpressed, which leads to a severe inflammation in lung tissues [46].

In vitro Studies with Hydrocarbon Oils:

Hydrocarbon oils TMPD and hex triggered the release of inflammatory cytokines IL-1α and IL-1β via inflammasome-dependent and -independent mechanisms, respectively [47]. In rat splenocytes and human cell line THP-1 cells (peripheral blood monocytes), IL-1α was found in the supernatants of cells treated with oil-beta cyclodextrin (β-CyD) complexes; the TMPD-complexes triggered more IL-1α release than hex-complexes. In THP-1 cells, direct treatment with TMPD increased release of IL-1β/proIL-1ß into the cellular supernatants, whereas direct exposure to hex did not. In rat splenocytes, direct application of the oils led to rapid cell death and did not increase IL-1β levels at all.

TMPD is a powerful inducer of apoptosis in cultured lymphoid cells, such as BW5147 (murine), Jurkat (human T cell lymphoma), and U266 (human myeloma) cells , and in freshly isolated murine peritoneal cells [48]. A previous study confirmed that TMPD-induced apoptosis is not due to β-CyD alone or a β-CyD emulsion containing hex, because no apoptosis was induced under either of these culture conditions. TMPD induced apoptosis in murine peritoneal cells in vivo, thus providing a potential mechanism by which a break in self-tolerance may occur in TMPD-induced lupus [48].

Cell death induced by hydrocarbon oils may initially generate the autoimmunogenic substrates responsible for the break of self-tolerance. The chronification of this process, most likely by an insufficient clearance may ultimately lead to the development of lupus-like or arthritogenic autoimmunity [47, 48].

Potentially, there may be differences in transmembrane transport of TMPD or permeability to this oil among dendritic cells (DCs), B cells, T cells, and monocytes, which may explain their differential susceptibilities to undergo apoptosis [48].

In studies using nuclear magnetic resonance imaging of TMPD uptake into lipid bilayers, it was shown that TMPD localizes to the hydrophobic compartment of the cell membrane [49]. It is therefore possible that TMPD may induce its early apoptotic effects by an indirect, passive, nonreceptor-mediated mechanism, causing changes in the biophysical properties of the membrane bilayers. However, one would expect that other alkanes, such as hex, should elicit similar cellular changes as TMPD, but it did not [48].

Significance:

There is minimal knowledge about the pathogenesis of DPH, a potentially fatal pulmonary condition that occurs due to exposure to environmental agents, recreational drugs, medications, autoimmune diseases and organ transplantation. The use of the induced DPH model permits investigations into the early pathogenetic events, which would otherwise not be possible using genetically susceptible models or human samples from diseased tissues.

Identification of specific immune abnormalities in the animal model may pave the way for their manipulation as novel therapeutic strategies for pulmonary hemorrhage and inflammation and related diseases. Depletion of B cells using rituximab is FDA approved to treat patients with vasculitis (Wegeners granulomatosis) that is known to cause DPH,

and rituximab is being used as an off-label treatment in other patients with DPH. Our novel findings demonstrating the role of one subset of B cells, B1 B cells, which is a numerically small subpopulation of B cells, paves the way for further studies to target B1 B cells, instead of current treatment with rituximab that indiscriminately targets all B cells. Furthermore, we identify the trafficking of innate B1 B cells from the peritoneum to the lungs as a specific, novel mechanism by which B1 B cells contribute to the development of lung inflammation and hemorrhage. Thus, future development of strategies to target this specific mechanism would lead to novel, highly specific treatments for these diseases. Our preliminary gene expression data identify specific chemokines which might be involved in the trafficking of B1 B cells to the lungs.

Intriguingly, TMPD is known to induce different pathologies (arthritis, nephritis, hepatitis, DPH, and plasmacytomas) in different genetically inbred strains of mice. This provides an opportunity to investigate gene-environment interactions in the pathogenesis of complex autoimmune and inflammatory diseases.

Our data add to the existing reports from other laboratories that exposure to hydrocarbon oils results in many changes in immune cells in different organs. Thus, investigations into immune effects of oils may identify, hitherto undiscovered effects of hydrocarbon oils on immunity, which may have broader implications for the role of exposure to hydrocarbon oils in various diseases. Our finding that the direct exposure of lungs to very low doses of hydrocarbon oil can elicit dramatic pathological changes in the lungs with early morbidity and even mortality has enormous implications for hydrocarbon oil as an environmental pollutant.

Innovation:

In this study, we have made several novel contributions: First, this study demonstrates the role of innate B1 B cells in the development of pneumonitis and DPH. Second, the trafficking of innate B1 B cells from the peritoneum to the lung tissue in the pathogenesis of pneumonitis and DPH has not been reported previously, to the best of our knowledge. Third, direct lung exposure to low doses (4 µl) of hydrocarbon oils such as TMPD and hexadecane via oropharyngeal aspiration can induce pneumonitis and/or DPH. Fourth, oropharyngeal aspiration of hydrocarbon oils in relatively low doses (6 µl to 40 µl) can induce acute toxicity with elevated muscle and liver enzymes including early mortality. Finally, we have established a clinical parameter that can predict the development of DPH, and developed semi-quantitative and quantitative measures of DPH severity, which would be helpful in future studies of pneumonitis and DPH in animal models.

In summary, our novel findings in this animal model form the basis to investigate the role of trafficking of B1/B1-like B cells to the lungs in humans with DPH and inflammatory lung diseases. Our results also highlight the need to investigate the role of hydrocarbon oil as important environmental pollutants in the pathogenesis of human inflammatory diseases, especially when individuals are acutely exposed to hydrocarbon oil such as during large oil spills.

CHAPTER 2

Hydrocarbon Oil Induced Lung Inflammation and Diffuse Pulmonary Hemorrhage:

Characterization and Assessment of Disease using Clinical, Semi-quantitative, and Quantitative Measures

ABSTRACT

When we started this project, there were only two publications on TMPD-induced lung inflammation and hemorrhage. We established the TMPD-induced pneumonitis and DPH mouse model in our laboratory and performed a detailed clinico-pathological characterization of the model. Compared to none of the controls [control oil hexadecane or PBS (500 µl, ip), sham-injected or unmanipulated; n=50], 73% of TMPD-exposed (500 µl, ip; n=62) young C57BL/6 mice developed DPH/pneumonitis/vasculitis after 10-30 days of exposure. To investigate the long-term effects of hydrocarbon oils, we monitored TMPD-injected animals that do not develop DPH within four weeks for a longer term and monitored animals injected with another hydrocarbon oil hexadecane for up to 11 months. 33% of the hexadecane-exposed mice developed ascites and mild lung inflammation but no hemorrhage and no obvious pathology in kidney, spleen, liver, and intestines. Analyses of data in all animals revealed that 20% weight loss correlates with the presence of DPH. We also developed semi-quantitative scoring of inflammation and hemorrhage and a quantitative measurement of DPH by eosin-stained lung area to assess DPH severity. In summary, TMPD induces DPH as early as 10 days post-exposure, whereas another hydrocarbon oil hexadecane does not induce DPH up to 11 months after a single large exposure. Furthermore, the recognition of weight loss as a clinical parameter to predict the presence of DPH as well as semi-quantitative and quantitative measurements to assess DPH severity would be helpful in future studies to manipulate TMPD-induced pneumonitis and DPH.

INTRODUCTION

Exposure to hydrocarbon oils such as 2,6,10,14-tetramethylpentadecane (TMPD) and hexadecane (Hex) that are found in crude/petroleum oils as well as in plants and other organisms, food items, cosmetics, and laxatives can cause inflammatory diseases in humans and animals. TMPD ($C_{19}H_{40}$) is an isoprenoid alkane present in crude oils and as a major component of mineral oil [5]. Studies by my mentor and others have shown that a single intraperitoneal (ip) injection of 0.5 ml of TMPD causes a variety of inflammatory diseases in different mouse strains, including diffuse pulmonary hemorrhage (DPH) in C57BL/6 (B6) and C57BL/10 (B10) mice [3, 4]. The pathology of DPH in animals resembles DPH in humans, which is fatal and has no specific treatment.

We used Hex ($C_{16}H_{34}$) as a control oil, since like TMPD it is also a component of medicinal mineral oils. In a previous study, a single ip injection of 0.5 ml of Hex in female BALB/cJ mice induced chronic peritoneal inflammation, but no lung hemorrhage [19]. Thus, Hex induces a different type of immune/inflammatory response compared to TMPD, this may be due to the difference in their structures (Figure 2.1) and ability of the body to metabolize them.

In this chapter, we established the animal model in B6 mice in our laboratory to investigate the pathogenesis of TMPD upon systemic exposure, performed a detailed clinico-pathological characterization of the model, and investigated the short-term and long-term effects of hydrocarbon oils TMPD and hexadecane.

METHODS

Mice

Wild-type C57BL/6J (WT B6; Black 6; Stock No: 000664) mice were purchased from the Jackson Laboratory and housed in the UCLA Warren Hall (WAH) Barrier Facility. To establish the TMPD-DPH animal model in our laboratory, mice of both sexes, aged 2-6 months (n=112) were used. For the TMPD dose response experiment: 2 months old male mice (n=23) were used. For long term effect of Hex experiment: 2.5 months old (n=6), 3 months old (n=5) and 4.5 months old (n=4) male mice were used.

The UCLA Institutional Animal Care and Use Committee, known as the Chancellor's Animal Research Committee (ARC), approved the protocol for this study.

Dose Administration and Bodyweight Assessment

TMPD-DPH Animal Model Experiments:

Control oil (Hex)/ PBS/sham-injected/unmanipulated (n=50), and TMPD-exposed (n=62) WT B6 mice were administered 500 µl PBS/Hex/TMPD via ip route under isoflurane anesthesia. The day of TMPD administration was Day 0 for each experiment and their bodyweight was monitored at different time points for up to 30 days post exposure.

Hex Long Term Experiment:

The mice (n=9) were weighed on a scale prior to hexadecane administration. Controls were unmanipulated mice (n=6). Under isoflurane anesthesia, the mice were administered an ip injection with a 500 µl dose of hexadecane, and the day of hexadecane administration was Day 0 for this experiment. The bodyweights of the mice were then monitored for eleven months.

Reagents

2,6,10,14-Tetramethylpentadecane BioReagent (TMPD, Molecular Weight 268.52, CAS Number 1921-70-6), synthetic, liquid, sterile-filtered, purity ≥95% (Sigma-Aldrich Corp., St. Louis, MO; Lot Nos. RNBB3307 and RNBB3307V). Hexadecane *ReagentPlus*® (Hex,

Molecular Weight 226.44, CAS Number 544-76-3) liquid, purity 99% (Sigma-Aldrich Corp., St. Louis, MO; Lot No. SHBD2368V). Isoflurane USP (Piramal Healthcare Limited, Bethlehem, PA) was used to anesthetize/euthanize the mice. Dulbecco's Phosphate Buffered Saline [DPBS **(**1X**)** Gibco™; Thermo Fisher Scientific Inc., Waltham, MA] was used to perfuse the lungs, and to clean the small and large intestines. Ethyl alcohol (Decon Laboratories, King of Prussia, PA) was used to clean the mouse prior to necropsy and preserve tissues for histology. Formalin 10% (Fischer Scientific Company LLC, Kalamazoo, MI) was used to fix the tissues for histology.

Necropsy

Necropsy was performed on those mice that showed a reduction in bodyweight by 20% of their initial weight at Day 0. On the day of necropsy, each mouse was placed in a chamber that contained isoflurane for 3-5 minutes until it was euthanized. After the mouse ceased to breathe, it was taken out of the chamber and placed on a dissection mat. The mouse's body was cleaned with alcohol and its outer skin was cut. Cardiac blood was collected for serum analysis. The lungs were perfused via the heart, with DPBS 1X to remove the blood from them after the aorta was cut.

The lungs, liver (left lateral and right medial lobes), spleen, kidney (right), 2 sections each of small intestine, and large intestine were fixed in 10% formalin for at least 24 hours. The small and large intestine sections were cleaned with DPBS 1X solution before they were preserved for histology.

Histopathological Assessment

Histopathology was conducted at the UCLA Translational Pathology Core Laboratory (TPCL). Tissues were embedded in paraffin. Tissue sections were stained with

hematoxylin and eosin (H&E). All slides were examined independently by a pathologist in a blinded manner for hemorrhage and inflammation.

Scoring for Lung Inflammation and Hemorrhage

Lungs were scored for hemorrhage (hem), and the grading criteria was: grade 0, normal; grade 1, minimal hem; grade 2, mild hem; grade 3, moderate hem; grade 4. Lungs were scored for inflammation (inf), and the grading criteria was: grade 0, normal; grade 1, minimal inf; grade 2, mild inf; grade 3, moderate inf; grade 4. severe inf. Scoring was conducted independently by a pathologist in a blinded manner.

Morphometric Analysis for Quantifying Hemorrhage

H&E-stained slides were digitized on a ScanScope AT (Leica Biosystems, Inc., Vista, CA), and scanned at 40X objective magnification. Morphometric analysis was performed with *Definiens'* Tissue Studio (Definiens Inc., Parsippany, NJ) to determine the area of eosin staining in a non-biased method. Briefly, a stain specific algorithm was created using the pre-defined marker area detection module and classification tool. Thresholds were set to classify eosin stain for the entire tissue area. The data were exported to Microsoft Excel for further statistical analysis.

Data Analysis

Data was analyzed utilizing Microsoft Excel and Prism 6.0 (GraphPad Software, San Diego, CA).

RESULTS

To establish the TMPD-DPH model in our laboratory we injected a single dose of TMPD/Hex/PBS (0.5 ml, ip) once to B6 mice, and euthanized them at 1, 1.5, 2, 3 and 4 weeks post injection. At 1-week timepoint, none of the TMPD-injected mice (n=12) had

DPH, vasculitis or pneumonitis. We did detect a subtle increase in macrophage infiltration in the interstitium of the lungs in 25% of the TMPD-injected mice. There were no histopathological changes observed in the bone marrow, spleen, liver and kidney of all TMPD or Hex (n=8) or PBS (n=8)-injected mice. At Day 10, 2- weeks, 3-weeks, and 4 weeks timepoints, while other organs examined, including liver, kidney, and spleen, did not show any histopathological changes, 73% of TMPD-injected (n=50) mice but none of the controls (PBS/Hex) developed hemorrhage/pneumonitis/vasculitis in lungs (Figures 2.2 and 2.3). 50% animals succumbed to disease within 4 weeks of TMPD injection.

To quantify the extent of TMPD-induced disease in animals, we developed and used a semi-quantitative scoring system for inflammation and hemorrhage and a quantitative measure of DPH by measuring eosin-stained area by morphometric analysis, as described in Methods (Figure 2.4).

To assess the long-term effects of hydrocarbon oils, we monitored animals injected with TMPD or hex (500 µl, ip, single dose) and euthanized them when they became moribund or 2 months (TMPD) or 11 months (hex-injected or age-matched uninjected controls) (Figures 2.5-2.7). Four of six animals lost $\geq$ 20% bodyweight within 10-14 days post-TMPD (500 µl, ip); all had DPH. The two TMPD-injected animals that did not have weight loss did not have DPH, when euthanized at 2 months (Figure 2.5).

Analysis of data from this and other experiments in our laboratory revealed that a reduction in body weight by ~20% correlated with the development of DPH in mice (Figure 2.8). Hence, we used 20% weight loss as a clinical parameter to predict the development of DPH.

None of the Hex-injected mice lost 20% bodyweight, in contrast 3/9 Hex-injected mice gained 20-35% bodyweight 50 days post-Hex injection (Figure 2.5). The three animals that gained abnormal amount of weight were diagnosed with ascites, and euthanized on Days 52, 58 and 79. Lung pathology showed minimal inflammation, few oil droplets however there was no hemorrhage in the animals that had ascites. The remaining six mice were monitored up to 11 months for bodyweight and there was no increase/decrease $\geq$ 20% bodyweight (Figure 2.6). At 11 month timepoint (age 13.5-15.5 months), both the unmanipulated controls (n=6) and Hex-injected (n=6) animals showed similar lung pathology which included minimal lymphocytic infiltrates/focal inflammatory cells or a combination of these conditions (Figure 2.7). Oil droplets were present, however there was no lung hemorrhage in the Hex-injected animals. Focal, minimal lymphocytic infiltrates were present in the liver of both controls and Hex-injected animals. We also observed focal, minimal lymphocytic infiltrates in the medulla of kidneys of both controls and Hex-injected animals. The spleen and intestines were normal in all the animals. Inflammation and fat necrosis was observed outside intestines, liver, kidney, pancreas and spleen, if fat was present in tissue sections from Hex-injected animals. Acute and chronic granuloma were seen outside intestines in Hex-injected animals.

DISCUSSION

Administration of a single dose 500 µl ip TMPD induces DPH in B6 mice within 2 weeks and 50% mortality within 3-4 weeks, which is consistent with a previous report [4]. A relatively rapid development of inflammatory disease makes TMPD-DPH an efficient animal model to study mechanisms of autoimmune and inflammatory diseases in the laboratory. Furthermore, administration of TMPD (500 µl, ip), has been shown to induce

different autoimmune manifestations in different mouse strains [5, 6, 13, 17, 22], making this as an excellent model to investigate gene-environment interactions in the pathogenesis of autoimmune disease with heterogeneous manifestations such as lupus. Furthermore, the establishment of clinical parameter and semi-quantitative and quantitative measures in our study would be helpful in future studies to predict the presence of DPH and assess its severity, respectively.

While TMPD induced pneumonitis, vasculitis and DPH within two weeks of exposure, hexadecane did not elicit DPH up to 11 months after exposure, although, it did cause inflammation in lungs. Hexadecane-exposed mice at 11-months showed no evidence of prior hemorrhage since there were no hemosiderin-laden macrophages. Instead, 33% of hexadecane injected animals developed peritoneal inflammation and ascites, which is similar to a previous study, where a single hexadecane-injection (500 µl, ip) in female BALB/cJ mice (3 months old) induced chronic peritoneal inflammation within 2.5 months, but no lung hemorrhage. Granuloma formation and diffuse inflammatory tissue were seen in the peritoneum, diaphragm, liver, and spleen and they concluded that ascites resulted from the chronic peritoneal inflammation induced by hexadecane [19].

The different effects of the two hydrocarbon oils on lung pathology may be owing to their biodegradation properties. TMPD, a branched-chain alkane, is hardly biodegradable compared to n-alkanes such as hexadecane [24]. The fatty acid oxidation scheme works neatly for even-numbered chain lengths, it does not work completely for fatty acids that contain an odd number of carbons, β-oxidation of these compounds leads to propionyl-CoA and acetyl-CoA, rather than to two acetyl-CoA at the final step, this may be a factor for the different responses to different hydrocarbon oils. The fate of TMPD has

been studied in rats after a single per os administration of 3H-labeled TMPD. The balance study showed an extensive fecal excretion (66%) mainly as unchanged hydrocarbon, whereas about 14% of ingested TMPD was excreted in urine as TMPD metabolites and tritiated water. After one week, 8.3% of the ingested 3H still was stored in the carcass, and radioactive distribution in tissues and organs showed a preferential incorporation into adipose tissue and liver. Over 75% of the radioactivity stored in the carcass was associated with TMPD/pristane metabolites and tritiated water. Tissue metabolites were characterized by thin layer chromatography, gas chromatography and mass spectrometric analyses. Four metabolites were identified: pristan-1-ol, pristane-2-ol, pristanic acid and 4,8,12-trimethyltridecanoic acid. This study showed that TMPD undergoes subterminal hydroxylation or terminal oxidation followed by the classical beta-oxidation process [25]. Future studies are needed to elucidate whether different types of inflammatory reactions caused by the two hydrocarbon oils are indeed due to their different metabolic pathways in the body. Such studies may pave the way for developing strategies to enhance the degradation of difficult to biodegrade oils such as TMPD.

FIGURES

Hexadecane: $C_{16}H_{34}$

MW: 226.44

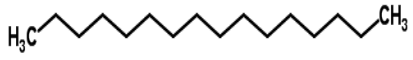

TMPD: $C_{19}H_{40}$

MW: 268.53

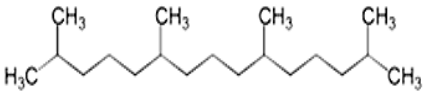

Fig 2.1 Structure and Molecular weight of Hydrocarbon oils: Hexadecane and 2,6,10,14-Tetramethylpentadecane (TMPD).

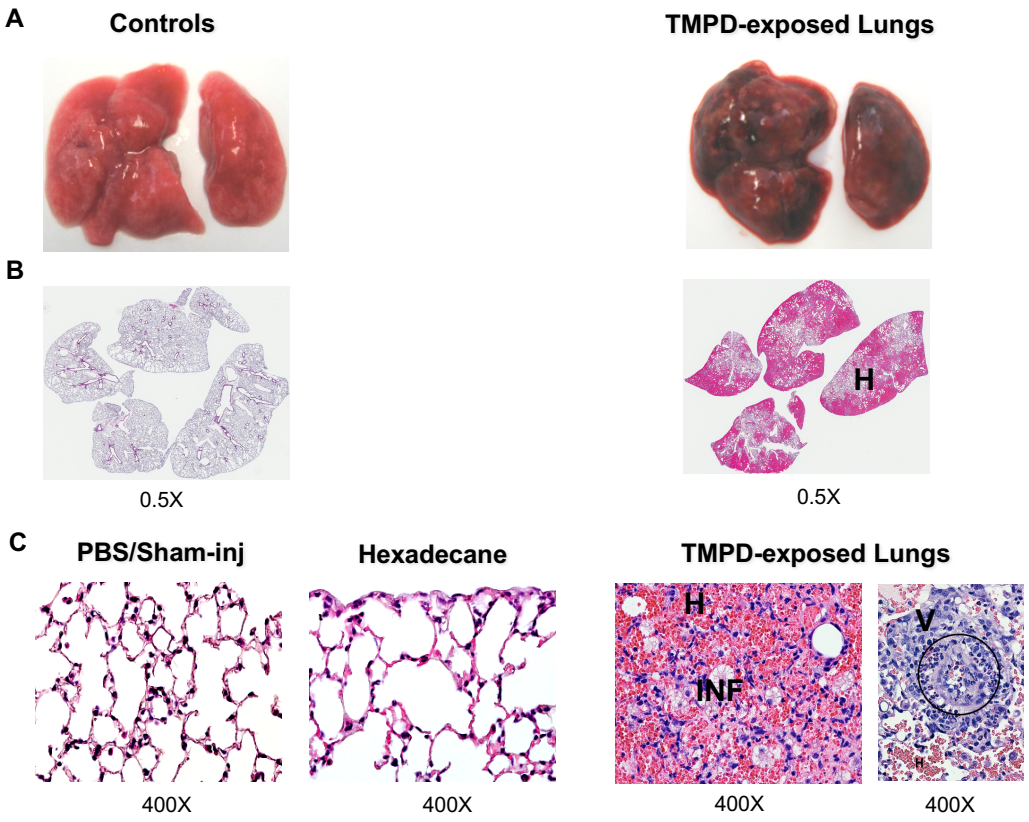

Fig 2.2 Gross Morphology and Histopathology of Lungs.

(A) Representative gross morphology of lungs from control (Hexadecane/PBS/sham-injected or unmanipulated) and TMPD-injected B6 mice (all injections of 0.5 ml, ip). Control groups had normal appearing lungs at all timepoints tested (1, 1.5, 2, 3, 4-weeks and 2 months) in contrast to dark pigmented lungs suggestive of hemorrhage in TMPD-exposed mice (0.5 ml, ip) mice at 1.5, 2, 3, and 4-week timepoints.

(B) Representative hematoxylin and eosin (H&E) stained lung tissue sections of all lobes at 2-weeks post-injection. Slides of whole lungs sections were digitized on a ScanScope AT (Leica Biosystems, Inc) and viewed with Aperio ImageScope 12.3.0.5 software at 0.5X low magnification. Control mouse lungs show normal histology, whereas TMPD-exposed mice exhibit diffuse hemorrhage.

(C) Representative lung tissue sections from control (PBS/sham or hexadecane injected) and TMPD-injected mice. Note hemorrhage ('H'), inflammation ('INF'), and/or vasculitis/arteritis ('V'). Arteritis (circled) and hemorrhage in surrounding alveoli are highlighted. Magnification 40X and 400X, as indicated on figure panels.

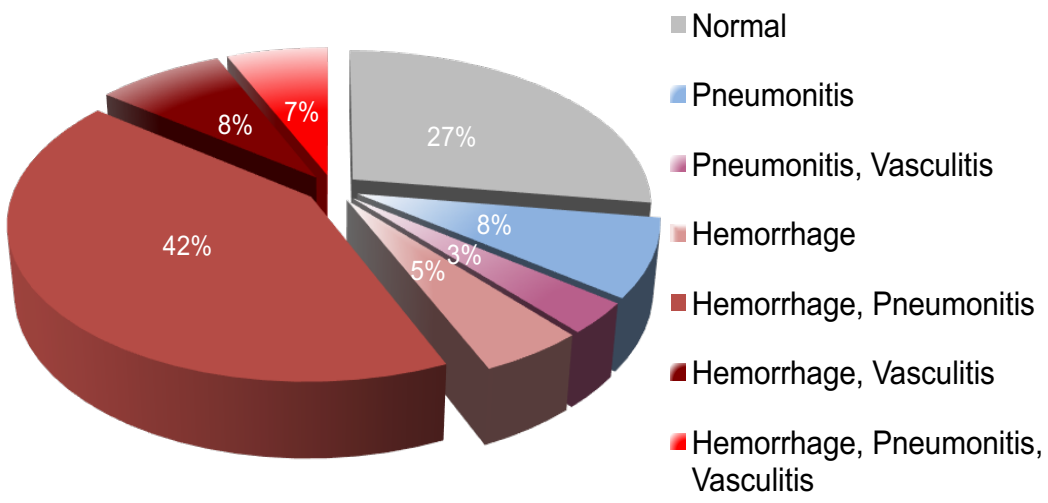

Fig 2.3 Summary of Histopathological Changes in the Lungs of TMPD-injected B6 Mice. Results from 62 animals that received 0.5 ml of TMPD ip are represented in this pie chart. Most animals were euthanized at ~2-weeks timepoint, unless they were moribund and/or had lost 20% bodyweight. The pathological changes in the lungs were detected as early as day 10 post-injection in a few animals. Some animals were monitored up to 4 weeks after injection. 73% animals exhibited pathological changes in various combinations, shown in the pie chart.

A

Lung Pathology Scoring Method

Score	Hemorrhage	Inflammation
0	None	None
1	Minimal	Minimal
2	Mild	Mild
3	Moderate	Moderate
4	Severe	Severe

B

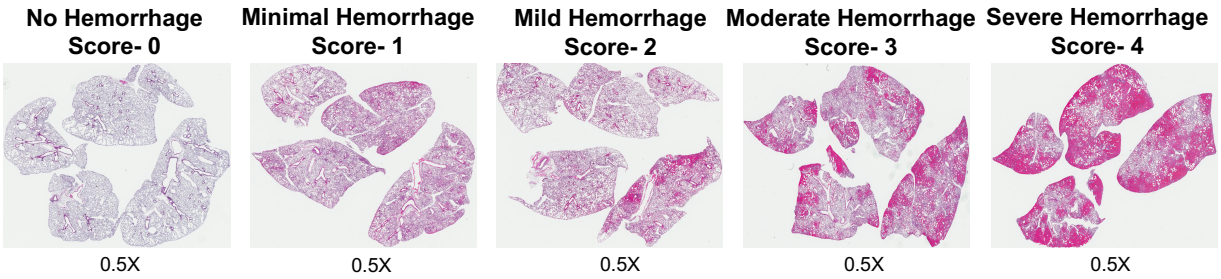

Fig 2.4 Semi-quantitative Scoring and Quantitative Measurements for TMPD Induced Lung Disease. H&E-stained lung tissue sections were scored independently by a pathologist in a blinded manner for hemorrhage and inflammation.

(A) and **(B)** Hemorrhage was scored on the following scale: score 0, normal; 1, minimal hemorrhage; 2, mild hemorrhage; 3, moderate hemorrhage; 4, severe hemorrhage. Slides were also scored for inflammation on the following scale: score 0, normal; 1, minimal inflammation; 2, mild; 3, moderate; and 4, severe inflammation. All the slides were examined. For quantitation of hemorrhage severity, morphometric analysis was performed on digitized slides of whole lungs to measure the area of eosin staining in a non-biased manner, as described in Methods. Briefly, tissue slides were digitized on a ScanScope AT. Using the *Definiens'* Tissue Studio, a stain specific algorithm was created using the pre-defined marker area detection module and classification tool. Thresholds were set to classify eosin stain for the entire tissue area. The data were exported to Microsoft Excel for further statistical analysis.

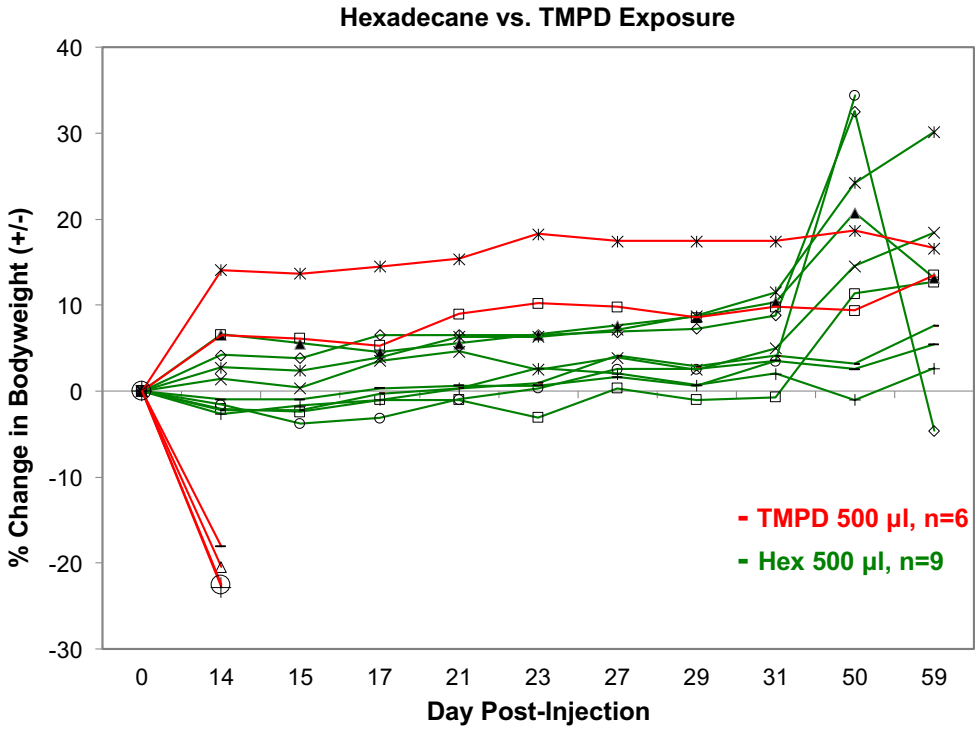

Fig 2.5 Clinical and Pathological Effects of Hexadecane versus TMPD. WT B6 males were injected with TMPD (n=6, 2-month-old) or Hexadecane (hex; n=5, 3-month-old; n=4, 4.5-month-old), both at 500 µl, ip dose. Each mouse was weighed prior to TMPD or Hex administration (Day 0). In the TMPD group, 4/6 mice lost 20% bodyweight within 14 days post-injection and correlated with severe lung hemorrhage. None of the mice in Hexadecane group lost weight; 3/9 mice gained 20-35% bodyweight 50 days post-injection, and were found to have ascites. Lung pathology in these three animals showed a minimal inflammation and a few oil droplets, but no hemorrhage. The remaining six mice were monitored for a longer term.

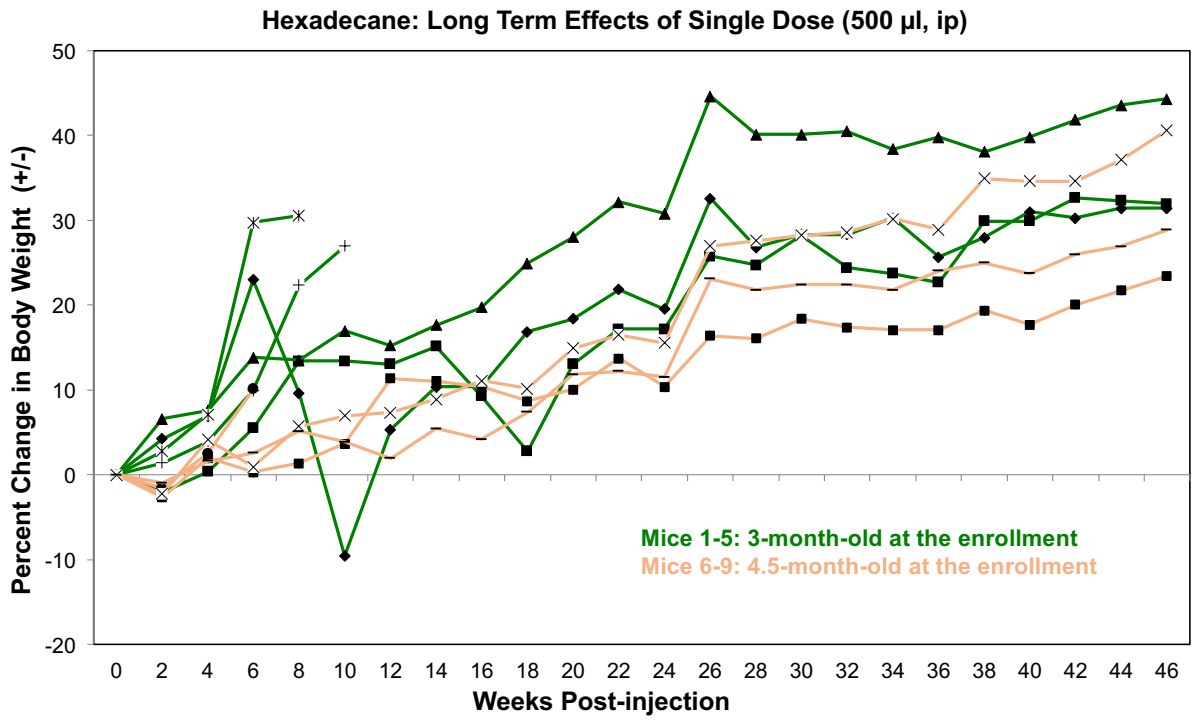

Fig 2.6 Long Term Effects of Hexadecane. Three to 4.5-month-old B6 mice were injected with hexadecane (500 µl, ip), as described in previous figure. Animals were monitored for up to 11 months. As stated in previous figure, 3/9 mice developed peritoneal inflammation and ascites within 50 days of injection. The remaining six mice appeared healthy up to 11 months.

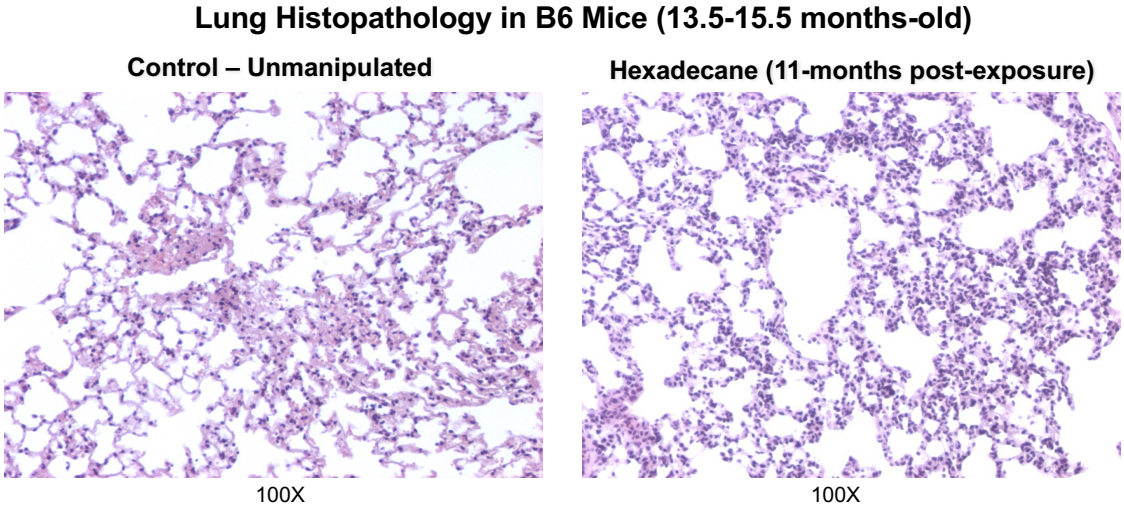

Fig 2.7 Lung Histopathology 11 Months after Hexadecane Administration and in Age-matched Unmanipulated Mice. B6 mice injected with hexadecane (500 µl, ip) at the age of 3-4.5 months, as in Figure 2.6, and 6 unmanipulated controls (2.5-month-old) mice were monitored up to 11 months. As stated in Figure 2.5, 3/9 hexadecane injected mice developed ascites within 50 days post-injection. The remaining hexadecane-injected mice (n=6) and control mice (n=6) were monitored up to the age of 13.5-15.5 months, when various organs were harvested and tissue sections subjected to H&E staining. Most organs did not show any inflammatory changes. Minimal lymphocytic infiltrates with focal inflammatory cells were present in the lungs of both hexadecane-injected and control mice. Specific lung areas 400X high magnification.

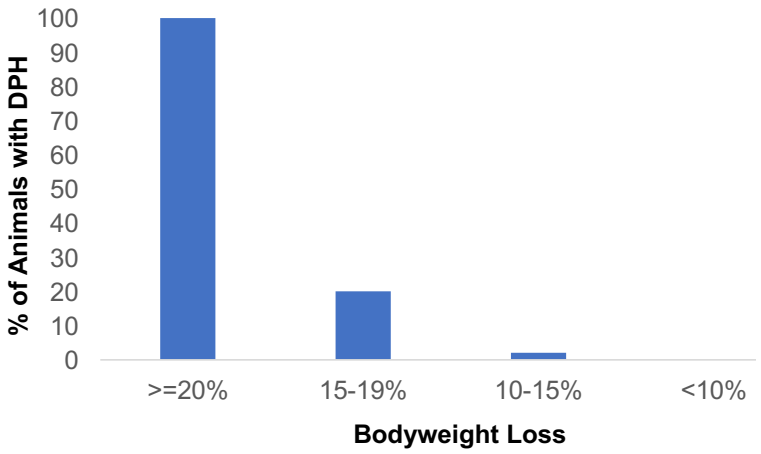

Fig 2.8 Weight Loss (20%) as a Clinical Parameter to Predict the Development of TMPD-induced DPH. B6 mice were weighed prior to administration of TMPD or hexadecane, and daily thereafter. In some experiments, animals were monitored daily for general health and weighed if moribund or on day 7 and daily or alternate day thereafter. Pooled data from 4 separate experiments involving 45 mice are shown.

CHAPTER 3

Hydrocarbon Oil Induced Lung Inflammation and Diffuse Pulmonary Hemorrhage: Effects of Different Dose Regimens and Routes of Exposure

ABSTRACT

A single intraperitoneal (ip) injection of 500 µl of TMPD in B6 mice consistently induces pneumonitis and DPH that pathologically mimics DPH in humans. Although, this serves as an excellent model to study mechanisms of DPH, acute high-dose exposures rarely occur in humans. Humans are exposed to hydrocarbon oils via inhalation (diesel exhaust, oil mists, aspiration of ingested mineral oil), ingestion (foods, medications), skin absorption (cosmetics, skin contact) or injection (immunization). To begin to address these issues, we conducted a dose-response study of hydrocarbon oils administered via ip and oropharyngeal aspiration. We found that ip administration of lower doses of TMPD (125 µl and 250 µl) were not effective in inducing DPH. While animals in 500 µl group developed weight loss and DPH (67%) and pneumonitis (81%), only 14% of animals in 250 µl group developed DPH and 42% pneumonitis. None of the animals in 125 µl developed DPH and 14% developed pneumonitis. A single oropharyngeal aspiration of 40 µl, 20 µl, 8 µl, and 6 µl of TMPD led to rapid morbidity and mortality, whereas 40 µl of PBS via this route had no adverse effect on health. Whole body necropsy of animals in 6 µl group showed lung inflammation, and serum chemistry revealed elevated creatinine kinase, glucose and aspartate aminotransferase. Mice given 4 µl TMPD or hexadecane via this route did not experience acute morbidity, and developed lung inflammation (TMPD/hexadecane) and/or hemorrhage (TMPD). Thus, oropharyngeal aspiration of 4 µl hydrocarbon oils may serve as a model to study the effects of low-dose direct lung exposure on pneumonitis and DPH, however, higher doses elicit acute toxicity. Studies are needed to determine the effect of repeated/chronic exposures to lower doses of hydrocarbon oils via different routes on the development of inflammation.

INTRODUCTION

A single intraperitoneal injection of high dose (0.5 ml) of hydrocarbon oil such as 2,6,10,14-tetramethylpentadecane (TMPD) and hexadecane (Hex) can cause various inflammatory diseases in rodent models. However, as it is unlikely for humans to be exposed to such a high dose of TMPD. Due to lack of published reports on the effect of different doses of TMPD, we conducted dose response studies to elucidate clinico-pathological changes in lungs and other organs at lower doses.

Epidemiological reports suggest an association between hydrocarbon oils and inflammatory diseases such as lupus and glomerulonephritis in humans. However, the presumption in such instances is of high levels of exposure by inhalation or via the skin [50]. Humans can be exposed to hydrocarbon oils via inhalation (diesel exhaust, oil mists, aspiration of ingested mineral oil), ingestion (foods, food contaminants, food packaging, and medications), skin absorption (cosmetics, skin contact) or injection (immunization) [8, 10, 11]. There is a paucity of experimental studies on the effect of hydrocarbon oils administered via oral or inhalation routes.

Dietary exposure to mineral oils did not provoke autoimmune responses in a previous study [50]. In a recent study, Dark Agouti (DA) rats given feed containing 4000 mg/kg TMPD or a broad mineral oil saturated hydrocarbons mixture in various concentrations (0-4000 mg/kg) for 90 days did not develop arthritis, whereas a single intradermal injection of 200 µl TMPD induced arthritis in all rats [51]. In another study, BALB/c mice given six intermittent oral doses of 0.1 ml TMPD (via a syringe and needle introduced into the lower esophagus) within a period of 9 weeks developed amyloidosis in the liver and spleen at 37-38 weeks and chronic renal lesions with papillary necrosis,

scars and cystic change later in life [52]. These studies suggest that oral exposure of TMPD causes varied effects in different rodents, and that different routes of exposures might cause different pathologies in the same animal strain.

To elucidate clinico-pathological changes in lungs and other organs upon exposure to lower doses of hydrocarbon oils via different routes, we administered different doses of TMPD or hexadecane given ip or via oropharyngeal aspiration.

METHODS

Mice

C57BL/6J (WT B6; Black 6; Stock No: 000664) mice were purchased from the Jackson Laboratory and housed in the UCLA Warren Hall Barrier Facility. Mice of both sexes, aged 2-5 months were used.

The UCLA Institutional Animal Care and Use Committee, known as the Chancellor's Animal Research Committee (ARC), approved the protocol for this study.

Dose Administration and Bodyweight Assessment

TMPD Dose Response Experiment:

Twenty mice were divided into three groups consisting of the low-dose group (125 µl TMPD), n=7; mid-dose group (250 µl TMPD), n=7; and high-dose group (500 µl TMPD), n=6. Controls were unmanipulated mice (n=3). Each mouse was weighed on a scale prior to TMPD administration. Under isoflurane anesthesia, the mice were administered an ip injection with a single dose (low/mid/high) of TMPD, and the day of TMPD administration was Day 0 for this experiment. The bodyweights of the mice were then monitored up to 2 months.

Oropharyngeal Aspiration of Hydrocarbon Oils in Mice

Each animal was lightly anesthetized with Ketamine/Xylazine solution (100 μl, ip). Oropharyngeal aspiration (OA) was performed as described in previous studies [53, 54]. Mice were fixed on a surgery board, the tongue was pulled out with a forceps, and the liquid (TMPD/Hex/PBS) was placed onto the distal part of the oropharynx using a micropipette, while the nose was gently closed.

To establish whether TMPD-DPH occurs via OA route, we performed experiments with different doses (40 μl, 20 μl, 8 μl, 6 μl, and 4 μl) of TMPD in B6 mice. Control B6 mice were given OA of 40 μl PBS. Hexadecane was tested only at two doses 6 μl and 4 μl in WT B6 mice.

For OA with low doses of 6 μl, and 4 μl TMPD/Hex, each animal was given OA of 6μl sterile DPBS (1X) immediately after to assure that the oil is flushed down, and not stuck at the oropharyngeal opening.

Reagents

2,6,10,14-Tetramethylpentadecane BioReagent (TMPD, Molecular Weight 268.52, CAS Number 1921-70-6), synthetic, liquid, sterile-filtered, purity ≥95% (Sigma-Aldrich Corp., St. Louis, MO; Lot Nos. RNBB3307 and RNBB3307V). Hexadecane *ReagentPlus*® (Hex, Molecular Weight 226.44, CAS Number 544-76-3) liquid, purity 99% (Sigma-Aldrich Corp., St. Louis, MO; Lot No. SHBD2368V). Ketamine Hydrochloride injection USP (Ketalar®; Par Pharmaceuticals Cos., Inc., NY), Xylazine injection (AnaSed®; Lloyd, Inc., IA), or Isoflurane USP (Piramal Healthcare Limited, Bethlehem, PA) was used to anesthetize/euthanize the mice. Dulbecco's Phosphate Buffered Saline [DPBS (1X) Gibco™; Thermo Fisher Scientific Inc., Waltham, MA] was used to perfuse the lungs, and to clean the small and large intestines. Ethyl alcohol (Decon Laboratories, King of Prussia,

PA) was used to clean the mouse prior to necropsy and preserve tissues for histology. Formalin 10% (Fischer Scientific Company LLC, Kalamazoo, MI) was used to fix the tissues for histology.

Necropsy

Necropsy was performed on those mice that were found dead/moribund or showed a reduction in bodyweight by 20% of their initial weight at Day 0. Animals given OA of TMPD at doses of 40 μl or 20 μl were euthanized using Ketamine/Xylazine solution (200 μl, ip). For all other experiments, on the day of necropsy, each mouse was placed in a chamber containing isoflurane for 3-5 minutes until it was euthanized. After the mouse ceased to breathe, it was taken out of the chamber and placed on a dissection mat. The mouse's body was cleaned with alcohol and its outer skin was cut. Cardiac blood was collected for serum analysis. The lungs were perfused via the heart, with DPBS 1X to remove the blood from them after the aorta was cut.

The lungs, liver (left lateral and right medial lobes), spleen, kidney (right), 2 sections each of small intestine, and large intestine were fixed in 10% formalin for at least 24 hours. The small and large intestine sections were cleaned with DPBS 1X solution before they were preserved for histology. Since majority of the animals given OA of 40μl TMPD died immediately after treatment, no tissues were collected.

For animals given OA of TMPD/Hex at dose of 6 μl, UCLA-DLAM technicians collected whole blood for serum and performed whole body necropsy. Each mouse was placed in a chamber that contained carbon dioxide for 3-5 minutes until it was euthanized. The lungs were perfused via the heart, with 10% formalin to remove the blood after the aorta was cut. Whole lungs, brain, trachea, heart, stomach, cecum, intestines, colon, liver

(median lobe), gallbladder, spleen, kidneys (half of each one) were collected and fixed in 10% formalin for at least 24 hours.

Histopathological Assessment

UCLA Translational Pathology Core Laboratory (TPCL) embedded the tissues in paraffin. Sections were stained with hematoxylin and eosin (H&E) for all the experiments. All the sections were examined independently by a pathologist in a blinded manner for hemorrhage and inflammation.

Serum Analysis

For animals given OA of TMPD/Hex at dose of 6 μl, the serum chemistry analysis was performed by a UCLA-DLAM technician. The serum samples (undiluted) were run on the Vet Axcel® Chemistry Analyzer (Alfa Wassermann Diagnostic Technologies, NJ). The Vet Axcel® Chemistry Analyzer automatically dilutes the serum sample for specific parameters. Serum samples were analyzed for alkaline phosphatase, alanine aminotransferase, aspartate aminotransferase, gamma-glutamyl transpeptidase, creatine kinase, blood urea nitrogen, creatinine, glucose, cholesterol, triglycerides, bilirubin (total), calcium, inorganic phosphorus, sodium, potassium, chloride, bicarbonate, albumin, and total protein levels. The normal range of these parameters in mice is based on a previous study [55], and was provided by UCLA-DLAM.

Data Analysis

Data was analyzed utilizing Microsoft Excel and Prism 6.0 (GraphPad Software, San Diego, CA).

RESULTS

Effect of different doses of systemic (intraperitoneal) administration of TMPD

In our previous experiments, a reduction in body weight of ~20% following TMPD injection (500 µl, ip) correlated with the development of DPH in mice. Hence, we used this parameter to monitor animals and euthanized them at ≥20% weight loss. In the first TMPD dose-response study, animals were monitored after a single ip injection with three different doses (125 µl, 250 µl, and 500 µl) of TMPD. Four of 6 mice in the 500 µl group and 1/7 in the 250 µl group had a significant reduction in bodyweight (>20%) within 18 days of TMPD injection; all had DPH (Figures 3.1, 3.2). The remaining 15 mice showed consistent/slightly increased bodyweights during the two-month period (Figure 3.1).

In the 500 µl group, there was focal granulomatous inflammation in the lungs in 5/6 mice; the two mice that survived up to 2 months had no hemorrhage, but had oil droplets in the lungs and one had granulomatous inflammation. In the 250 µl group, 3/7 animals had several foci of inflammation with focal areas of macrophage infiltration, mild inflammation or presence of lipid droplets or combination of these at 2 months timepoint (Figure 3.2). No histopathological changes in the lungs were detected in all unmanipulated controls, 6/7 animals in the 125 µl group, 3/7 in the 250 µl group, and 1/6 in 500 µl group.

The liver was mostly normal in all the animals at all doses of TMPD. Few mice showed the presence of prominent Kupffer cells and focal inflammation. The latter was observed in occasional unmanipulated controls. The spleen was normal in unmanipulated controls and in 125 µl group, however, there were increased megakaryocytes and lipid droplets in 5/7 in 250 µl group and 5/6 in 500 µl group. The kidneys and intestines were normal in all animals. Granulomatous reaction and fat necrosis was seen outside

intestines, liver, kidney, and spleen, if fat was present in tissue sections of TMPD-injected mice at all doses.

Effect of different doses of oropharyngeal aspiration of hydrocarbon oils

We investigated the effect of oropharyngeal aspiration (OA) of TMPD at different doses in B6 mice (Figure 3.3). We started the study with a dose of 40 μl TMPD via OA route, since it was >10X lower than the established ip dose of 500 μl TMPD that induces DPH within 2 weeks in WT B6 mice. After OA of 40 μl TMPD, 4/5 died soon after exposure, and the remaining animal was moribund and euthanized 18 hours later. All animals given the same amount of PBS (40 μl) remained healthy and were euthanized 4 weeks later.

We repeated the OA route experiments using 20 μl, 8 μl, 6 μl, and 4 μl doses in B6 mice (n=4-8/group, six independent experiments). At all doses tested except 4 μl, the animals became moribund and started dying within 18 to 72 hours post exposure**.** At all doses of TMPD, B6 mice developed lung inflammation, however, lung hemorrhage only occurred in mice that died after OA. No histopathological changes were detected in the trachea by light microscopy in all animals in all experiments conducted.

Lung tissue sections from mice administered 20 μl TMPD via OA showed moderate lung hemorrhage and inflammation in one of four mice that died at 18 hours post-exposure. All the other mice appeared moribund, had 10-15% bodyweight loss, and were euthanized after 24 hours. Lungs of these animals showed minimal to mild inflammation, but no hemorrhage (Figure 3.3).

In TMPD 8 µl OA experiment, all mice were moribund, had 10-15% bodyweight loss, and were euthanized on day 2. None of the animals had hemorrhage, and one of four animals showed minimal inflammation in the lungs. There was hyaline membrane formation in one mouse that died at 36 hours after TMPD exposure, indicative of acute lung injury (Figure 3.3).

We then repeated the OA experiment at 6 µl dose and included a control group of mice given OA of hexadecane that does not induce DPH when given via ip route. At this dose, 2/5 in the TMPD group died at 72 hours and one had a minimal lung hemorrhage. The remaining four TMPD-exposed mice were moribund, had 15-20% loss of bodyweight, and were euthanized on day 3. These animals had minimal to moderate inflammation in the lungs (Figure 3.4). Hexadecane recipients appeared less moribund than TMPD-exposed mice, none of them died, and were euthanized at 72 hours. All hexadecane-exposed mice had mild to moderate lung inflammation. Histopathology of other tissues (brain, trachea, heart, stomach, cecum, intestines, colon, liver, gallbladder, spleen and kidney) did not reveal any abnormality on light microscopy. Serum chemistry analysis showed elevated creatinine kinase and glucose in all animals given hexadecane or TMPD. The liver enzyme aspartate aminotransferase (AST) serum levels were elevated in 2 animals in each group (Figure 3.4). Blood could not be collected for two TMPD-exposed mice that were found dead on day 3 morning. Serum levels of alkaline phosphatase, alanine aminotransferase, gamma-glutamyl transpeptidase, blood urea nitrogen, creatinine, cholesterol, triglycerides, bilirubin (total), calcium, inorganic phosphorus, sodium, potassium, chloride, bicarbonate, albumin, and total protein levels were within the normal range in both TMPD and hexadecane exposed animals.

Next, we administered 4 µl hexadecane or TMPD via OA in two independent experiments (Figure 3.5). In the first experiment in 3-month-old females, 2/4 animals had a 15-20% loss of bodyweight within 3-days post-TMPD exposure, however, the mice gained weight after day 4 and appeared healthy thereafter. Necropsy was performed on day 17. In the second experiment in 2-month-old males, 2/4 animals had a 20% loss of bodyweight by day 4 in the TMPD group and were euthanized on day 4. In the hexadecane group, 3/4 animals had a 10-18% loss of bodyweight within 2-days, however the mice gained weight on day 3 onwards and appeared healthy thereafter. All four hexadecane and 2/4 TMPD exposed animals were euthanized on day 17. Histopathology of lungs showed minimal/mild hemorrhage in 3/8 TMPD-exposed and none in the hexadecane group. 6/8 TMPD-exposed and 3/4 hexadecane-exposed animals had lung inflammation.

DISCUSSION

Intraperitoneal administration of a single dose of 500 µl of TMPD consistently induced lung hemorrhage within 2 weeks in B6 mice, whereas 125 µl (ip) dose did not induce DPH and induced mild lung inflammation in 1/7 mice. The 250 µl ip dose caused DPH in 1/7 mice by day 18 and mild inflammation in the lungs by 2 months. TMPD (500 µl, ip) also induces other autoimmune manifestations in other mouse strains, but at later timepoints [5, 6, 13, 17, 22]. Thus, TMPD-DPH induced by 500 µl ip regimen of TMPD is an efficient animal model to study autoimmune disease pathogenesis in the laboratory.

To the best of our knowledge, this is the first study to show that oropharyngeal aspiration of TMPD and hexadecane induces pneumonitis and/or DPH in mice. It is

intriguing that B6 mice survive a large dose of 500 μl TMPD or hexadecane via ip route, however, show rapid morbidity/mortality when exposed to 6-40 μl TMPD via OA route. Compared to the ip route of TMPD administration that induces prominent lung hemorrhage and inflammation, OA route induces a prominent inflammatory response with minimal hemorrhage, likely because it may take time for lung hemorrhage to develop.

There are no published TMPD inhalation studies and limited animal studies on the effects via oral exposure. TMPD does not seem to induce the same disease via different routes in animals. TMPD induces arthritis in rats after an intradermal injection, but not after oral exposure via diet [51]. Amyloidosis involving the liver and spleen was observed in BALB/c mice administered 100 μl TMPD orally directly into the lower esophagus [52].

A recent study showed that BW5147 cells (murine thymoma cell line) exposed in vitro to TMPD (emulsified in PBS and BSA) exhibited dose-dependent induction of cell death within 24 hours. However, RAW 264.7 cells (murine macrophage cell line) were resistant to the cytotoxic effects of TMPD [26]. In the OA route, the epithelial cells in the oral cavity and trachea which are in direct contact with TMPD may undergo early cell death, whereas after ip exposure the peritoneal cells that largely consist of macrophages might be more resistant to cell death.

The whole body necropsy of animals given OA of 6 μl Hex or TMPD showed inflammation in the lungs, whereas all other tissues (brain, trachea, heart, stomach, cecum, intestines, colon, liver, gallbladder, spleen and kidney) tested did not show any histopathological changes. Animals did have elevated creatinine kinase and aspartate aminotransferase (AST) in both hexadecane and TMPD exposed animals. This may suggest an acute skeletal muscle or myocardial injury or liver damage. However, light

microscopy did not show changes in the liver and heart. In future studies, we will harvest muscle to examine any evidence of muscle damage. Animals also had increased blood glucose levels, for which we will examine pancreas in future studies.

Both TMPD and Hex (4 and 6 μl) induced pneumonitis via OA route, however lung hemorrhage was only observed in animals given TMPD. Thus, both ip and OA routes of exposure suggest a unique effect of TMPD in inducing lung hemorrhage.

Our novel observations demonstrating the effect of oropharyngeal aspiration of hydrocarbon oils are relevant to humans since the major route of exposure to TMPD is via inhalation (diesel exhaust, oil mists, aspiration of ingested mineral oil). However, the latter exposures are more likely to occur at a lower dose over a long period of time. Hence, studies are needed to examine the effect of repeated exposures to doses lower than 4 μl of hydrocarbon oil on local lung and systemic inflammation.

FIGURES

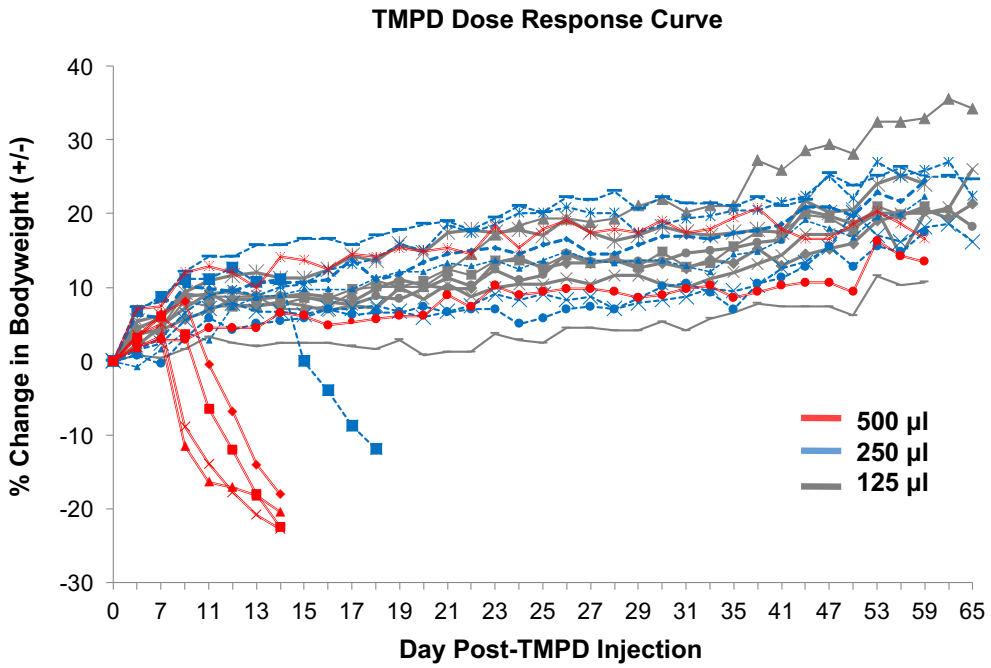

Fig 3.1 Clinical Effects of Different Doses of TMPD in B6 mice. Two-month-old B6 males were given a single ip injection of TMPD at 125 µl (n=7); 250 µl (n=7); and 500 µl (n=6). Each mouse was weighed prior to TMPD administration (Day 0). Four of 6 mice in 500 µl group and 1/7 in 250 µl group had a significant reduction in bodyweight (≥20%) within 18 days of injection. The remaining 15 mice were monitored up to 2 months post-injection, and then lungs harvested for histopathology.

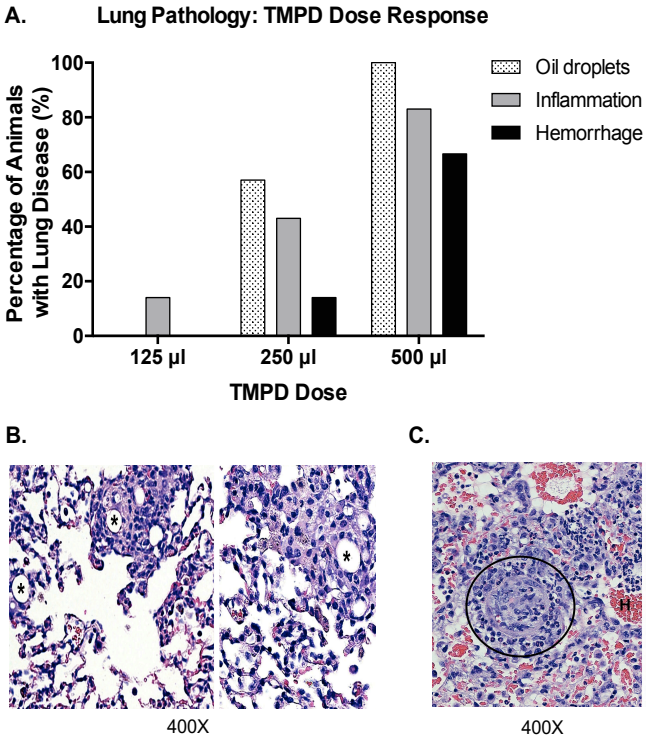

Fig 3.2 Lung Pathology in Mice Injected with Different Doses of TMPD. Animals injected with different doses of TMPD, in Figure 3.1, were euthanized at 2 months or sooner if they had ≥20% weight loss and/or appeared moribund. Lungs were harvested and tissue sections stained with H&E. **(A)** Histopathological changes: DPH was observed in 4/6 mice in high-dose group, 1/7 in medium-dose group, and in none in the low-dose group. Lung inflammation was seen in 5/6 mice in the 500 µl dose group (focal granulomatous inflammation), 3/7 in the 250 µl dose (several foci of inflammation), and 1/7 in the 125 µl dose group. Oil droplets in lungs were seen in all animals in 500 µl dose and 4/7 in 250 µl dose. **(B)** Representative photomicrographs showing granulomatous reaction to oil droplets in the mid- and high- dose groups at 2 months. **(C)** Arteritis (circled) and hemorrhage in lungs of high-dose TMPD group. Specific lung areas 400X high magnification.

A

PBS	TMPD Dose					Hexadecane	
40 µl	40 µl	20 µl	8 µl	6 µl	4 µl	6 µl	4 µl
All 3 normal up to 4 weeks	4/5 died soon after exposure; surviving mouse euthanized at 18 hrs	1/4 mouse died within 18 hrs. All mice moribund, euthanized at 24 hrs	4/4 mice moribund, euthanized at 48 hrs	2/5 died at 72 hours; remaining mice moribund, euthanized at 72 hrs.	Expt 1: 4/4 healthy up to 17 days. Expt 2: 2/4 moribund/ euthanized at 96 hrs	5/5 moribund; euthanized at 72 hrs	4/4 mice healthy up to 17 days
Lung pathology normal	N/A	1/4 DPH; 3/4 Inf	0 DPH; 1/4 Inf	1/5 DPH; 4/5 Inf	3/8 DPH; 6/8 Inf	0 DPH; 5/5 Inf	0 DPH; 3/4 Inf

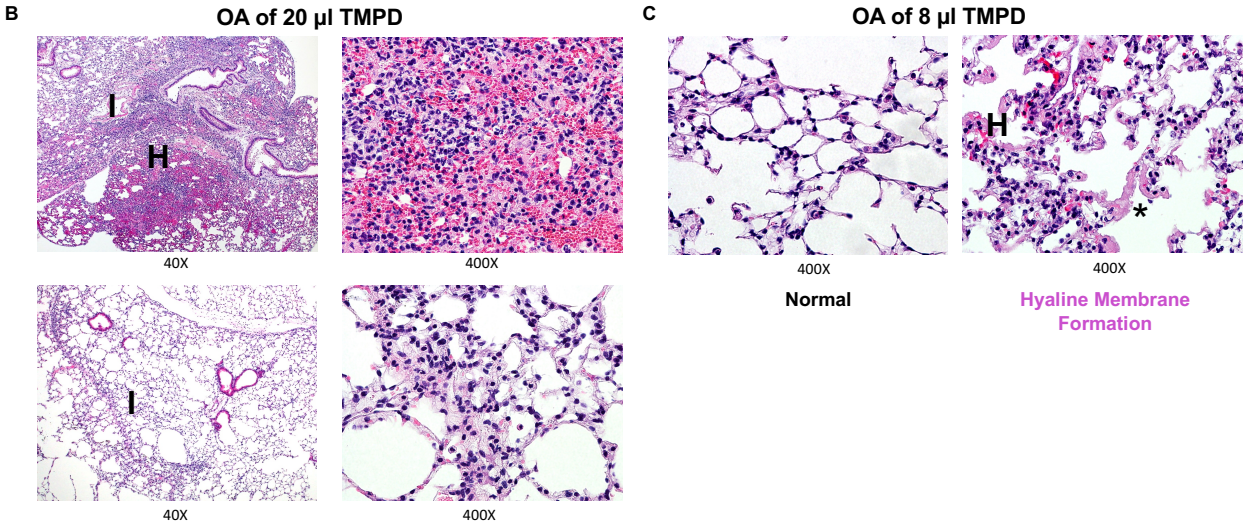

Fig 3.3 Oropharyngeal Aspiration of Hydrocarbon Oils at Different Doses.

(**A**) Effect on general health. B6 mice were administered with PBS, TMPD or hexadecane in different doses, as indicated, via oropharyngeal aspiration (OA) route. 2-5-month-old males and females were used in six separate experiments. While none of PBS or hexadecane injected animals died, TMPD-injected animals died or were severely moribund within a few days of exposure to doses of 40 µl, 20 µl, 8 µl, and 6 µl.

(B) Lung histology in B6 mice administered OA with TMPD 20 µl. One mouse that died within 18 hours had moderate hemorrhage (H) and inflammation (I) (upper panels). The remaining three animals that were euthanized when moribund showed minimal to mild

inflammation (lower panels). Representative lung areas at 40X and 400X high magnification.

(C) Lung histology in B6 mice administered OA with TMPD 8 µl. Hyaline membrane formation (*) in one mouse that died within 36 hours of exposure with TMPD, indicative of acute lung injury. A control normal lung is shown for comparison. Representative lung areas at 400X high magnification.

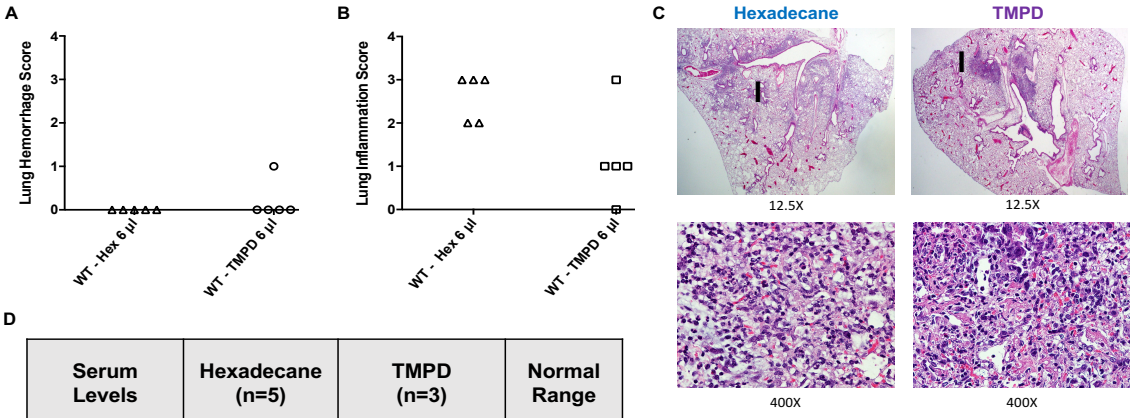

D

Serum Levels	Hexadecane (n=5)	TMPD (n=3)	Normal Range
Creatine kinase (U/L)	685.80±439.41	1450.33±209.19	112-236
Glucose (mg/dL)	207.20±83.93	181.67±53.27	60-133
Aspartate aminotrasferase (AST; U/L)	179.20±138.92	304±141.10	46-221

Fig 3.4 Oropharyngeal Aspiration of 6 µl Hexadecane and TMPD in WT B6 Mice: Changes in lungs and serum chemistry. B6 mice (males; 5 months old) were administered OA with hexadecane or TMPD 6 µl. Lung sections were stained with H&E, and scored for lung hemorrhage and inflammation. All sections were scored by a pathologist in a blinded manner. **(A)** Lung hemorrhage scores in both groups. Only one TMPD-exposed B6 mouse that died on Day 3 morning post exposure had minimal hemorrhage. All other mice were moribund, and were euthanized on Day 3, however none of them had hemorrhage. (**B)** Lung inflammation scores in both groups. Majority of the mice showed inflammation in both groups. **(C)** Specific lung areas with inflammation (I) in both groups. Representative lung areas at 12.5 X and 400X high magnification. **(D)** Serum chemistry analysis showed increased levels of creatinine kinase and glucose in both groups. Liver enzyme aspartate aminotransferase (AST) levels were elevated in 2 animals in each group. Data are shown as the mean±SD. Blood could not be collected for two TMPD-exposed mice that were found dead on Day 3 morning.

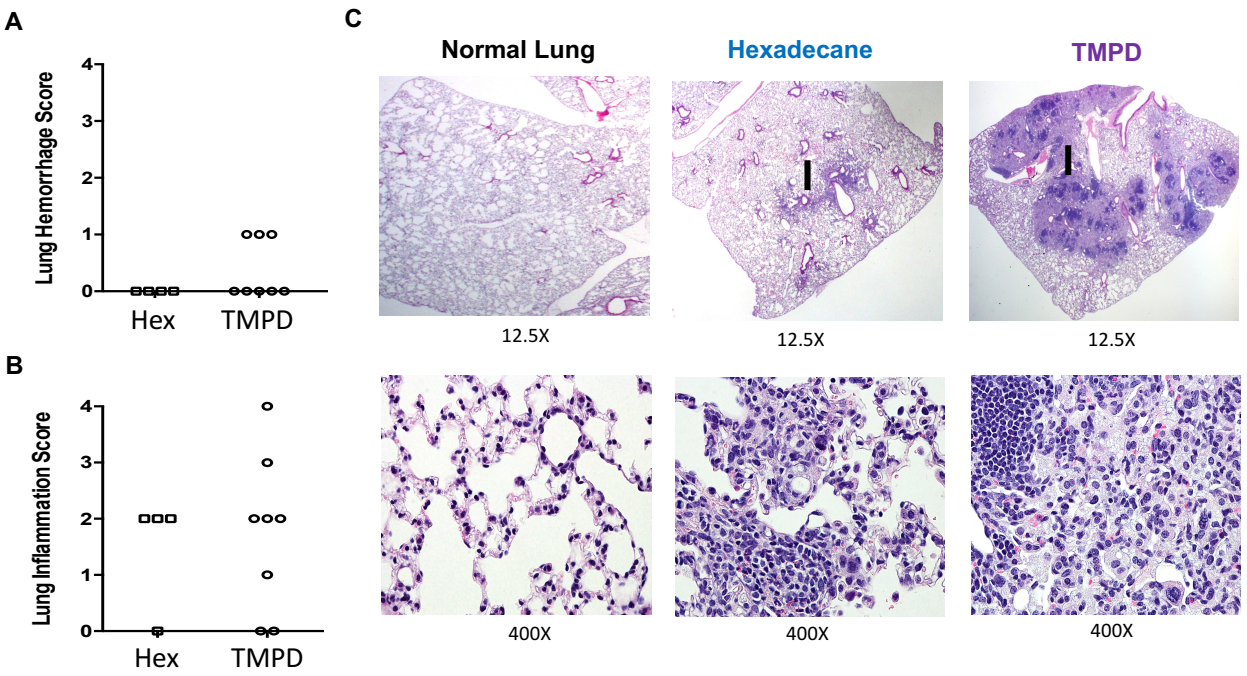

Fig 3.5 Effects of OA of 4 µl Hexadecane and TMPD in B6 mice. Mice (n=4-8/group; females and males; 2-3 months old) were administered OA with 4 µl of hexadecane or TMPD. Moribund mice were euthanized on day 4; healthy appearing mice were euthanized on day 17. Lung sections were stained with H&E, and scored for lung hemorrhage and inflammation. All sections were scored by a pathologist in a blinded manner. **(A)** Lung hemorrhage scores in all 4 groups. TMPD-exposed (3/8 mice) had minimal/mild hemorrhage. (**B)** Lung inflammation scores. **(C)** Specific lung areas with inflammation (I) in both groups compared to a normal lung. Representative lung areas at 12.5 X and 400X high magnification.

CHAPTER 4

Hydrocarbon Oil Induced Lung Inflammation and Diffuse Pulmonary Hemorrhage: Immune Phenotypes and Response

ABSTRACT

Intraperitoneal administration of a single dose of TMPD induces lung hemorrhage, pneumonitis and/or vasculitis in B6 mice at 2-4 weeks. At 1-week timepoint, none of the TMPD-injected mice had any major histopathological changes in the lungs, except for a subtle increase in macrophage infiltration in the interstitium of the lungs in 25% mice. At the 2-weeks timepoint, flow cytometry analysis showed that there was an increase in proportions of $TCR\beta^+$ T cells, $CD19^+$ B cells, and $CD11b^+CD11c^-$ cells (macrophages and neutrophils) in the lungs of TMPD-injected mice compared to controls. Abnormalities in almost all immune cell types analyzed at 2-4 weeks timepoint suggested that some of these findings likely represented a consequence of disease, rather being a primary driver of pathology. At 1-week timepoint, prior to any histopathological changes, while both hexadecane and TMPD caused abnormalities of myeloid cells, only TMPD caused increased infiltration of lungs with B cells, most of which expressed the markers of B1 B cell subset ($CD19^+CD11b^+$/$CD19^+CD5^+$). The proportions and numbers of these B1 B cells were simultaneously reduced in their usual location, i.e., peritoneal cavity in TMPD-exposed mice. These data suggest a possible role of B1 B cells in the pathogenesis of TMPD-DPH and guide us to posit that TMPD drives the trafficking of innate B1 B cells from the peritoneum to the lungs, where they play a role in the pathogenesis of DPH.

INTRODUCTION

Pathogenesis of DPH is unclear. Advances in the pathogenesis of DPH have been hampered due to the heterogeneity of clinical findings, a paucity of access to clinical tissues from early stages of disease, and the lack of suitable animal models. Thus, the recent discovery of TMPD-DPH provides a model system to study DPH pathogenesis [3,

4]. Using this model, the prevalence of DPH was lower in Rag1$^{-/-}$ B6 mice than in WT B6 controls, although 50% of Rag1$^{-/-}$ mice did develop DPH. This suggests that DPH can develop in the absence of T and B cells, although they may play a role in promoting DPH. Interestingly, Ig$\mu^{-/-}$ B6 mice had a strikingly reduced prevalence of DPH (7% vs 84% in WT B6), and reconstitution of Ig$\mu^{-/-}$ B6 mice with wild-type splenic B cells increased the DPH prevalence to 50%, thereby suggesting a possible role of B cells in development of DPH [4]. However, no immune complexes or complement deposition was detected in the DPH lungs. Furthermore, the transfer of serum from DPH mice to naive mice did not induce DPH, although the sample size was too small in this experiment [4].

A community study from New Mexico showed that people living near an oil field waste site with increased levels of TMPD in house dust had increased proportions of CD19^{+} B cells in their peripheral blood compared to the control population [12]. Furthermore, my mentor's lab reported an increase in marginal zone B (MZB) cells, and immunoglobulin isotypes produced by these MZB cells in BALB/c mice injected with TMPD [30].

MZB cells and another B cell type, called, B1 B cells, provide an initial and prompt antibody response, mainly to T cell-independent antigens. Due to their anatomical location, these B cells are the first cell populations to encounter antigens acquired through the peritoneum and blood stream [31], [32]. B1 B cells are innate-like lymphocytes that generate natural antibodies with important functions in tissue homeostasis and immune defense. While B1 B cells frequencies in secondary lymphoid tissues are low, relative high frequencies are found within peritoneal and pleural cavities of mice [33]. Guided by our preliminary data, we focused on these cells.

B1 B cells are divided into three different subsets, B1a, B1b, and B1c, on basis of CD5 and CD11b expression. They represent reservoirs of B1 cells that can be activated for migration to lymphoid tissues to secrete antibodies and/or cytokines. B1a cells are $CD11b^{+}CD5^{+}$, B1B cells are $CD11b^{+}CD5^{-}$, and the newly described rare and unique subpopulation of B1c cells is $CD11b^{-}CD5^{+}$ (they can develop into B1a cells) [56], [57]. B1a and B1c cells express CD5 that is known to function as a negative regulator of B cell receptor (BCR) signaling that may help prevent inappropriate activation of autoreactive B1a cells. B1a cells produce natural antibodies, while B1b cells are critical in development of IgM memory cells [58]. The functional properties of B1c are essentially similar to those of B1a and B1b B cells [57].

The unique markers for B1 cells in humans are not well defined yet, since activated human B cells express CD5. However, recent studies have characterized human B1 cell surface phenotype and function, which resembles the properties of murine B1 cells very closely [59], [60]. Immune regulation produced by B cells has been attributed to production and secretion of interleukin (IL)-10, which is a characteristic of mouse B1 cells [60].

B1b cells express Mac-1 (CD11b/CD18), a leukocyte adhesion molecule that is also expressed on many myeloid cell types. Mac-1 plays a role in inflammation by regulating migration of leukocytes into injured tissue. A recent study showed that depletion of neutrophils and eosinophils or adoptive transfer of classically activated macrophages resulted in the exacerbation of TMPD-DPH in both WT and Mac-$1^{-/-}$ B6 mice. However, the peritoneal transfer of $F4/80^{hi}MMR^{+}$ (mannose receptor) alternatively activated macrophages reduced the prevalence of DPH in WT mice. Thus, Mac-1 can promote acute inflammatory responses in the peritoneal cavity and lungs by

downregulating granulocyte migration and subsequent phenotypic conversion of macrophages in the TMPD-lupus model [34]. In atherosclerosis, a chronic inflammatory disease of the arterial wall, B1 cells are believed to secrete protective IgM antibodies that act as scavenger of deleterious molecules whereas B2 lymphocytes probably worsen the disease by activating proinflammatory T lymphocytes [36].

Chowdhary et al. found that 2 weeks after TMPD injection (0.5 ml, ip) the bronchoalveolar lavage (BAL) fluid from B10 mice was consistently bloody and filled predominantly with macrophages and neutrophils [3]. In another previous study, when the cells in BAL from TMPD-injected (0.5 ml, ip) B6 mice were examined via flow cytometry, the numbers of monocytes, granulocytes, $CD19^+$ B cells, $CD4^+$ and $CD8^+$ T cells were increased over the 2- weeks period [4].

In summary, little is known about the role of innate B cells in vascular inflammation, and their role is unknown in DPH. None of the previous studies reported flow cytometry data regarding the lungs, our study provides detailed cellular analysis of the lungs, peritoneal fluid (PF) and the spleen in the TMPD-DPH model.

METHODS

Mice

Wild-type C57BL/6J (WT B6; Black 6; Stock No: 000664) mice were purchased from the Jackson Laboratory and housed in the UCLA WAH Barrier Facility. For flow cytometry experiments at different timepoints, male mice aged 3-8 months were used.

The UCLA Institutional Animal Care and Use Committee, known as the Chancellor's Animal Research Committee (ARC), approved the protocol for this study.

Dose Administration and Bodyweight Assessment

TMPD-DPH Animal Model Experiments:

WT B6 mice were administered PBS/Hex/TMPD (500 µl, ip) under isoflurane anesthesia. Shan-injected and unmanipulated WT B6 were used as controls for some experiments. The day of TMPD administration was Day 0 for each experiment and their weight was monitored at different time points post-TMPD exposure.

Reagents

2,6,10,14-Tetramethylpentadecane BioReagent (TMPD, Molecular Weight 268.52, CAS Number 1921-70-6), synthetic, liquid, sterile-filtered, purity ≥95% (Sigma-Aldrich Corp., St. Louis, MO; Lot Nos. RNBB3307 and RNBB3307V). Hexadecane *ReagentPlus*® (Hex, Molecular Weight 226.44, CAS Number 544-76-3) liquid, purity 99% (Sigma-Aldrich Corp., St. Louis, MO; Lot No. SHBD2368V). Isoflurane USP (Piramal Healthcare Limited, Bethlehem, PA) was used to anesthetize/euthanize the mice. Dulbecco's Phosphate Buffered Saline [DPBS (1X) Gibco™; Thermo Fisher Scientific Inc., Waltham, MA] was used to perfuse the lungs, and to clean the small and large intestines. Ethyl alcohol (Decon Laboratories, King of Prussia, PA) was used to clean the mouse prior to necropsy and preserve tissues for histology. Formalin 10% (Fischer Scientific Company LLC, Kalamazoo, MI) was used to fix the tissues for histology. The lungs were digested with Collagenase, Type 1 (Worthington Biochemical Corporation, Lakewood, NJ) and Deoxyribonuclease I from bovine pancreas (DNase; Sigma-Aldrich Corp., St. Louis, MO**),** and the enzymatic digestion process was stopped with UltraPure™ EDTA (Invitrogen™, Thermo Fisher Scientific Inc., Waltham, MA**)**. Red blood cells (RBCs) in spleen, bone marrow and lungs were removed with lysis buffer BD Pharm Lyse™ (BD Biosciences, San Jose, CA). For flow cytometry, the tissues were collected and cells washed with RPMI 1640 Medium (Gibco™; Thermo Fisher Scientific Inc., Waltham, MA).

FACS buffer for immunostaining was made with PBS 10X (Fischer Scientific Company LLC, Fair Lawn, NJ) and Bovine serum albumin (BSA; Fischer Scientific Company LLC, Fair Lawn, NJ). Trypan blue (MP Biomedicals LLC, Solon, OH) was used to count viable cells for immunostaining.

Necropsy

On the day of necropsy, each mouse was placed in a chamber that contained isoflurane for 3-5 minutes until it was euthanized. After the mouse ceased to breathe, it was taken out of the chamber and placed on a dissection mat. The mouse's body was cleaned with alcohol and its outer skin was cut. The peritoneum was infused with 10 ml of cold DPBS 1X, lavage was performed peritoneal fluid collection. Cardiac blood was collected for serum analysis. The lungs were perfused via the heart, with DPBS 1X to remove the blood from them after the aorta was cut. The lungs were incubated at 37^{o}C in RPMI medium with Collagenase and DNase for one hour, and digestion was stopped by adding EDTA.

The lungs (lower right lobe), liver (left lateral and right medial lobes), spleen (lower part small piece), kidney (right), 2 sections each of small intestine, and large intestine were fixed in 10% formalin for at least 24 hours. The small and large intestine sections were cleaned with DPBS 1X solution before they were preserved for histology.

Histopathological Assessment

UCLA Translational Pathology Core Laboratory (TPCL) embedded the tissues in paraffin. Sections were stained with hematoxylin and eosin (H&E) for all the experiments. All the sections were examined independently by a pathologist in a blinded manner for hemorrhage and inflammation.

Flow Cytometric Analysis

Cells from lungs, peritoneal fluid, spleen and bone marrow were washed with RPMI medium. Red blood cells (RBCs) in spleen, bone marrow and lungs were removed with lysis buffer, then kept in FACS buffer. After blockade of Fc receptors with purified anti-mouse CD16/CD32 mAb (clone 2.4G2; Tonbo Biosciences, San Diego, CA), cells were stained with the corresponding Ab mixtures. The following mAbs were used: APC-labeled anti-mouse CD19 (clone 1D3; Tonbo Biosciences, San Diego, CA), PE-labeled anti-mouse CD21/35 (clone 4E3; eBiosciences, San Diego, CA), PerCP Cy5.5-labeled anti-mouse CD23 (clone B3B4; eBiosciences, San Diego, CA), PE-labeled anti-mouse CD5 (clone 53-7.3, eBiosciences, San Diego, CA), and PerCP-Cyanine5.5-labeled anti-human/mouse CD11b (clone M1/70; Tonbo Biosciences, San Diego, CA). Cells were acquired using a BD FACSCalibur™ flow cytometry system (BD Biosciences) in our laboratory. All the data were analyzed using the FlowJo software Version 8.7 (Ashland, OR).

Data Analysis

For the phenotypic characterization of the immune cells found in the lungs, peritoneal fluid, spleen and bone marrow, differences between groups were statistically analyzed by unpaired Student's t-test with Welch's correction method with $P < 0.05$ considered to be significant. Data are presented as mean±SEM. Data were analyzed utilizing Microsoft Excel and Prism 6.0 (GraphPad Software, San Diego, CA).

RESULTS

We analyzed immune cells in the lungs and lymphoid organs of TMPD injected WT B6 mice. At the 2-weeks timepoint, there was an increase in proportions of $TCR\beta^+$ T cells,

$CD19^+$ B cells, and $CD11b^+CD11c^-$ cells (macrophages and neutrophils) in the lungs of TMPD-exposed mice compared to controls. In addition, we found a higher proportion of $CD11c^+$ dendritic cells (DC) in lungs and bone marrow (BM). In particular, there was a statistically significant increase in $PDCA1^+$ $CD11c^+$ plasmacytoid DC (pDC) in the BM, and $CD11b^+$ $CD11c^+$ myeloid DC (mDC) in the lungs of TMPD injected mice (n=11) as compared to controls (PBS, n=9). Immunostaining with anti-S100 antibody indicated increased $S100^+$ cells in alveolar spaces and septae of TMPD-exposed mice versus saline (n=3/group), at 2-weeks timepoint. At 3-4 weeks after TMPD injection, flow cytometry studies showed increased DCs along with a profound cellular infiltration with mDCs, and granulocytes in lungs, and pDCs in bone marrow of TMPD exposed mice (data not shown).

Abnormalities in almost all immune cell types analyzed at 2-4 weeks timepoint suggested that some of these findings likely represent a consequence of disease, rather being a primary driver of pathology. Hence, to glean into early events leading to the development of DPH, we analyzed immune cells at the 1-week timepoint, when animals had not developed DPH based on histopathology.

At the 1-week timepoint, flow cytometry analyses of immune cells showed similar numbers and proportions of $TCR\beta^+$ T cells in the lungs, spleen and peritoneum in all groups of mice. There were similar numbers and proportions of mDCs and pDCs in the lungs. However, consistent with the finding at the 2-week timepoint, $MHCII^{lo}$ $PDCA1^+$ $CD11c^+$ pDCs were significantly increased in the BM of TMPD-exposed mice as compared to both controls. Granulocytes ($CD11b^+$ $Gr1^+$) were significantly

increased in the lungs, BM and spleen of mice injected with both hydrocarbon oils (TMPD or Hex) as compared to PBS-injected mice. Specifically, there was a 3-fold increase in the number of $Gr1^{+}CD11b^{+}CD11c^{-}$ cells, $CD11b^{+}Ly6G^{+}$ cells, and $CD11b^{+}Ly6C^{+}$ cells in the lungs of TMPD and Hex-injected mice compared to the saline group (data not shown).

Analysis of B cells in different organs at the 1-week timepoint showed an interesting pattern. Importantly, the proportions and numbers of $CD19^{+}$ B cells were significantly higher in the lungs of TMPD-injected versus PBS/Sham-injected mice (Figure 4.1). The proportions and numbers of $CD19^{+}$ B cells were significantly reduced in the peritoneal fluid (PF) and bone marrow (BM) of mice injected with TMPD or Hex as compared to the PBS group (Figures 4.1 and 4.2). The proportions and numbers $CD19^{+}$ B cells were unchanged in the spleen within the three groups (Figure 4.3). In the spleen, the proportions of innate B cells, specifically MZB cells, defined as $CD19^{+}CD21^{hi}CD23^{lo}$ cells were similar in all the groups of mice (Figure 4.3).

The most interesting finding was that only TMPD caused increased infiltration of $CD19^{+}$ B cells and the subset B1 B cells ($CD19^{+}CD11b^{+}$/$CD19^{+}CD5^{+}$) in the lungs. The proportions and numbers of these B1 B cells were simultaneously reduced significantly in their usual location, i.e., peritoneal cavity in TMPD- and Hex- versus PBS/Sham-injected mice. (Figure 4.4).

These data guided us to hypothesize that *while both hydrocarbon oils induce an egress of B1 B cells from the peritoneal cavity, only TMPD induces the trafficking of these cells to the lung*. *The peritoneal innate B1 B cells may migrate to the lung after TMPD injection and contribute to the development of DPH* (Figure 4.5).

DISCUSSION

We analyzed cells isolated from the lungs, spleen, BM, peritoneal fluid (PF), for B and T cells, DCs and granulocytes after 1- and 2-weeks of injecting B6 mice with TMPD, Hex or PBS (0.5 ml, ip). While most immune cell types were increased in the lungs at 2 weeks, only B1 B cells were increased in the lungs at 1-week timepoint in TMPD injected mice as compared to Hex-injected mice.

Chowdhary et al. found that 2 weeks after TMPD injection (0.5 ml, ip) the BAL fluid from B10 mice was consistently bloody, and filled predominantly with macrophages and neutrophils [3]. In another previous study, when the cells in BAL from TMPD-injected (0.5 ml, ip) WT B6 mice were examined via flow cytometry, the numbers of monocytes, granulocytes, $CD19^+$ B cells, $CD4^+$ and $CD8^+$ T cells were increased over the 2-weeks period [4]. Our immune cell findings in the lungs are similar to the findings in BAL fluid in these published studies.

A community study showed that people living near an oil field waste site with increased levels of TMPD in house dust had increased proportions of B cells in their peripheral blood compared to the control population [12], suggesting a possible role of B cells in TMPD-induced immune pathology. This assumption is supported by an animal study that showed that TMPD-DPH is markedly reduced in B cell-deficient ($Ig\mu^{-/-}$) mice; and the reconstitution with B cells reverses the protection from DPH in $Ig\mu^{-/-}$ B6 mice [4]. Another study showed a sharp increase in serum IgM levels within a few days of TMPD-injection in mice [61]. However, the mechanism by which B cells contribute to the pathogenesis of TMPD-DPH is unclear.

Our findings of the increased proportions of B1 B cells in the lungs and reduced

proportions in the peritoneum of TMPD-injected mice as compared to controls in the peritoneal fluid were unexpected, and may be critical in the pathogenesis of DPH. B1 B cell is subset of innate B cells that rapidly produce IgM. We posit that TMPD that induces DPH, as compared to Hex that does not, induce a different set of genes in the target organ prior to the onset of DPH. Our specific **hypothesis** was that *TMPD-induced molecular changes in the lungs are conducive to the recruitment of B1 B cells from their peritoneal and pleural locations.*

Based on these findings we decided to investigate the effects of TMPD in $CD19^{-/-}$ B6 mice since they have significantly decreased B1a B cells in the peritoneum compared to WT B6 mice [43], and showed decreased incidence of lung fibrosis in a bleomycin animal model [45].

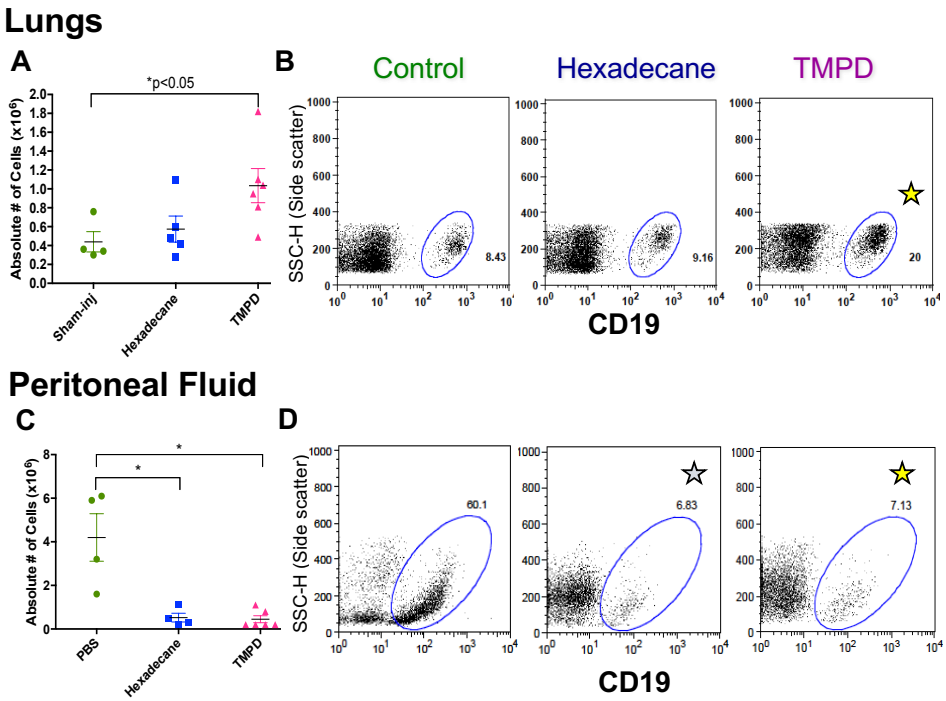

Fig 4.1 Flow cytometry analysis of B cells in Lungs, and Peritoneal Fluid at 1-week Timepoint. WT B6 mice (males) were injected with TMPD, Hex or PBS (0.5 ml, ip), and euthanized at 1-week time point. Cells were gated on $CD19^+$ live lymphocytes. **(A)** Lungs showed a significant increase in absolute cell counts of $CD19^+$ B cells in TMPD-exposed mice. **(B)** Increased percentage of $CD19^+$ B cells in lungs of TMPD-exposed mice (representative of all 4 independent experiments). **(C)** Decreased absolute cell counts $CD19^+$ B cells in PF of Hex- and TMPD-exposed mice **(D)** Decreased percentage of $CD19^+$ B cells in PF of Hex- and TMPD-exposed mice (representative of all 4 independent experiments). For absolute cells counts data shown from two experiments since age of mice different within 4 independent experiments, and in two experiments the lower right lobe of lungs were taken for histology. TMPD (n=12), hexadecane (n=10), controls (PBS/sham-injected, n=8). Numbers on a representative dot plot indicate percentage of cells. 1 $X10^6$ cells were stained. Data are presented as mean±SEM, *P<0.05

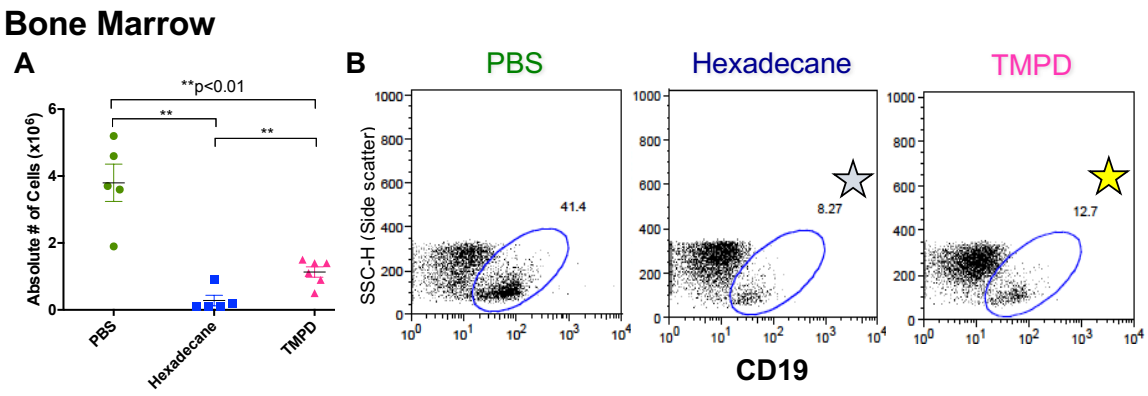

Fig 4.2 Flow cytometry analysis of B cells in Bone Marrow at 1-week Timepoint. WT B6 mice (males) were injected with TMPD, Hex or PBS (0.5 ml, ip), and euthanized at 1-week time point. Cells were gated on $CD19^+$ live lymphocytes. **(A)** BM showed a significant decrease in absolute cell counts of $CD19^+$ B cells in TMPD-exposed mice. **(B)** Decreased percentage of $CD19^+$ B cells in BM of TMPD-exposed mice. Data representative of two independent experiments. TMPD (n=6), hexadecane (n=5), and PBS (n=5). Numbers on a representative dot plot indicate percentage of cells. 1 $X10^6$ cells were stained. Data are presented as mean±SEM. **P<0.01

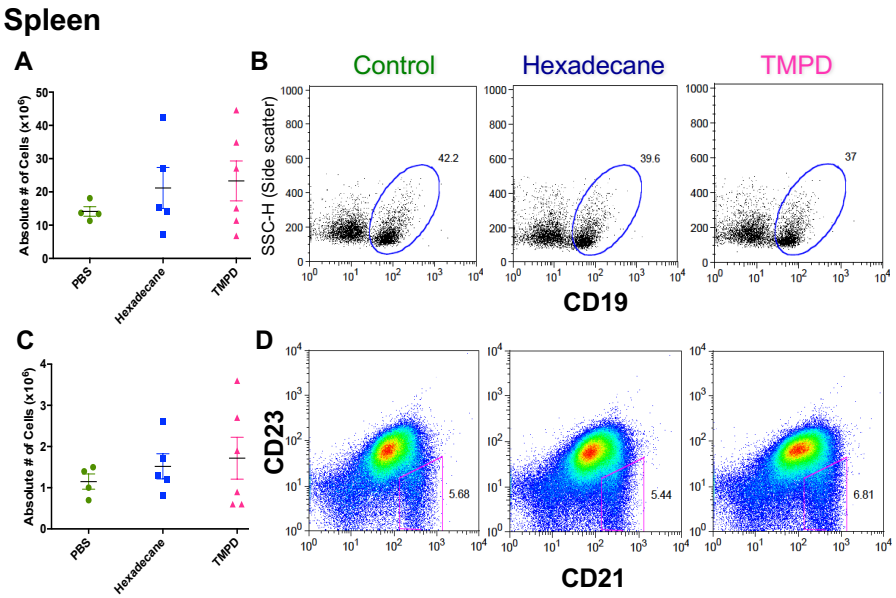

Fig 4.3 Flow cytometry analysis of B cells in Spleen at 1-week Timepoint. WT B6 mice (males) were injected with TMPD, Hex or PBS (0.5 ml, ip), and euthanized at 1-week time point. Cells were gated on $CD19^{+}$ live lymphocytes. **(A)** Spleen showed a no significant change in absolute cell counts of $CD19^{+}$ B cells between the groups. **(B)** Similar percentage of $CD19^{+}$ B cells in spleen of all groups (representative of all 4 independent experiments). **(C)** Similar proportions of MZB cells ($CD19^{+}CD21^{hi}CD23^{lo}$) cells in spleen of all groups **(D)** Similar percentage of MZB cells in spleen of all groups (representative of all 4 independent experiments). For absolute cells counts data shown from two experiments since age of mice different within 4 independent experiments, and in two experiments a small piece of the lower part of spleen was taken for histology. TMPD (n=12), hexadecane (n=10), controls (PBS/sham-injected, n=9). Numbers on a representative dot plot indicate percentage of cells. 1 $X10^{6}$ cells were stained. Data are presented as mean±SEM.

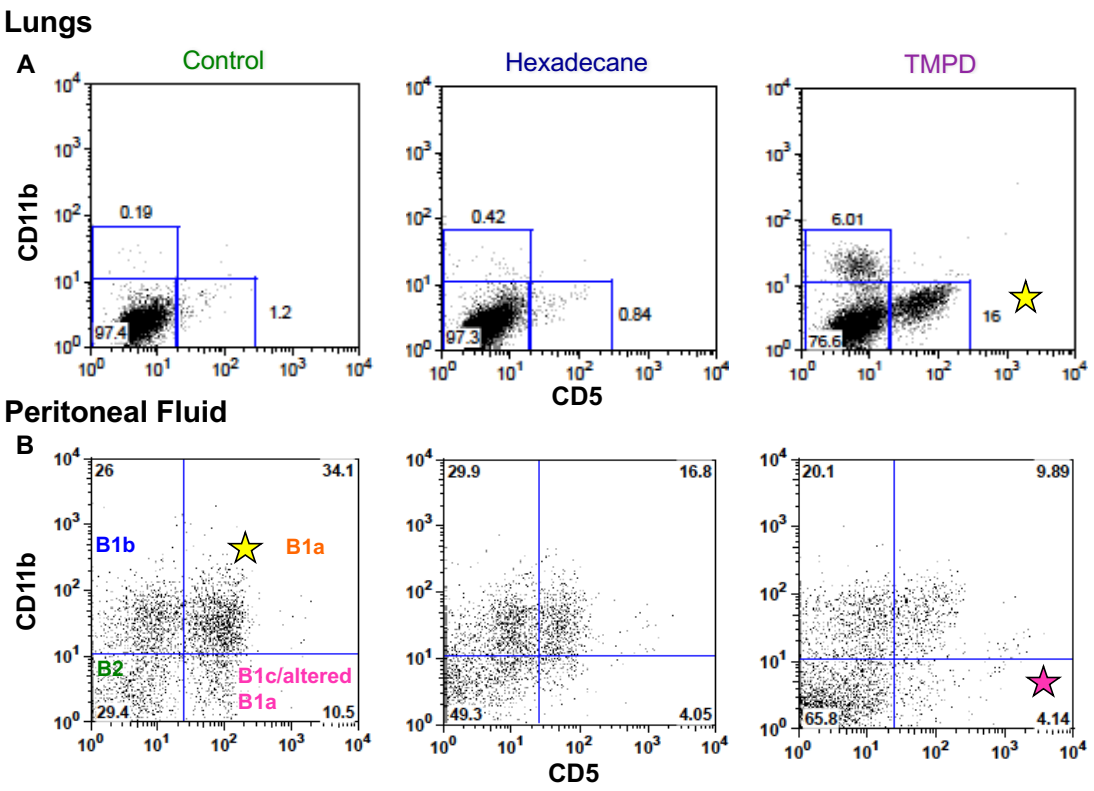

Fig 4.4 Flow cytometry analysis of B1 B cells in Lungs and Peritoneal Fluid at 1-week Timepoint. WT B6 mice (males) were injected with TMPD, Hex or PBS (0.5 ml, ip), and euthanized at 1-week time point. Cells were gated on $CD19^+$ live lymphocytes. **(A)** Lungs: increased proportions of B1b ($CD19^+CD11b^+CD5^-$), and B1c B cells in TMPD-exposed mice vs. controls **(B)** Peritoneal Fluid: decreased proportions of B1a ($CD19^+CD11b^+CD5^+$), B1b, and B1c B cells in TMPD-exposed mice vs. controls. Data representative of all 4 independent experiments. TMPD (n=12), hexadecane (n=10), controls (PBS/sham-injected, n=8). Numbers on a representative dot plot indicate percentage of cells. 1 $X10^6$ cells were stained.

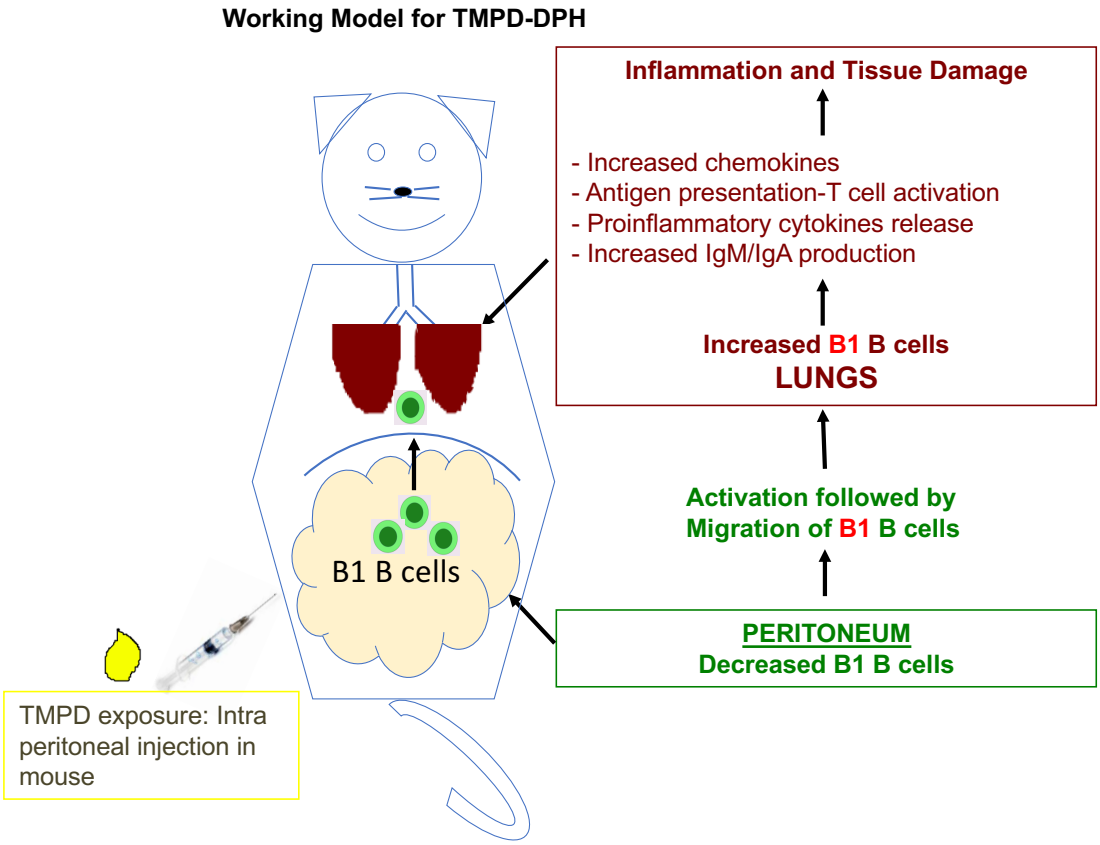

We hypothesize that *innate B1 B cells contribute to the pathogenesis of DPH*

Fig 4.5 Working model for TMPD-DPH. Based on our B cell findings, we hypothesized that a single dose TMPD ip injection leads to an activation of B1 B cells in the peritoneal/pleural cavities, resulting in their reduced expression of integrins and an increased expression of chemokine/chemokine receptors which leads to an increased trafficking of B1 B cells to the lungs, where they secrete IgM/IgA antibodies, cytokines and chemokines and serve as efficient antigen presenting cells to activate T cells, which may result in local inflammation and DPH.

CHAPTER 5

Role of B1 B cells in the Pathogenesis of Hydrocarbon Oil Induced Lung Inflammation and Diffuse Pulmonary Hemorrhage

ABSTRACT

The complete deficiency of B cells in Igμ$^{-/-}$ mice reduced the prevalence of DPH. However, there are different subsets of B cells, which have different functions. We found that prior to any histopathological changes, TMPD-injected animals had infiltration of lungs with B cells that expressed the markers of B1 B cell subset (CD19^{+}CD11b^{+}/CD19^{+}CD5^{+}). To elucidate role of B1 B cells in DPH development, we used CD19$^{-/-}$ mice that have significantly reduced B1a B cells in the peritoneal cavity compared to wild-type (WT) B6 mice. TMPD (500 μl, ip) was administered to CD19$^{-/-}$ B6 mice (n=18) and WT B6 mice (n=17). Results show that CD19$^{-/-}$ mice developed significantly less DPH, with reduced lung hemorrhage scores ($P<0.05$) and reduced DPH severity as measured by the percentage of eosin-stained area ($P<0.01$), than WT B6 mice. Immunofluorescence staining showed less leukocytes (CD45^{+}) and less B cells (CD45^{+}IgM^{+}) in the lungs of TMPD-injected CD19$^{-/-}$ vs. WT B6 mice. In a previous chapter, we showed the induction of pneumonitis and DPH upon oropharyngeal administration of 4μl of TMPD and rapid morbidity and mortality at higher doses of oropharyngeal aspiration of TMPD. To investigate whether B cells play a role in disease when the lungs are directly exposed to TMPD, we administered different doses of TMPD via oropharyngeal aspiration in CD19$^{-/-}$ and Igμ$^{-/-}$ and WT B6 mice. There was no significant difference in the development of TMPD-induced lung inflammation and hemorrhage in WT vs. CD19$^{-/-}$ vs. Igμ$^{-/-}$ B6 mice. Thus, B1 B cells play a critical role in the development of pneumonitis and DPH when animals are exposed to TMPD via a systemic (ip) route, but not upon the direct exposure of lungs to TMPD via oropharyngeal aspiration.

INTRODUCTION

A previous study suggested the role of B cells in the pathogenesis of TMPD-induced DPH. Ig$\mu^{-/-}$ MT B6 mice that do not have any B cells had a strikingly reduced prevalence of DPH (7% vs 84% in WT B6); reconstitution of Ig$\mu^{-/-}$ B6 mice with wild-type splenic B cells increased the DPH prevalence to 50%, thereby suggesting a possible role of B cells in development of DPH [4]. However, no immune complexes or complement deposition was detected in the DPH lungs. Furthermore, the transfer of serum from DPH mice to naive mice did not induce DPH, although the sample size was too small in this experiment [4]. In a more recent study, the susceptibility to DPH was restored in Ig$\mu^{-/-}$ MT mice by infusing IgM. C3$^{-/-}$ and CD18$^{-/-}$ mice were also resistant to DPH [35]. These observations suggest a role of B cells and IgM as well as Mac-1 (CD18) in the pathogenesis of DPH. T cells are not required for the development of TMPD-induced DPH [4]. Among different B cell subsets, marginal zone B cells and B1 B cells rapidly produce large amounts of IgM during early T-independent phase of immune responses [32]. B1 B cells also express CD18. Furthermore, our studies in the previous chapter showed that at day 7 timepoint, prior to any histopathological changes, TMPD caused increased infiltration of CD19^{+} B cells and subset B1 B cells (CD19^{+}CD11b^{+}/CD19^{+}CD5^{+}) in lungs. B1 B cells were simultaneously reduced significantly in their usual location, peritoneal cavity in TMPD-exposed mice. Taken together, these observations led us to hypothesize that B1 B cells are involved in the pathogenesis of TMPD-DPH.

CD19-deficient mice were generated to examine the role of CD19 in B cell regulation in vivo. Deletion of CD19 had no deleterious effects on the generation of B cells in the bone marrow, but there was a significant reduction in the number of B cells in

peripheral lymphoid tissues. To selectively modify genes in B lymphocytes, Rickert et al. generated mice (designated $CD19^{-/-}$ (Cre); B6 background) which express cre under the transcriptional control of the B lineage-restricted CD19 gene. In a model system involving the cross of $CD19^{-/-}$ (Cre) mice with mice bearing a loxP-flanked substrate, they found a deletion efficiency of 75–80% in bone marrow-derived pre-B cells and 90–95% in splenic B cells [41]. We have used these $CD19^{-/-}$ (Cre) mice to study the pathogenesis of TMPD-DPH for the following reason.

The B-1 subpopulation of B lymphocytes is particularly sensitive to CD19 regulation, since their development is severely decreased in $CD19^{-/-}$ mice. Specifically, development of $CD5^{+}$ B cells was severely decreased in $CD19^{-/-}$ mice [42]. The frequencies of peritoneal B-1a and B-1b cells were clearly different between $CD19^{-/-}$ B6, WT B6, and hCD19Tg mice when CD5 expression was used to differentiate peritoneal B1a ($CD5^{+}CD11b^{+}$) and B1b ($CD5^{-}CD11b^{+}$) cells. Although the peritoneal $CD11b^{+}$ B cell population exhibited an IgM^{hi} phenotype in all mice, the vast majority of $CD11b^{+}B220^{+}$ cells were $CD5^{-}$ in $CD19^{-/-}$ mice [43].

The $CD19^{-/-}$ B6 mouse model has been utilized to study atopic dermatitis, skin and lung fibrosis [44, 45]. Suppressed allergic skin inflammation in $CD19^{-/-}$ mice is likely due to the decreased B-cell numbers and/or impaired proliferation capacity of B cells [44]. CD19 deficiency also inhibited the development of skin and lung fibrosis and autoantibody production in a bleomycin-induced scleroderma model [45].

Here, we compared the development of TMPD-DPH and B cell infiltration and IgM deposition in the lungs between $CD19^{-/-}$ mice and WT B6 mice after a systemic (ip) as well direct (oropharyngeal aspiration) exposure to TMPD.

METHODS

Mice

Wild-type C57BL/6J (WT B6; Black 6; Stock No: 000664), and CD19$^{-/-}$ (CD19 cre; B6.129P2(C)-*Cd19*$^{tm1(cre)Cgn}$/J; Stock No: 006785) B6 mice (only breeder pairs), and Igμ$^{-/-}$ (muMt^{-}; B6.129S2-*Ighm*^{tm1Cgn}/J; Stock No: 002288) B6 mice were purchased from the Jackson Laboratory and housed in the UCLA Warren Hall (WAH) Barrier Facility. The CD19$^{-/-}$ B6 mouse colony was expanded at UCLA WAH, and blood phenotyping via flow cytometry was performed to confirm genotype of mice.

The UCLA Institutional Animal Care and Use Committee, known as the Chancellor's Animal Research Committee (ARC), approved the protocol for this study.

Dose Administration and Bodyweight Assessment

TMPD-DPH Model in CD19$^{-/-}$ B6 vs. WT B6 Experiments:

To establish whether TMPD-DPH occurs in CD19$^{-/-}$ B6 mice, we administered TMPD (500 µl, ip) under isoflurane anesthesia to CD19$^{-/-}$ B6 (n=18), and WT B6 (n=17) mice. The day of TMPD administration was Day 0 for each experiment and their bodyweight was monitored at different timepoints for up to 2-weeks post exposure. Controls were unmanipulated CD19$^{-/-}$ B6 (n=4) and WT B6 (n=4). Both males and females, 3-4 months old mice were used in the experiments.

To investigate the early cellular changes that occur in CD19$^{-/-}$ B6, and WT B6 mice (n=5/group, males, 3 months old) were used. We administered TMPD (500 µl, ip) to the mice under isoflurane anesthesia, and their bodyweight was monitored up to Day 7 post exposure.

Oropharyngeal Aspiration of TMPD in Mice

Each animal was lightly anesthetized with Ketamine/Xylazine solution (ip, 100 μl). OA was performed as described in previous studies [53, 54]. Mice were fixed on a surgery board, the tongue was pulled out with a forceps, and the liquid (TMPD/Hex/PBS) was placed onto the distal part of the oropharynx using a micropipette, while the nose was gently closed.

WT and $CD19^{-/-}$ B6 mice were given OA of 40 μl PBS, and different doses (40 μl, 20 μl, 8 μl, and 4 μl) of TMPD. Males and females, 2-5 months old mice were used in the experiments.

Only the low dose of 4 μl TMPD was tested in $Ig\mu^{-/-}$ B6 mice (n=4; males; 2 months old).

For OA with low dose of 4 μl TMPD, each animal was given OA of 6 μl sterile DPBS (1X) immediately after to assure that the oil is flushed down, and not stuck at the oropharyngeal opening.

Reagents

2,6,10,14-Tetramethylpentadecane BioReagent (TMPD, Molecular Weight 268.52, CAS Number 1921-70-6), synthetic, liquid, sterile-filtered, purity ≥95% (Sigma-Aldrich Corp., St. Louis, MO; Lot Nos. RNBB3307V and RNBF1748). Ketamine Hydrochloride injection USP (Ketalar®; Par Pharmaceuticals Cos., Inc., NY), Xylazine injection (AnaSed®; Lloyd, Inc., IA), or Isoflurane USP (Piramal Healthcare Limited, Bethlehem, PA) was used to anesthetize/euthanize the mice. Dulbecco's Phosphate Buffered Saline [DPBS (1X) Gibco™; Thermo Fisher Scientific Inc., Waltham, MA] was used to perfuse the lungs, and to clean the small and large intestines. Ethyl alcohol (Decon Laboratories, King of Prussia, PA) was used to clean the mouse prior to necropsy and preserve tissues for histology. Formalin 10% (Fischer Scientific Company LLC, Kalamazoo, MI) was used to fix the

tissues for histology. The lungs were digested with Collagenase, Type 1 (Worthington Biochemical Corporation, Lakewood, NJ) and Deoxyribonuclease I from bovine pancreas (DNase; Sigma-Aldrich Corp., St. Louis, MO**),** and the enzymatic digestion process was stopped with UltraPure™ EDTA (Invitrogen™, Thermo Fisher Scientific Inc., Waltham, MA**)**. Red blood cells (RBCs) in spleen were removed with lysis buffer BD Pharm Lyse™ (BD Biosciences, San Jose, CA). For flow cytometry, the tissues were collected and cells washed with RPMI 1640 Medium (Gibco™; Thermo Fisher Scientific Inc., Waltham, MA). FACS buffer for immunostaining was made with PBS 10X (Fischer Scientific Company LLC, Fair Lawn, NJ) and Bovine serum albumin (BSA; Fischer Scientific Company LLC, Fair Lawn, NJ). Trypan blue (MP Biomedicals LLC, Solon, OH) was used to count viable cells for immunostaining. Tissue freezing medium (Triangle Biomedical Sciences, Durham, NC) was used to freeze lung tissue.

Necropsy

On the day of necropsy, each mouse was placed in a chamber that contained isoflurane for 3-5 minutes until it was euthanized. After the mouse ceased to breathe, it was taken out of the chamber and placed on a dissection mat. The mouse's body was cleaned with alcohol and its outer skin was cut. The peritoneum was infused with 10 ml of cold DPBS 1X, lavage was performed for peritoneal fluid (PF) collection. Cardiac blood was collected for serum analysis. The lungs were perfused via the heart, with DPBS 1X to remove the blood from them after the aorta was cut.

For TMPD 2-weeks timepoint, WT B6 vs. $CD19^{-/-}$ B6 experiments: The lungs (except lower right lobe), liver (left lateral and right medial lobes), spleen (lower part small piece), kidney (right), 2 sections each of small intestine, and large intestine were fixed in

10% formalin for at least 24 hours. The small and large intestine sections were cleaned with DPBS 1X solution before they were preserved for histology. The lower right lobe of the lungs were fixed with tissue freezing medium, flash frozen with liquid nitrogen and then stored at -80° C. Cells from PF and spleen were analyzed by flow cytometry.

For TMPD Day 7 timepoint, WT B6 vs. $CD19^{-/-}$ B6 experiments: The whole lungs were incubated at 37°C in RPMI medium with Collagenase and DNase for one hour, and digestion was stopped by adding EDTA. Cells from PF and lungs were analyzed by flow cytometry.

For animals given OA of TMPD at doses of 40 μl or 20 μl, each animal was euthanized with Ketamine/Xylazine solution (ip, 200 μl). Since majority of the animals given OA of 40 μl TMPD, died immediately after treatment no tissues were collected. For all the other OA experiments the cardiac blood, whole lungs and trachea was collected.

Immunofluorescence (IF) Staining

Paraffin embedded sections of lungs were used for IF staining with mAbs specific for lymphocytes. UCLA Translational Pathology Core Laboratory (TPCL) performed the IF staining for the slides. For TMPD 2-weeks timepoint, WT B6 vs. $CD19^{-/-}$ B6 experiments: Purified anti-mouse CD45 (Clone 30-F11 (RUO); BD Biosciences, San Jose, CA) at a dilution 1:200 was used. To identify lymphocytes specifically producing IgM, we used Alexa Fluor 488 anti-mouse IgM (Cat. A21042; Life Technologies Corp., Carlsbad, CA) at a dilution 1:200. Deparaffinized and hydrationed sections were treated with blocking reagent (PerkinElmer antibody diluent buffer) for 10 minutes at room temperature. Sections were then incubated with primary antibody working solution (conditions specific to antibody). Sections were then incubated (30 minutes) with a

secondary anti-mouse antibody followed by a horseradish peroxidase conjugated complex. For signal amplification, each slide was incubated at room temperature for 10 minutes with opal Fluorophore Working Solution (1:50 dilution). Applied DAPI (ProLong® Gold Antifade Mountant with DAPI; Invitrogen, Carlsbad, CA) at a dilution of 1:2000 for 5 minutes in a humidity chamber, and then placed coverslip.

Histopathological Assessment

UCLA TPCL embedded the tissues in paraffin. Sections were stained with hematoxylin and eosin (H&E) for all the experiments. Lungs were scored for hemorrhage (hem), and the grading criteria was: grade 0, normal; grade 1, minimal hem; grade 2, mild hem; grade 3, moderate hem; grade 4. Lungs were scored for inflammation (inf), and the grading criteria was: grade 0, normal; grade 1, minimal inf; grade 2, mild inf; grade 3, moderate inf; grade 4. severe inf. All the slides were examined independently by a pathologist in a blinded manner for hemorrhage and inflammation.

H&E slides were digitized on a ScanScope AT (Leica Biosystems, Inc., Vista, CA), all the slides were scanned at 40X objective magnification. Morphometric analysis was performed with *Definiens'* Tissue Studio (Definiens Inc., Parsippany, NJ) to determine the area of eosin staining in a non-biased method. Briefly, a stain specific algorithm was created using the pre-defined marker area detection module and classification tool. Thresholds were set to classify eosin stain for the entire tissue area. The data were exported to Microsoft Excel for further statistical analysis.

Fluorescent images were acquired and analyzed using the Leica Versa (Applied Imaging Corp., San Jose, CA). The Versa scanner is based on a Leica DM600 B microscope with motorized stage and autofocus capabilities. Slides were scanned at 20X

or 40X objective magnification with the DAPI, FITC and TRITC filters. Optimal exposure times were determined before automated scanning. After scanning, images were exported for subsequent analysis.

Using the Definiens Tissue Studio™ product, stain specific algorithms were created, utilizing Definiens eCognitionNetwork Language™ for the pre-defined cellular detection modules and classification tools, to identify positive stained cells and cells with colocalized staining within each tissue region. Thresholds were set to classify the following: blue channel for DAPI, green channel for IgM and red channel for CD45. The data were exported to Microsoft Excel for further statistical analysis.

Scanning and analyses were performed through TPCL, Department of Pathology and Laboratory Medicine, David Geffen School of Medicine at UCLA.

Flow Cytometric Analysis

Cells from lungs, peritoneal fluid, and spleen were washed with RPMI medium. Red blood cells (RBCs) in spleen were removed with lysis buffer, then kept in FACS buffer. After blockade of Fc receptors with purified anti-mouse CD16/CD32 mAb (clone 2.4G2; Tonbo Biosciences, San Diego, CA), cells were stained with the corresponding Ab mixtures. The following mAbs were used: APC-labeled anti-mouse CD19 (clone 1D3; Tonbo Biosciences, San Diego, CA), FITC-labeled anti-mouse CD19 (clone 1D3; Tonbo Biosciences, San Diego, CA), PerCP-Cyanine5.5-labeled anti- mouse CD19 (clone 1D3; Tonbo Biosciences, San Diego, CA), PE-labeled anti-mouse CD19 (clone 1D3; Tonbo Biosciences, San Diego, CA), APC-labeled anti-mouse CD45.1 (clone A20; BioLegend Inc., San Diego, CA), Alexa Fluor 700-labeled anti-mouse B220 (clone RA3-682; BioLegend Inc., San Diego, CA), PerCP Cy5.5-labeled anti-mouse B220 (clone RA3-682;

BD Biosciences, San Jose, CA), FITC-labeled anti-mouse IgM (clone RMM-1; BioLegend Inc., San Diego, CA), eFluor NC-650-labeled anti-mouse IgM (clone 11/41; eBiosciences, San Diego, CA), PE-labeled anti-mouse CD5 (clone 53-7.3, eBiosciences, San Diego, CA), PerCP-Cyanine5.5-labeled anti-human/mouse CD11b (clone M1/70; Tonbo Biosciences, San Diego, CA), APC-labeled anti-mouse CD11b (clone M1/70; Tonbo Biosciences, San Diego, CA), V500-labeled CD11b (clone M1/70; BD Biosciences, San Jose, CA), and PE-labeled anti-mouse TCRß (clone H57-597, Tonbo Biosciences, San Diego, CA).

For the WT B6 vs. $CD19^{-/-}$ experiments (TMPD 1-week and 2-weeks), the cells were acquired using the LSR Fortessa BV605 FACS, at the UCLA Immune Assessment Core (IAC). All the data were analyzed using the FlowJo software Version 8.7 (Ashland, OR).

Data Analysis

The lung hemorrhage and inflammation scores for histopathology were statistically analyzed by Chi-square test. For the bodyweight changes, quantitative assessment of eosin staining in lungs, and total cells counts in the lungs, peritoneal fluid, the differences between groups were statistically analyzed by unpaired Student's t-test with Welch's correction method with $P < 0.05$ considered to be significant. Data are presented as mean±SEM. Data was analyzed utilizing Microsoft Excel and Prism 6.0 (GraphPad Software, San Diego, CA).

RESULTS

CD19-deficiency ameliorates TMPD-induced DPH.

To determine the effect of B1 B cells on TMPD-induced DPH, we injected CD19$^{-/-}$ mice and WT B6 mice with TMPD. Animals were monitored for weight loss and euthanized on or before day 14 for lung histopathology studies. As compared to 70% of wild-type animals, only 11% of CD19$^{-/-}$ mice lost 20% bodyweight within 14 days post-TMPD (Figure 5.1A). All animals with 20% weight loss, but none of the remaining animals, had lung hemorrhage.

To assess TMPD-induced lung pathology, we established a semi-quantitative system to score lung hemorrhage (Figure 5.1B) and inflammation on a scale of 0-4. We further established a morphometric analysis that was performed using *Definiens'* Tissue Studio (Definiens Inc.) on digitized slides to measure the area of eosin staining in a non-biased method, which served as a quantitative estimate of lung hemorrhage.

The prevalence of lung hemorrhage was significantly lower (55%) in CD19$^{-/-}$ mice than WT B6 mice (76%) (Figure 5.1C). The prevalence of severe DPH was rare (6%) in CD19$^{-/-}$ mice compared to wild-type mice (53%). The lung hemorrhage scores were significantly lower in CD19$^{-/-}$ than WT B6 mice (Figure 5.1D). However, the lung inflammation scores were not significantly different between CD19$^{-/-}$ and wild-type mice, although there was a trend towards less inflammation in CD19$^{-/-}$ mice **(**Figure 5.1F). Finally, the quantitative estimate of lung hemorrhage, as measured by the percentage of lung area eosin stain, showed a highly significant decrease in CD19$^{-/-}$ mice compared to WT B6 mice **(**Figure 5.1E). These results clearly demonstrate a protective effect of CD19-deficiency on TMPD-induced DPH.

The histopathologic evaluation of liver, spleen, kidney, small intestine, and large intestine showed no changes in both wild-type and CD19$^{-/-}$ TMPD-injected mice (not

shown). Animals in both groups had a focal chronic inflammation/fibrosis and granulation in the outer fat of intestines/liver/spleen.

CD19-deficient mice have reduced TMPD-induced infiltration with leukocytes and B cells and IgM deposition in the lungs.

To determine the effect of CD19 deficiency on lung infiltration with total leukocytes and B cells as well as for local IgM deposition, we conducted immunofluorescence staining of the lungs. Few B cells were detected in the lungs of unmanipulated WT mice and even fewer in $CD19^{-/-}$ mice. At 2-weeks post-TMPD, total leukocyte infiltration and IgM^+ B cells as well as IgM deposition in the lungs were increased as compared to unmanipulated controls in both WT and $CD19^{-/-}$ B6 mice, however, all three parameters were lower in $CD19^{-/-}$ than in WT B6 mice (Figure 5.2A-D).

Consistent with the above immunostaining data showing less leukocytes ($CD45^+$) and B cells ($CD45^+IgM^+$) in $CD19^{-/-}$ mice than in WT mice, flow cytometry analysis in lungs prior to any histopathological change (1 week post-TMPD) revealed less total cell count, and lower proportions of B cells ($B220^+IgM^+$) and B1 B cells ($B220^+IgM^+$ $CD5^+CD11b^+/CD5^-CD11b^+/CD5^+CD11b^-$) in $CD19^{-/-}$ mice than in WT mice (Fig. 5.2 E, F).

Peritoneal B1a B cells at 2-weeks post-TMPD are reduced from the baseline in WT mice, but not in CD19-deficient mice.

Analysis of peritoneal fluid cells showed that the total cellularity was significantly increased 2-weeks post-TMPD in both WT and $CD19^{-/-}$ mice as compared to their unmanipulated controls, but there was no significant difference in cell counts between WT and $CD19^{-/-}$ mice both at baseline and 2-weeks after TMPD injection (Figure 5.3). As

previously reported, all B cells and B1a B cells were lower in $CD19^{-/-}$ mice than in WT mice at the baseline. Furthermore, peritoneal B cells expressed higher levels of IgM and CD5 in $CD19^{-/-}$ mice than in WT mice. Post-TMPD, B cells were reduced by ~3.5-fold in WT and ~2.3-fold in $CD19^{-/-}$ mice as compared to their unmanipulated controls. However, IgM^{hi} B cells were dramatically reduced after TMPD injection in WT mice but not so much in $CD19^{-/-}$ mice. $CD19^{-/-}$ mice also had a higher proportion of B1a cells post-TMPD than at baseline, whereas the proportion of B1a cells among all B cells remained similar between baseline and 2-weeks post-TMPD in WT mice.

CD19-deficiency does not protect from disease when TMPD is administered via oropharyngeal aspiration.

We investigated the effect of oropharyngeal aspiration (OA) of TMPD at different doses in WT and $CD19^{-/-}$ B6 mice. At all doses tested except TMPD 4 μl, the animals became moribund and started dying within 18 to 36-hours post exposure. WT (n=4-8/group) and $CD19^{-/-}$ (n=3-8/group) B6 mice, were administered TMPD at different doses [40 μl, 20 μl, 8 μl, 6 μl (only WT mice), and 4 μl] via OA route. Controls were administered OA of 40 μl PBS (n=3/group). Both males and females, 2-5 months old mice were used, and six independent experiments were performed. For the OA of 40 μl TMPD experiment, WT and $CD19^{-/-}$ B6 mice were used (females; 5 months old) were used. WT mice (4/5) died immediately after exposure. One WT mouse and all $CD19^{-/-}$ mice (n=3) were moribund post-OA of 40 μl TMPD, and euthanized within 18 hours-post exposure. Controls (PBS; n=3/groups) were normal, no loss of bodyweight, and necropsy was performed on them at 4-weeks post-TMPD exposure. There was high mortality and animals were moribund within 24-48 hours post-OA with TMPD at doses of 20 μl, 8 μl, and 6 μl. At all doses of

TMPD the WT B6 mice developed lung inflammation, however lung hemorrhage only occurred in mice that were found dead post-OA. A similar response was observed in the $CD19^{-/-}$ B6 mice at all doses of TMPD (Figure 5.4).

WT and $CD19^{-/-}$ B6 mice (n=4/group; females; 5 months old) were administered OA of TMPD 20 µl. Lung sections were stained with H&E, and scored for lung hemorrhage and inflammation. All sections were scored by a pathologist in a blinded manner. Only one TMPD-exposed WT B6 mouse that died within 18 hours-post exposure had moderate lung hemorrhage and inflammation. All the other mice were moribund, 10-15% bodyweight loss, and were euthanized on Day 1. Majority of the mice showed minimal to mild inflammation, however there was no hemorrhage in the lungs in TMPD-exposed WT and $CD19^{-/-}$ B6 mice (Figure 5.4).

WT and $CD19^{-/-}$ B6 mice (n=4/group; males; 3 months old) were administered OA of TMPD 8 µl. Only one TMPD-exposed $CD19^{-/-}$ B6 mouse that died within 36 hours-post exposure had minimal lung hemorrhage. All the other mice were moribund, 10-15% bodyweight loss, and were euthanized on Day 2. None of the animals had hemorrhage, and only one animal showed minimal inflammation in the lungs. There was hyaline membrane formation in mice (1/group) that died within 36 hours-post exposure with TMPD, indicative of acute lung injury (Figure 5.4).

The effects of OA of 4 µl TMPD in WT vs. $CD19^{-/-}$ vs. $Ig\mu^{-/-}$ B6 mice on lungs were investigated. Two independent experiments were performed. In the first experiment conducted with OA of TMPD 4 µl in WT vs. $CD19^{-/-}$ B6 mice (n=4/group, females, 3 months), there was 15-20% loss of bodyweight in 50% animals within 3-days post

exposure, however the mice gained weight after Day 4 and were normal thereafter (data not shown). Necropsy was performed on Day 17, since we wanted to observe the short-term effects of OA of TMPD. In the second experiment performed, effects of OA of 4 µl TMPD in WT vs. CD19$^{-/-}$ vs. Igµ$^{-/-}$ B6 mice (n=4/group, males, 2 months old) were studied. In the WT and CD19$^{-/-}$ groups, the mice started dying by Day 3. In addition, by Day 4 the mice were moribund and 20% loss of bodyweight in mice (2/group) in the TMPD-exposed WT, CD19$^{-/-}$, Igµ$^{-/-}$ groups. Moribund mice were euthanized on Day 4, normal mice were euthanized on Day 17. TMPD-exposed WT (3/8 mice) and CD19$^{-/-}$ (2/8 mice) had minimal/mild hemorrhage. Majority of the mice showed minimal-severe inflammation in all groups (Figures 5.4 and 5.5).

DISCUSSION

Previous studies have shown that Igµ$^{-/-}$ MT B6 mice (do not have any B cells) had a strikingly reduced prevalence of DPH (7% vs 84% in WT B6) [4, 26]. However, the specific B cell subsets that may be involved in DPH pathogenesis have not been identified. Here, we have established that CD19$^{-/-}$ mice develop significantly less lung hemorrhage than WT B6 mice. The B-1 subpopulation of B lymphocytes is particularly sensitive to CD19 regulation, since their development is severely decreased in CD19$^{-/-}$ mice. Specifically, development of CD5^{+} B cells was severely decreased in CD19$^{-/-}$ mice [42]. The frequencies of peritoneal B-1a and B-1b cells were clearly different between CD19$^{-/-}$ and WT B6 mice when CD5 expression was used to differentiate peritoneal B1a (CD5^{+}CD11b^{+}) and B1b (CD5^{-}CD11b^{+}) cells [43]. We observed similar differences in the peritoneal B1a B cell population in CD19$^{-/-}$ and WT B6 mice.

The $CD19^{-/-}$ mouse model has been utilized to study atopic dermatitis, skin and lung fibrosis [44], [45]. Suppressed allergic skin inflammation in $CD19^{-/-}$ mice was likely due to the decreased B-cell numbers and/or impaired proliferation capacity of B cells, and reduced peritoneal B1a cells may decrease IL-17 secretion [44].

CD19 deficiency inhibited the development of skin and lung fibrosis, and autoantibody production by inhibiting TLR4 signals in a Bleomycin-induced scleroderma model. B-cell activation contributes to downstream inflammatory infiltration of other immune cells. CD19 deficiency inhibited the production of Th1, Th2 cytokines and TGF-β1 (except TNF-α), suppressed mast cell and macrophage infiltration [45].

The serum levels of all immunoglobulin isotypes examined were significantly reduced in $CD19^{-/-}$ mice when compared with WT B6 mice. On average, IgM levels were significantly reduced by 75%, IgG1 by 66%, IgG2a by 64%, IgG2b by 72%, IgG3 by 57%, and IgA by 46%. Thus, the combination of decreased B cell numbers along with the decreased proliferative responses of $CD19^{-/-}$ mice have a considerable impact on the immune status of these mice [40]. Our flow cytometry analysis also showed significantly less proportions of $B220^{+}IgM^{+}$ cells in the peritoneal fluid (PF) of unmanipulated $CD19^{-/-}$ vs WT B6 mice. Interestingly, after TMPD-injection at both 1- and 2-weeks timepoint the populations of B1a ($B220^{+}IgM^{+}CD5^{+}CD11b^{+}$) cells are reduced in the WT and $CD19^{-/-}$ mice vs. controls. At the 1-week timepoint the total cell counts and proportions of B1a cells are higher in WT vs. $CD19^{-/-}$ mice. This supported our hypothesis that peritoneal B1 B cells migrate to the lungs and play a role in DPH pathogenesis.

Intriguingly, $CD19^{-/-}$ and $Ig\mu^{-/-}$ mice were not protected from the development of TMPD-induced lung disease when these animals were exposed to 4 μl TMPD via OA

route. This may be due to a direct cytotoxic effect of TMPD in the oral cavity, and/or rapid absorption via blood. With an ip injection the peritoneal cells (macrophages, B cells, T cells, and dendritic cells) are exposed to TMPD, and it takes time for TMPD to enter the lymphatic/blood circulation. Potentially, there may be differences in transmembrane transport of TMPD or permeability to this oil among dendritic cells, B cells, T cells, and monocytes, which may explain their differential susceptibilities to undergo apoptosis [48].

Our findings are relevant to humans since the major route of exposure to TMPD is via inhalation (diesel exhaust, oil mists, aspiration of ingested mineral oil). Since B cells do not seem to be involved when mice are exposed to TMPD via OA route, further studies are required to establish which specific cell types are involved in the pathogenesis of pneumonitis/DPH.

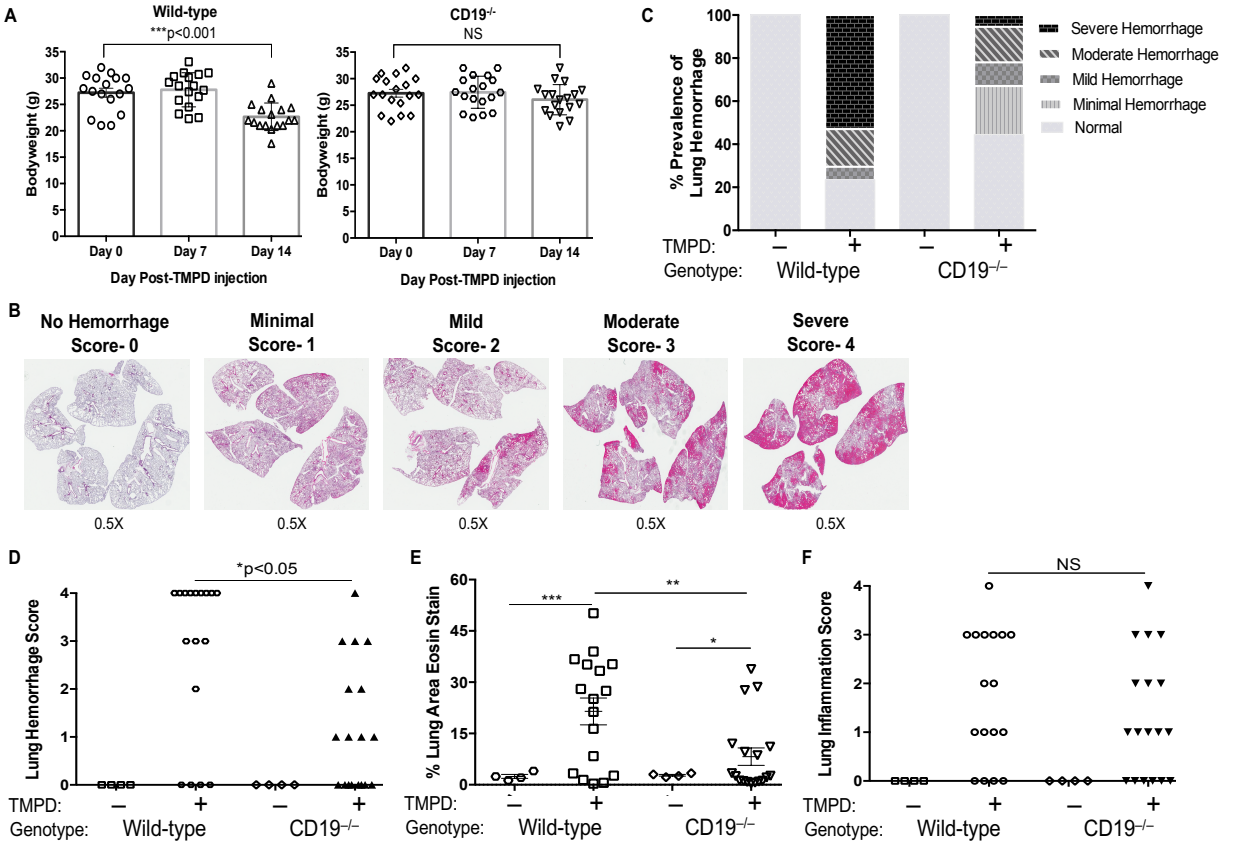

Fig 5.1 Effect of CD19-deficiency on TMPD-induced weight loss and lung inflammation and hemorrhage. Wild-type (WT; n=17) and CD19$^{-/-}$ (n=18) C57Bl/6 (B6) mice were administered TMPD (500 µl, ip). Unmanipulated WT and CD19$^{-/-}$ B6 mice (n=4/group) served as controls. Male and female mice at 3-4-months of age were used. Animals were monitored for general health and daily weight measurements. Animals were euthanized on day 14 or before if moribund or had 20% weight loss. Lung sections were stained with H&E, and scored by a pathologist in a blinded manner. **(A)** Bodyweights on days 0, 7 and 14 are shown in TMPD-injected WT and CD19$^{-/-}$ mice. Data are presented from individual animals and as the mean±SEM. **(B)** Lung histology was scored on a scale of 0-4 for lung hemorrhage. Whole lung sections were digitized on a ScanScope AT (Leica Biosystems, Inc) and viewed with Aperio ImageScope 12.3.0.5 software at a low

(0.5X) magnification. **(C)** Percent prevalence of lung hemorrhage are shown as stack bars. **(D, F)** Lung hemorrhage and inflammation scores (on a scale of 0-4) respectively, in individual WT vs. $CD19^{-/-}$ mice are shown as symbol plots. **(E)** Morphometric analysis was performed using *Definiens'* Tissue Studio (Definiens Inc.) on digitized slides to measure the area of eosin staining as a quantitative estimate of lung hemorrhage. Data are presented as the percent eosin-stained lung area from individual animals and as the mean±SEM. Results represent five independent experiments. *P<0.05, **P<0.01, ***P<0.001

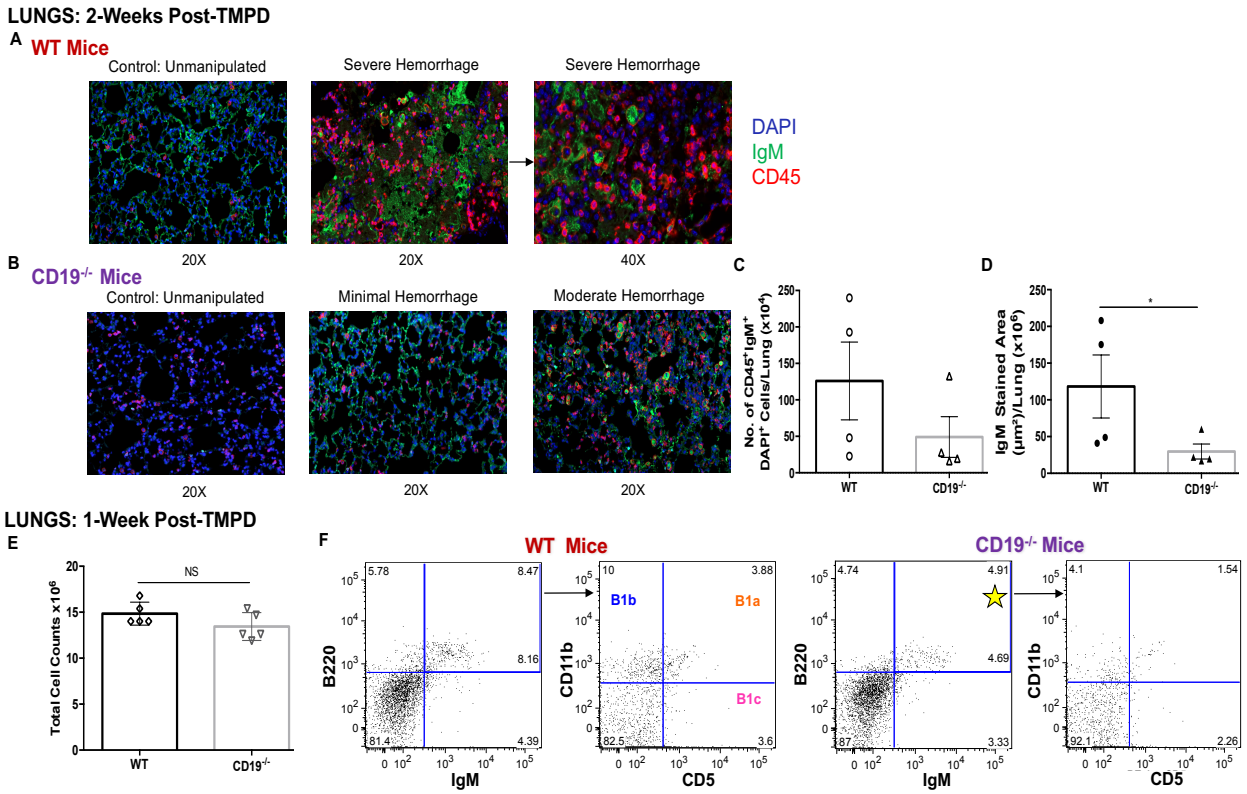

Fig 5.2 Effect of CD19-deficiency on TMPD-induced Infiltration with Leukocytes, B Cells, and IgM Deposition in the Lungs. (**A-D**) Four each of 3-month-old wild-type (WT) and CD19$^{-/-}$ B6 male mice were administered TMPD (500 μl, ip). Four each of age/sex-matched unmanipulated WT and CD19$^{-/-}$ B6 mice served as controls. Lungs were harvested at 2-weeks, and lung tissue sections immunostained to detect CD45, IgM, and DAPI. **(A, B)** Representative fluorescence microscopy images are shown from one each of unmanipulated WT and CD19$^{-/-}$ B6 lungs (left panels), one TMPD-DPH in WT and two TMPD-DPH in CD19$^{-/-}$ lungs at original magnification of 20X and a magnified (40X) area highlighting CD45^{+}IgM^{+} cells. Morphometric analyses were performed to enumerate leukocytes (CD45^{+}DAPI^{+}, red/blue) and B cells (CD45^{+}IgM^{+}DAPI^{+}, co-localized red/green/blue), and to measure IgM-staining (green) area that includes IgM deposition (green alone) and B cells. Note that in unmanipulated mice, while leukocyte numbers

were similar between WT and $CD19^{-/-}$ mice, B cells were fewer in $CD19^{-/-}$ mice than in WT mice (left panels). Leukocytes, B cells and IgM deposition were higher in TMPD-injected mice (middle and right panels) than in unmanipulated mice. **(C)** Higher number of co-localized $CD45^{+}IgM^{+}DAPI^{+}$ cells in lungs with hemorrhage in TMPD-injected WT vs. $CD19^{-/-}$ mice. **(D)** Total IgM^{+} area in lungs is significantly increased in TMPD-injected WT vs. $CD19^{-/-}$ B6 mice. * $P<0.05$.

(**E, F**) Five each of 3.5-month-old male wild-type (WT) and $CD19^{-/-}$ C57Bl/6 (B6) mice were administered TMPD (500 µl, ip). Animals were euthanized at 1-week timepoint, and lungs and peritoneal fluid harvested. Single cell suspension was analyzed on gated live lymphocytes for B cells ($B220^{+}IgM^{+}$), which were then analyzed for CD5 and CD11b. Numbers on representative dot plots indicate percentage of cells. **(E)** Total cell counts in lungs in $CD19^{-/-}$ vs. WT mice. Data are presented as individual values and as the mean±SEM. **(F)** Note the lower proportions of B cells ($B220^{+}IgM^{+}$) and of B1 B cells ($B220^{+}IgM^{+}$ $CD5^{+}CD11b^{+}$/$CD5^{-}CD11b^{+}$/$CD5^{+}CD11b^{-}$) in the lungs of $CD19^{-/-}$ mice than in WT mice.

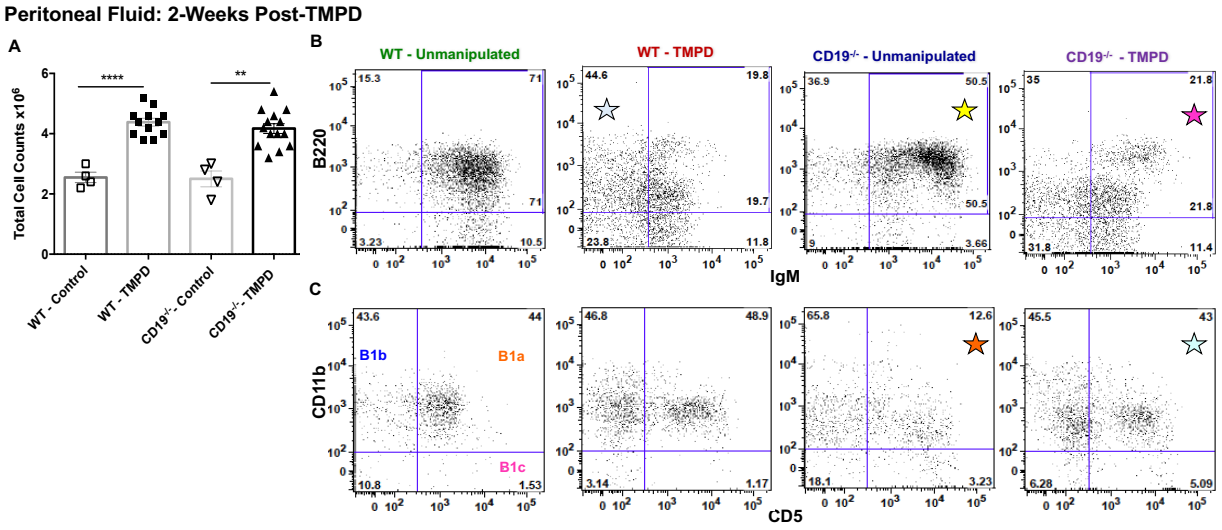

Fig 5.3 Effect of CD19-deficiency on Peritoneal Fluid B cells at 2-weeks post-TMPD.

Wild-type (WT; n=12) and CD19$^{-/-}$ (n=14) C57Bl/6 (B6) mice, 3-4 months old males, were administered TMPD (500 µl, ip). Unmanipulated WT and CD19$^{-/-}$ B6 mice (n=4/group) served as controls. Animals were euthanized at 2-weeks and peritoneal fluid cells collected, enumerated, and analyzed for B cells by flow cytometry. Numbers on representative dot plots indicate percentage of cells. **(A)** Total cell counts in peritoneal fluid. Data are presented as individual animal values and as the mean±SEM. **(B)** Peritoneal fluid cells were analyzed for B220^{+}IgM^{+} cells on gated live lymphocytes. Note a lower proportion of B cells (B220^{+}IgM^{+}) in unmanipulated CD19$^{-/-}$ mice than in unmanipulated WT mice, and a higher proportion of IgM^{high} cells in CD19$^{-/-}$ mice than in WT mice post-TMPD. **(C)** Gated B cells (B220^{+}IgM^{+}) were analyzed for B cell subsets: B1a (CD5^{+}CD11b^{+}), B1b (CD5^{-}CD11b^{+}) and B1c (CD5^{+}CD11b^{-}). Note a lower proportion of B1a B cells (B220^{+}IgM^{+}CD5^{+}CD11b^{+}) in CD19$^{-/-}$ mice than in WT unmanipulated mice. Post TMPD-injection, CD19$^{-/-}$ mice have a higher percentage of B1a cells than unmanipulated CD19$^{-/-}$ mice. Data shown are representative of 4 independent experiments. **P<0.01, ***P<0.001

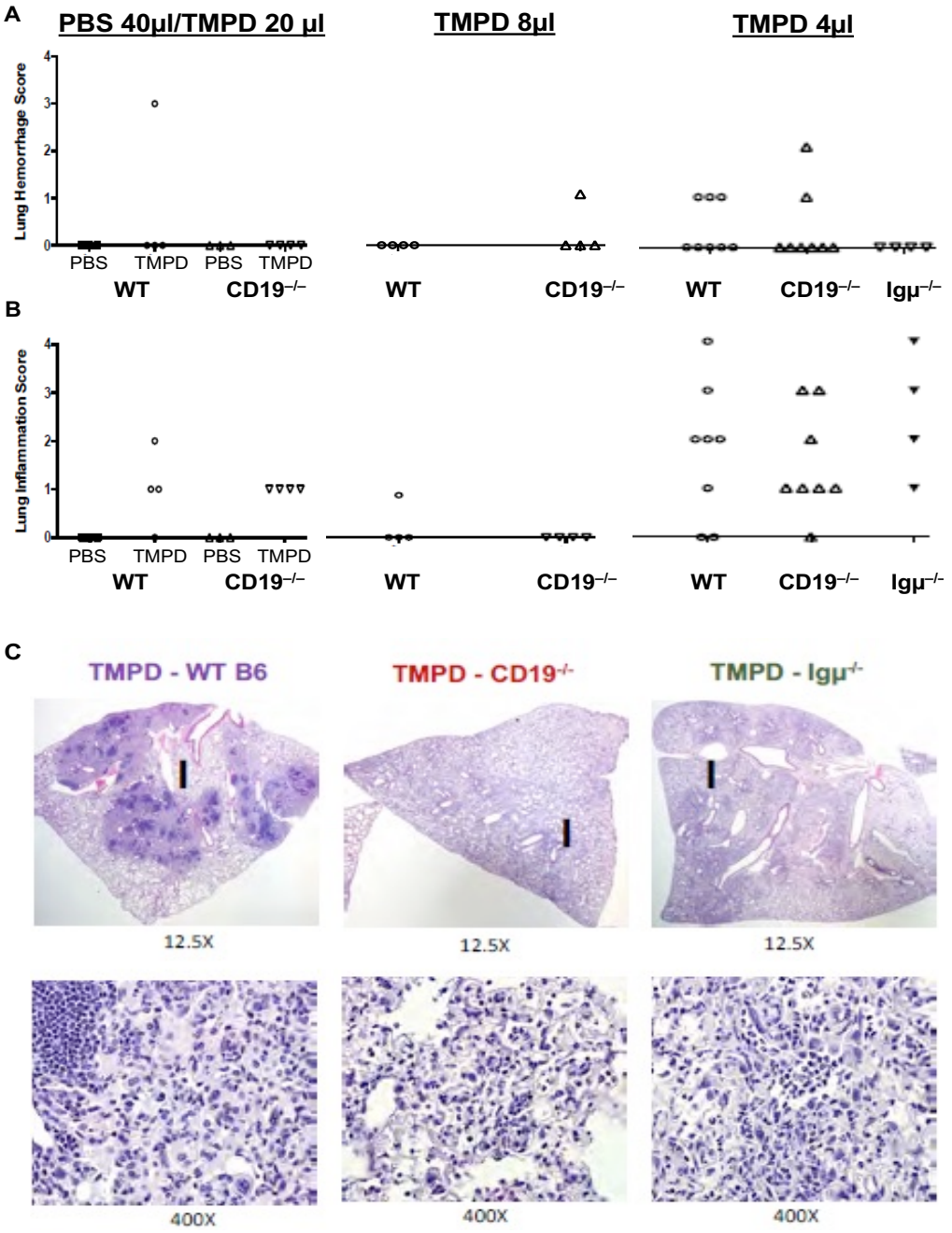

Fig 5.4 Effect of B cell Deficiency on Lung Inflammation and Hemorrhage upon Direct Exposure to TMPD via Oropharyngeal Aspiration. WT, CD19$^{-/-}$ or Igµ$^{-/-}$ B6 mice were administered TMPD or PBS at the doses indicated on the panels. Animals were euthanized at day 17 or sooner if moribund. Most animals at 20 µl and 8 µl dose were moribund within three days of oropharyngeal aspiration of TMPD. Lungs were harvested,

sections stained with H&E, and scored for hemorrhage and inflammation by a pathologist in a blinded manner, as indicated in Methods. **(A, B)** Similar scores were seen in WT, $CD19^{-/-}$ and $Ig\mu^{-/-}$ mice at all doses of TMPD. Each symbol represents individual mouse values. **(C)** Representative lung areas with inflammation (I) from 4 µl experiment at 12.5X and 400X magnification are shown. Five independent experiments using 2-5-month-old male and female mice were performed.

Effects of Hydrocarbon Oils (4 µl) via Oropharyngeal Aspiration in Different Strains of Mice				
Genotype	**WT B6**	**WT B6**	**CD19$^{-/-}$ B6**	**Igµ$^{-/-}$ B6**
Hydrocarbon Oil	**Hexadecane**	**TMPD**	**TMPD**	**TMPD**
Total number of mice (n)	**4**	**8**	**8**	**4**
Death/Euthanized due to loss of ≥20% bodyweight by Day 3-4	0	2	4	2
Lungs: Inflammation (score 1-4)	3	6	7	4
Lungs: Inflammation (score 3-4) and or any Hemorrhage	0	4	3	2

Fig 5.5 Effects of Hydrocarbon Oils (4 µl) via Oropharyngeal Aspiration in Different Strains of Mice. Mice (n=4-8/group; females and males; 2-3 months old) were administered OA with 4µl of hexadecane or TMPD. Moribund mice were euthanized on day 4 and healthy looking mice were euthanized on day 17. Lung sections were stained with H&E, and scored for lung hemorrhage and inflammation. All sections were scored by a pathologist in a blinded manner.

CHAPTER 6

Role of Trafficking of Peritoneal B1 B Cells to Lungs in TMPD Induced Lung Inflammation and Diffuse Pulmonary Hemorrhage

ABSTRACT

Upon exposure to TMPD, B cells expressing markers of B1 B cell subset infiltrate the lungs prior to any histopathological change while these cells are simultaneously reduced in their usual location, peritoneal cavity. Furthermore, $CD19^{-/-}$ mice that have reduced B1a B cells in the peritoneal cavity are protected from the development of TMPD-induced pneumonitis and DPH. Here, we tested the hypothesis that upon exposure to TMPD, B1 B cells traffic from the peritoneum to the lungs, where they induce pneumonitis and DPH. To test this hypothesis, we transferred peritoneal cells from the wild-type $CD19^{+}CD45.1^{+}$ B6 mice or control $CD19^{-/-}CD45.2^{+}$ B6 mice into the peritoneum of naïve $CD19^{-/-}$ $CD45.2^{+}$ or $Ig\mu^{-/-}$ B6 mice followed by an intraperitoneal injection of TMPD (500 μl) at 24 hours post-transfer. The $CD19^{-/-}$ recipients of $CD19^{+}$ cells developed more lung hemorrhage (70%) than the recipients of $CD19^{-}$ cells (10%). Similarly, $Ig\mu^{-/-}$ recipients of $CD19^{+}$ cells developed more lung inflammation (100%) than the recipients of $CD19^{-}$ cells (33%). In resonance with our hypothesis, the $CD19^{-/-}$ $CD45.2^{+}$ mice reconstituted intraperitoneally with peritoneal $CD19^{+}CD45.1^{+}$ cells showed presence of $CD45.1^{+}IgM^{+}$ cells in their lungs and had significantly higher IgM^{+} stained lung area than the control mice reconstituted with $CD19^{-}CD45.2^{+}$ cells. Finally, global gene expression analyses in lungs of TMPD-injected mice revealed a differential expression of a cohort of immune/inflammatory genes including a chemokine Cxcl13 that is known to drive migration of B1 B cells. Thus, we demonstrated the role of the trafficking of peritoneal B1 B cells to the lungs in the pathogenesis of TMPD-induced lung inflammation and hemorrhage. Ongoing studies will determine whether TMPD induces early changes in immune-response genes that drive the trafficking of innate B1 B cells to the lungs.

INTRODUCTION

B1 B cells mainly reside in the peritoneal and pleural cavities, but they do recirculate and migrate in response to various stimuli. In the previous chapter, we showed that $CD19^{-/-}$ mice that have a reduced development of CD5-expressing B1a B cells [42, 43] have a reduced prevalence and severity of DPH. We further found that at day 7 timepoint, prior to any histopathological changes, TMPD caused increased infiltration of $CD19^{+}$ B cells and subset B1 B cells ($CD19^{+}CD11b^{+}$/$CD19^{+}CD5^{+}$) in lungs of WT B6 mice. B1 B cells were simultaneously reduced significantly in their usual location, peritoneal cavity in TMPD-exposed mice. To test the hypothesis that innate B1 B cells migrate from the peritoneum into the lungs, where they promote the development of TMPD-DPH, we performed adoptive transfer experiments. Since peritoneum has a large population of B1 B cells, we used peritoneal B cells as a source of B1 B cells. To avoid activating the innate B1 B cell population, we did not positively select B cells during enrichment. Instead, we transferred all the peritoneal cells from $CD19^{+}$ WT mice into naïve $CD19^{-/-}$ B6 mice. The transferred cells were tracked by using $CD45.1^{+}$ donor cells and $CD45.2^{+}$ $CD19^{-/-}$ mice as recipients. To begin to identify potential molecular mechanisms, we performed microarray studies to identify genes that may be potentially involved in the migration of B1 B cells.

METHODS

Mice

$CD45.2^{+}$ wild-type C57BL/6J (WT B6; Stock No: 000664), breeder pairs of $CD19^{-/-}$ (CD19 cre; B6.129P2(C)-*Cd19*$^{tm1(cre)Cgn}$/J; Stock No: 006785) B6, and $Ig\mu^{-/-}$ ($muMt^{-}$; B6.129S2-*Ighm*^{tm1Cgn}/J; Stock No: 002288) B6 mice were purchased from the Jackson Laboratory and $CD45.1^{+}$ B6 WT mice expressing B6-Ly5.1/Cr ($CD45.1^{+}$ B6.SJL-

Ptprc^{a}*Pepc*^{b}/BoyCrCrl mice; Strain Code 564) were purchased from Charles River Laboratories. All mice were housed in a UCLA animal facility. The CD19$^{-/-}$ B6 mouse colony was expanded locally, and phenotyping via flow cytometry was performed to confirm the genotype of mice.

For the adoptive transfer experiments, 2-4-month-old male animals were used. For the microarray experiment, 5 month-old male mice (n=24) were used.

All animal studies were approved by the UCLA Institutional Animal Care and Use Committee.

Dose Administration and Bodyweight Assessment

Adoptive Transfer Experiments:

CD19$^{-/-}$ B6 Recipients:

For the preliminary adoptive transfer experiments (TMPD Day 7 and Day 11 timepoints), all the donors (2 months old), and recipients (2 months old) were male mice. Peritoneal B1 B cells were lavaged from donors CD19^{+}CD45.1^{+} WT B6 mice (n=16), the peritoneal fluid (PF) was pooled, and total viable cells counted. We administered 4 million total donor peritoneal cells suspended in 500 µl DPBS 1X (sterile) via ip route to each of the naïve CD19$^{-/-}$ CD45.2^{+} B6 recipients, and 24 hours post-transfer we injected TMPD (500 µl, ip) in all the recipients. Controls were unmanipulated CD19$^{-/-}$ CD45.2^{+} B6 mice (n=3). Necropsy was performed on Day 7 (n=3), and Day 11 (n=4) post TMPD-injection.

For the TMPD 2-weeks timepoint experiments, all the donors (3-4 months old), and recipients (2 months old) were female mice. Peritoneal B1 B cells were lavaged from donors CD19^{+}CD45.1^{+} WT B6 mice (n=16) or CD19$^{-/-}$ CD45.2^{+} B6 mice (n=16), the peritoneal fluid was pooled, and total viable cells counted. We administered 4 million total

donor peritoneal cells suspended in 500 µl DPBS 1X (sterile) via ip route to each of the naïve $CD19^{-/-}$ $CD45.2^{+}$ B6 recipients (n=10, received $CD19^{+}CD45.1^{+}$ WT B6 peritoneal cells; n=10, received $CD19^{-}CD45.2^{+}$ peritoneal cells). At 24 hours post-transfer, we injected all recipients with TMPD (500 µl, ip). Specifically, the control recipients did not receive any $CD19^{+}$ cells. All the recipients were monitored for bodyweight changes up to 2 weeks.

$Igμ^{-/-}$ B6 Recipients:

All the donors (2-3 months old), and recipients (2 months old) were male mice. Peritoneal B1 B cells were lavaged from donors $CD19^{+}CD45.1^{+}$ WT B6 mice (n=16) or $CD19^{-/-}$ $CD45.2^{+}$ B6 mice (n=16), the peritoneal fluid was pooled, and total viable cells counted. We administered 5 million total donor peritoneal fluid cells suspended in 500 µl DPBS 1X via ip route to each of the naïve $Igμ^{-/-}$ $CD45.2^{+}$ B6 recipients (n=6, received $CD19^{+}$ $CD45.1^{+}$ WT B6 peritoneal cells; n=6, received $CD19^{-}CD45.2^{+}$ peritoneal cells). At 24 hours post-transfer, we injected all recipients with TMPD (500 µl, ip). Specifically, the control recipients did not receive any $CD19^{+}$ cells. All the recipients were monitored for bodyweight changes up to 3 weeks.

Microarray Experiment

Male WT B6 mice were injected with a single dose of TMPD/Hex/PBS (500 µl, ip) under isoflurane anesthesia. The mice were divided in 5 groups: PBS (n=3); hex 1-week (n=3), TMPD 1-week (n=6), hex 2-weeks (n=6), TMPD 2-weeks (n=6). All the animals were monitored for changes in bodyweight, and euthanized at either 1- or 2-weeks timepoints.

Reagents

2,6,10,14-Tetramethylpentadecane BioReagent (TMPD, Molecular Weight 268.52, CAS Number 1921-70-6), synthetic, liquid, sterile-filtered, purity ≥95% (Sigma-Aldrich Corp., St. Louis, MO; Lot Nos. RNBB3307V). Isoflurane USP (Piramal Healthcare Limited, Bethlehem, PA) was used to anesthetize/euthanize the mice. Dulbecco's Phosphate Buffered Saline [DPBS (1X) Gibco™; Thermo Fisher Scientific Inc., Waltham, MA] was used to perfuse the lungs, and to clean the small and large intestines. Ethyl alcohol (Decon Laboratories, King of Prussia, PA) was used to clean the mouse prior to necropsy and preserve tissues for histology. Formalin 10% (Fischer Scientific Company LLC, Kalamazoo, MI) was used to fix the tissues for histology. The lungs were digested with Collagenase, Type 1 (Worthington Biochemical Corporation, Lakewood, NJ) and Deoxyribonuclease I from bovine pancreas (DNase; Sigma-Aldrich Corp., St. Louis, MO**),** and the enzymatic digestion process was stopped with UltraPure™ EDTA (Invitrogen™, Thermo Fisher Scientific Inc., Waltham, MA**)**. Red blood cells (RBCs) in spleen were removed with lysis buffer BD Pharm Lyse™ (BD Biosciences, San Jose, CA). For flow cytometry, the tissues were collected and cells washed with RPMI 1640 Medium (Gibco™; Thermo Fisher Scientific Inc., Waltham, MA). FACS buffer for immunostaining was made with PBS 10X (Fischer Scientific Company LLC, Fair Lawn, NJ) and Bovine serum albumin (BSA; Fischer Scientific Company LLC, Fair Lawn, NJ). Trypan blue (MP Biomedicals LLC, Solon, OH) was used to count viable cells for adoptive transfer/ immunostaining.

Necropsy

On the day of necropsy, each mouse was placed in a chamber that contained isoflurane for 3-5 minutes until it was euthanized. After the mouse ceased to breathe, it was taken

out of the chamber and placed on a dissection mat. The mouse's body was cleaned with alcohol and its outer skin was cut. The peritoneum was infused with 10 ml of cold DPBS 1X, lavage was performed for peritoneal fluid (PF) collection. Cardiac blood was collected for serum analysis. The lungs were perfused via the heart, with DPBS 1X to remove the blood from them after the aorta was cut.

For the preliminary adoptive transfer experiments (TMPD Day 7 and Day 11 timepoints) in $CD19^{-/-}$ $CD45.2^{+}$ B6 recipients: The whole lungs were incubated at 37°C in RPMI medium with Collagenase and DNase for one hour, and digestion was stopped by adding EDTA. Cells from peritoneal fluid (donors and recipients), spleen, and lungs were analyzed by flow cytometry.

For all the TMPD 2-weeks timepoint adoptive transfer experiments in $CD19^{-/-}$ and $Ig\mu^{-/-}$ $CD45.2^{+}$ B6 recipients: The whole lungs were collected from the recipients and fixed in 10% formalin for at least 24 hours. Cells from peritoneal fluid of both donors and recipients were analyzed by flow cytometry.

For the microarray experiment, the lungs were collected after perfusion and stored at **-** 80°C, except the lower right lobe which was fixed in 10% formalin for histology.

Immunofluorescence (IF) Staining

Paraffin embedded sections of lungs were used for IF staining with mAbs specific for lymphocytes. UCLA Translational Pathology Core Laboratory (TPCL) performed the IF staining for the slides. For the TMPD 2-weeks, adoptive transfer experiments to show migration of cells in $CD19^{-/-}CD45.2^{+}$ B6 recipients: Purified anti-mouse CD45.1 (Clone A20; BioLegend Inc., San Diego, CA) was used at a dilution of 1:500. To identify lymphocytes specifically producing IgM, we used Alexa Fluor 488 anti-mouse IgM

(Cat. A21042; Life Technologies Corp., Carlsbad, CA) at a dilution 1:200. Deparaffinized and hydrationed sections were treated with blocking reagent (PerkinElmer antibody diluent buffer) for 10 minutes at room temperature. Sections were then incubated with primary antibody working solution (conditions specific to antibody). Sections were then incubated (30 minutes) with a secondary anti-mouse antibody followed by a horseradish peroxidase conjugated complex. For signal amplification, each slide was incubated at room temperature for 10 minutes with opal Fluorophore Working Solution (1:50 dilution). Applied DAPI (ProLong® Gold Antifade Mountant with DAPI; Invitrogen, Carlsbad, CA) at a dilution of 1:2000 for 5 minutes in a humidity chamber, and then placed coverslip.

Histopathological Assessment

UCLA TPCL embedded the tissues in paraffin. Sections were stained with hematoxylin and eosin (H&E) for all the experiments. Lungs were scored for hemorrhage (hem), and the grading criteria was: grade 0, normal; grade 1, minimal hem; grade 2, mild hem; grade 3, moderate hem; grade 4. Lungs were scored for inflammation (inf), and the grading criteria was: grade 0, normal; grade 1, minimal inf; grade 2, mild inf; grade 3, moderate inf; grade 4. severe inf. All the slides were examined independently by a pathologist in a blinded manner for hemorrhage and inflammation.

H&E slides were digitized on a ScanScope AT (Leica Biosystems, Inc., Vista, CA), all the slides were scanned at 40X objective magnification.

Fluorescent images were acquired and analyzed using the Leica Versa (Applied Imaging Corp., San Jose, CA). The Versa scanner is based on a Leica DM600 B microscope with motorized stage and autofocus capabilities. Slides were scanned at 20X

or 40X objective magnification with the DAPI, FITC and TRITC filters. Optimal exposure times were determined before automated scanning. After scanning, images were exported for subsequent analysis.

Using the Definiens Tissue Studio™ product, stain specific algorithms were created, utilizing Definiens eCognitionNetwork Language™ for the pre-defined cellular detection modules and classification tools, to identify positive stained cells and cells with colocalized staining within each tissue region. Thresholds were set to classify the following: blue channel for DAPI, green channel for IgM and red channel for CD45.1 (for the TMPD 2-weeks, adoptive transfer experiments to show migration of cells in $CD19^{-/-}$ $CD45.2^{+}$ B6 recipients). The data were exported to Microsoft Excel for further statistical analysis.

Scanning and analyses were performed through TPCL, Department of Pathology and Laboratory Medicine, David Geffen School of Medicine at UCLA.

Flow Cytometric Analysis

Cells from lungs, peritoneal fluid, and spleen were washed with RPMI medium. Red blood cells (RBCs) in spleen were removed with lysis buffer, then kept in FACS buffer. After blockade of Fc receptors with purified anti-mouse CD16/CD32 mAb (clone 2.4G2; Tonbo Biosciences, San Diego, CA), cells were stained with the corresponding Ab mixtures. The following mAbs were used: APC-labeled anti-mouse CD19 (clone 1D3; Tonbo Biosciences, San Diego, CA), FITC-labeled anti-mouse CD19 (clone 1D3; Tonbo Biosciences, San Diego, CA), PerCP-Cyanine5.5-labeled anti- mouse CD19 (clone 1D3; Tonbo Biosciences, San Diego, CA), PE-labeled anti-mouse CD19 (clone 1D3; Tonbo Biosciences, San Diego, CA), APC-labeled anti-mouse CD45.1 (clone A20; BioLegend

Inc., San Diego, CA), Alexa Fluor 700-labeled anti-mouse B220 (clone RA3-682; BioLegend Inc., San Diego, CA), PerCP Cy5.5-labeled anti-mouse B220 (clone RA3-682; BD Biosciences, San Jose, CA), FITC-labeled anti-mouse IgM (clone RMM-1; BioLegend Inc., San Diego, CA), eFluor NC-650-labeled anti-mouse IgM (clone 11/41; eBiosciences, San Diego, CA), PE-labeled anti-mouse CD5 (clone 53-7.3, eBiosciences, San Diego, CA), PerCP-Cyanine5.5-labeled anti-human/mouse CD11b (clone M1/70; Tonbo Biosciences, San Diego, CA), APC-labeled anti-mouse CD11b (clone M1/70; Tonbo Biosciences, San Diego, CA), V500-labeled CD11b (clone M1/70; BD Biosciences, San Jose, CA), and PE-labeled anti-mouse TCRß (clone H57-597, Tonbo Biosciences, San Diego, CA).

For the adoptive transfer experiments with $CD19^{-/-}$ $CD45.2^{+}$ B6 recipients, the cells were acquired using the LSR Fortessa BV605 FACS, at the UCLA Immune Assessment Core (IAC).

The donor cells for all the adoptive transfer experiments were acquired using the BD FACSCalibur™ flow cytometry system (BD Biosciences) in our laboratory. All the data were analyzed using the FlowJo software Version 8.7 (Ashland, OR).

Data Analysis

The lung hemorrhage and inflammation scores for histopathology were statistically analyzed by Chi-square test. For the bodyweight changes, and total cells counts in the lungs, peritoneal fluid, and spleen, the differences between groups were statistically analyzed by unpaired Student's t-test with Welch's correction method with $P < 0.05$ considered to be significant. Data are presented as mean±SEM. Data was analyzed utilizing Microsoft Excel and Prism 6.0 (GraphPad Software, San Diego, CA).

Microarray Analysis

We performed a global gene expression analysis in the lungs at 1 and 2 weeks after an injection (0.5 ml, ip) of TMPD, Hex or PBS in 15 lung samples (n=3 per group). University of Texas Southwestern Medical Center performed RNA extraction from the lungs, and the gene expression data were obtained using an Affymetrix mouse 430 2.0 array. To screen for a differential gene expression profile between the groups, we analyzed the microarray data with assistance from the UCLA Biostatistics Core (Director: Dr. David Elashoff). Empirical Bayes Moderated t-test was used for analysis, since the sample size was small (3 per group). The Empirical Bayes Moderated t-test method is similar to t-test but helps use the other genes to get a better idea for the true variability (for which the t-test and p-value is based on). In case of a gene with unusually low variability, it can be shown as slightly larger and a weighted average between the observed variability in the gene and pool the estimated variability from the overall set to give a more stable variance estimate. This gives information about the true variances by using both the observed and pooled estimate across the sequence of transcripts. A marginally significant $p<0.10$ and fold change (FC) >1.5 was initially utilized as a cutoff to compare all the groups. To investigate the biological significance of our findings, we established collaboration with Dr. Matteo Pellegrini (UCLA Bioinformatics Collaboratory). To assess the biological significance of the differential gene response, we utilized the computational tool DAVID-Database for Annotation, Visualization and Integrated Discovery Bioinformatics Resources 6.7, NIAID/NIH [62, 63]. Heatmaps were generated using MATLAB software (Natick, MA).

RESULTS

Our data in the previous chapter led us to hypothesize that *after systemic (ip) exposure to TMPD, peritoneal B cells migrate to the lungs, where they induce changes leading to the development of pneumonitis and DPH*. To test this hypothesis, we conducted adoptive transfer studies where peritoneal cells were transferred from unmanipulated donor $CD19^{+}$ $CD45.1^{+}$ WT mice and control $CD19^{-/-}$ $CD45.2^{+}$ B6 mice into naive recipient $CD19^{-/-}$ $CD45.2^{+}$ B6 mice. Total cell counts in peritoneal fluid were similar between the WT B6 and $CD19^{-/-}$ donor mice (Figure 6.1A). As previously reported, $CD19^{-/-}$ $CD45.2^{+}$ donor mice had lower proportions of B cells ($B220^{+}IgM^{+}$) and B1a cells ($B220^{+}IgM^{+}CD5^{+}CD11b^{+}$) than $CD19^{+}CD45.1^{+}$ WT donor mice (Figure 6.1).

Four million peritoneal fluid cells from the unmanipulated donor B6 mice ($CD19^{+}CD45.1^{+}$ or $CD19^{-}CD45.2^{+}$) were injected ip into naïve $CD19^{-/-}$ $CD45.2^{+}$ recipient B6 mice. After 24 hours of transfer, the recipient mice were injected with TMPD (0.5 ml, ip), and mice were euthanized on days 7, 11 or 14. Total cell counts in peritoneal fluid were significantly increased in $CD19^{-/-}$ $CD45.2^{+}$ recipients injected with donor B6 WT cells on all timepoints as compared to controls (Figure 6.2A). Flow cytometry confirmed the presence of transferred $CD19^{+}CD45.1^{+}$ live lymphocytes in peritoneal fluid of $CD19^{-/-}$ $CD45.2^{+}$ recipients (Figure 6.2B). We did not detect the transferred cells in the peritoneum on days 11 and 14, as would be expected from studies in the previous chapter showing reduced peritoneal B cells after a TMPD injection. The transferred cells $CD19^{+}CD45.1^{+}$ were not present in the spleen of the recipient mice on Day 7 or Day 11 (data not shown). In fact, peritoneal B cells were lower at all timepoints after TMPD injection as compared to the baseline (unmanipulated $CD19^{-/-}CD45.2^{+}$ mice) (Figure 6.2C). Simultaneously,

total leukocyte cell count and absolute count of B cells, especially $B220^{low}IgM^{+}$ cells, in the lungs were higher in the reconstituted animals than in the unmanipulated controls (Figure 6.3).

At 2-weeks timepoint, 60% animals (n=10) reconstituted with WT ($CD19^{+}$) cells had 20% weight loss compared to only 10% recipients (n=10) reconstituted with $CD19^{-}$ cells. All animals with 20% weight loss had lung hemorrhage that was more prevalent in the recipients of $CD19^{+}$ cells as compared to the recipients of $CD19^{-}$ cells (70% vs. 10%). Lung hemorrhage scores were significantly higher in $CD19^{+}$ cell-recipients than in $CD19^{-}$ cell-recipients ($P<0.01$). Although, there was a trend towards more inflammation in $CD19^{+}$ cell-recipients than in $CD19^{-}$ cell-recipients, the differences were not statistically significant (Figure 6.4). These results clearly demonstrate a pathogenic role of peritoneal $CD19^{+}$ B cells in the pathogenesis of TMPD-DPH.

To reproduce our findings in another B cell-deficient model, we adoptively transferred peritoneal B cells isolated from $CD45.1^{+}CD19^{+}$ (WT) or control $CD19^{-/-}$ $CD45.2^{+}$ into the peritoneum of naïve $Ig\mu^{-/-}CD45.2^{+}$ recipients that have no B cells. After 24 hours of transfer, recipient mice were injected with TMPD (0.5 ml, ip). Animals were monitored for weight-loss and all euthanized at 3-weeks to harvest lungs for histopathology. One of 6 $CD19^{+}$ cell-recipients and none of 6 $CD19^{-/-}$ cell-recipients lost 20% bodyweight, and the animal with weight loss had DPH. Lung inflammation was more prevalent and inflammation scores were significantly higher in $CD19^{+}$ cell-recipients than in $CD19^{-}$ cell-recipients (Figure 6.5). Taken together, data in this chapter support the hypothesis that peritoneal B cells mediate TMPD-induced inflammatory lung disease.

To directly test our hypothesis that peritoneal B cells migrate from the peritoneum to lungs after TMPD-injection, we stained the lungs of $CD19^{-/-}CD45.2^{+}$ B6 recipients injected ip with peritoneal cells isolated from $CD19^{+}CD45.1^{+}$ or control $CD19^{-/-}$ $CD45.2^{+}$ mice followed by a TMPD injection. In the $CD19^{+}CD45.1^{+}$ cell-recipient group, the normal lungs had a few $CD45.1^{+}$ leukocytes, but were abundant in recipients that had DPH. As expected, $CD19^{-}CD45.2^{+}$ cell-recipients had no staining for CD45.1. These control mice also had no IgM staining, whereas $CD19^{+}CD45.1^{+}$ cell-recipients with hemorrhage had co-localized $CD45.1^{+}IgM^{+}DAPI^{+}$ cells and increased IgM stained lung tissue ($P<0.0001$) (Figure 6.6). Consistently, the recipients of $CD19^{+}$ cells had less IgM^{+} B cells remaining in the peritoneum compared to $CD19^{-/-}$ cell-recipients (Figure 6.7). These data clearly demonstrate that in response to TMPD, B cells traffic from the peritoneum into the lungs.

We performed a global gene expression analysis in the lungs of WT B6 mice at 1- and 2-weeks after an injection of TMPD, Hex or PBS (0.5 ml, ip) using Affymetrix Gene ST 2.0 mRNA microarray in 15 lung samples (n=3/group). Using this analysis, we found 559, 307, and 161, genes to be differentially expressed between PBS vs. TMPD, Hex vs. TMPD, and PBS vs. Hex, respectively, at the 1-week timepoint. At the 2-weeks timepoint when animals begin to exhibit features of DPH, 1,751 genes were differentially expressed between PBS and TMPD groups, 409 genes in Hex vs. TMPD, and 559 genes in PBS vs. Hex groups. 1,071 genes were different in 1- week TMPD vs. 2-week TMPD groups, using $p<0.10$ and $FC>1.5$ as a cutoff. Histopathology revealed normal lung tissues in all mice at the 1-week timepoint, however at the 2-weeks timepoint two of three TMPD-exposed mice exhibited severe DPH and one with minor pulmonary inflammation. The two TMPD-exposed mice with DPH exhibited a dramatically altered gene expression response in the

microarray data (Figure 6.8B, C).

Specifically, the microarray data analyses also showed that as compared to Hex controls, TMPD-injected mice have a significantly increased lung expression of chemokine *Cxcl13* at both timepoints (Figure 6.8A). *Cxcl13* is known to be required for the peritoneal/pleural homing as well as egress of B1 B cells [64].

For a more stringent differential gene expression profile, we further analyzed the data with $p < 0.05$ and fold-change >1.5 as the cutoff, which identified 96 genes that were significantly different between the three groups (PBS vs. Hex vs. TMPD) at the 1-week timepoint. A functional analysis of these differentially expressed genes utilizing DAVID revealed a functional annotation cluster of 16 genes involved in immune system development, cell migration, cell motility, secreted proteins, inflammation, chemotaxis, response to wounding and defense response pathways. The immune response genes that were differentially expressed in the TMPD vs. both controls at both 1-week and 2-weeks timepoints included *Ccl5, Ly96, S100a8, CD14, C1q, Ccl6, Ccl7, Ccl12, IL-6, Mpo, Marco,* and *Cxcl13* (Figure 6.8B, C).

DISCUSSION

We demonstrated that the reconstitution of B6 mice that are deficient in all B cells ($Ig\mu^{-/-}$) or in B1a B cells ($CD19^{-/-}$) with peritoneal cells that are enriched in B1 B cells increases the prevalence and severity of TMPD-induced lung inflammation/hemorrhage compared to when the two knockout animals are reconstituted with $CD19^{-}$ peritoneal cells that are deficient in B1a B cells. The donor cells ($CD45.1^{+}$) injected into the peritoneum of $CD45.2^{+}$ recipients were detected in the lungs of recipients at 15 days post-transfer. Simultaneously, the transferred cells were reduced in the peritoneum of recipients. These

results clearly demonstrate that in response to TMPD, B1 B cells migrate from the peritoneum into the lungs and promote the development of lung inflammation and hemorrhage.

Mechanisms underlying the trafficking of B1 B cells from the peritoneum into the lungs are unclear. In preliminary work, we analyzed global gene expression in the lungs of animals injected with TMPD, control hydrocarbon oil hexadecane or control PBS (0.5 ml, ip) with a goal to identify genes that could potentially modulate B1 B cell migration. As compared to control hexadecane-injected animals, TMPD-injected mice have an increased expression of chemokine *Cxcl13* that is known to be required for the peritoneal/pleural homing as well as egress of B1 B cells [64]. *Ly96* expression is also significantly higher in TMPD-exposed mice as compared to both controls across all conditions ($p = 0.002$ to 0.03; FC>1.5). *Ly96*, also known as myeloid differentiation factor-2, encodes a protein that associates with TLR4 on the cell surface and confers responsiveness to lipopolysaccharide (LPS), thus providing a link between the receptor and LPS signaling. The cellular source and functions of Ly96 are not well delineated. In competitive transfer experiments, peritoneal B1 B cells isolated from *TLR4*$^{-/-}$ mice exhibit an impaired egress compared with those from normal mice [65]. Hence, given an association of Ly96 with TLR4, it is possible to posit a role of *Ly96* in B1 B trafficking to lungs in TMPD-injected mice. Upon activation of B1 B cells through the TLR, integrins and tetraspanin, such as CD9 that regulates cell motility, are reduced, resulting in the detachment and migration of B1 B cells from the peritoneum. Ongoing studies will investigate the role of these genes as well as other potential mechanisms by which TMPD induces the migration of B1 B cells and their trafficking to the lungs. Identification of

mechanisms that induce the migration of B cells to the lung in this model may pave the way for further studies to modulate B cell migration to target organs as a therapeutic strategy.

It remains to be determined whether B1 or B1-like B cells infiltrate the lung in patients with a variety of conditions that can manifest with DPH, such as vasculitis, lupus, organ transplant, cocaine abuse, and pesticide exposure. These studies are timely because rituximab is currently being used in the treatment of some patients with DPH, however it indiscriminately depletes most B cells. Identification of *the pathogenic* subset of B cells in DPH and mechanisms underlying the B cell subset's contribution to DPH pathogenesis may open new strategies to develop highly specific therapies to treat DPH.

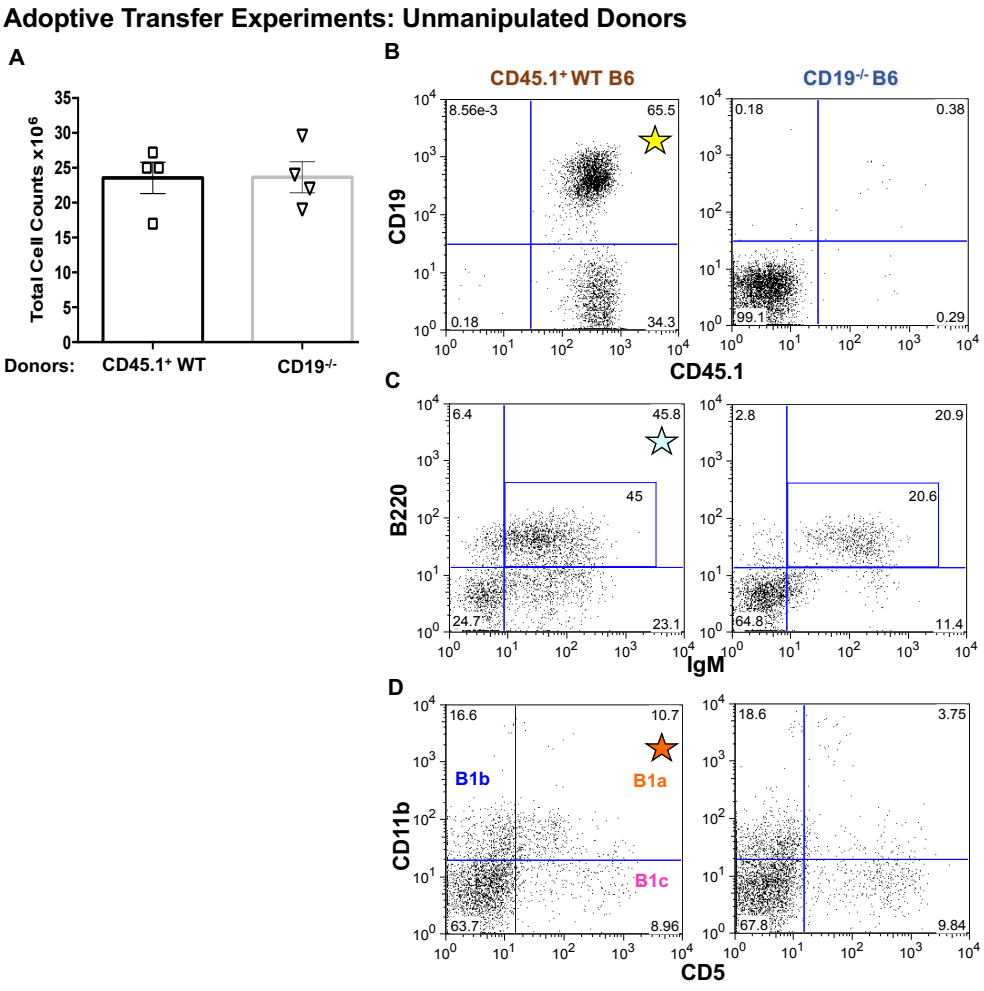

Fig 6.1 Adoptive Transfer Experiments: Characterization of donor cells. Donors were unmanipulated $CD19^{+}$ $CD45.1^{+}$ WT B6 (n=32) and $CD19^{-/-}$ $CD45.2^{+}$ B6 mice (n=32), age 2-4 months old. Peritoneal fluid cells were harvested, counted, and analyzed by flow cytometry. Numbers on representative dot plots indicate percentage of cells. **(A)** Total cell counts in peritoneal fluid were similar in WT B6 and $CD19^{-/-}$ donor mice. Each symbol represents pooled peritoneal fluid samples from 8 mice. **(B)** Peritoneal fluid cells were gated on $CD19^{+}CD45.1^{+}$ live lymphocytes. Peritoneal fluid had 65% $CD19^{+}CD45.1^{+}$ cells

in donor WT mice vs. none in $CD19^{-/-}$ $CD45.2^{+}$ donor mice. **(C)** PF cells were gated on $B220^{+}IgM^{+}$ live lymphocytes. $CD19^{-/-}$ $CD45.2^{+}$ donor mice had lower proportions of B cells ($B220^{+}IgM^{+}$) than $CD19^{+}CD45.1^{+}$ WT donor mice. **(D)** $CD19^{-/-}$ $CD45.2^{+}$ donor mice had lower proportions of B1a cells ($B220^{+}IgM^{+}CD5^{+}CD11b^{+}$) vs. $CD19^{+}CD45.1^{+}$ WT mice. Data are representative of 4 independent experiments.

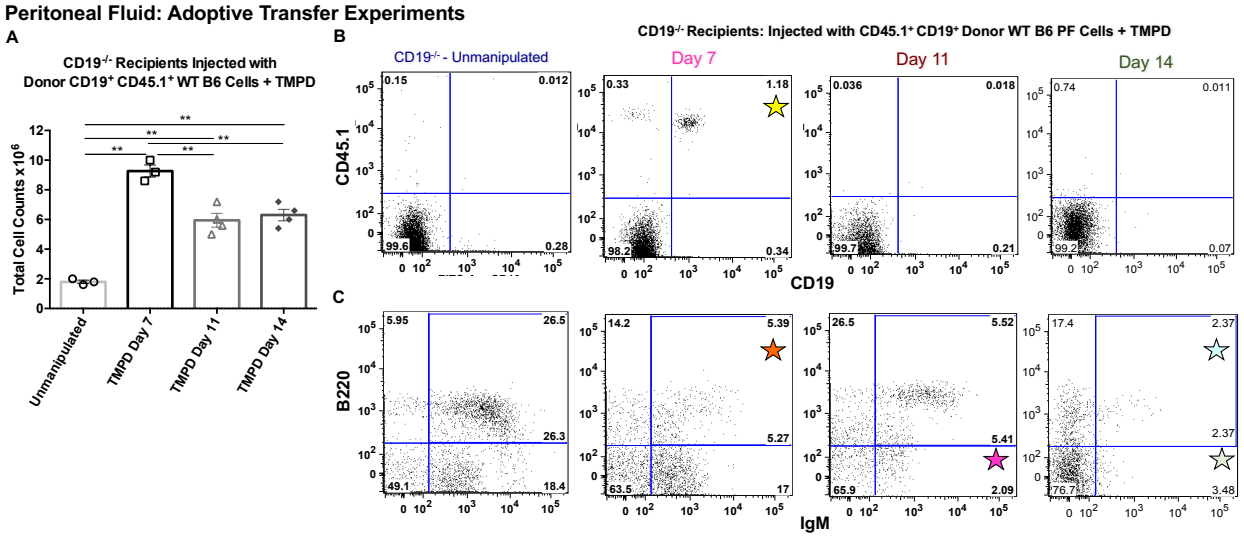

Fig 6.2 Intraperitoneal transfer of donor cells. Naïve CD19$^{-/-}$ CD45.2^{+} mice were injected (ip) with 4 million peritoneal cells isolated from unmanipulated donor WT B6 mice (CD19^{+}CD45.1^{+}). After 24 hours of transfer, recipient mice were injected with TMPD (0.5 ml, ip). Animals were euthanized on days 7, 11 or 14 post-TMPD exposure. Unmanipulated CD19$^{-/-}$ CD45.2^{+} mice were used as controls. **(A)** Total cell counts in peritoneal fluid were significantly increased in CD19$^{-/-}$ CD45.2^{+} recipients injected with donor B6 WT cells at all timepoints vs. baseline controls. **(B)** Peritoneal fluid cells were gated on CD19^{+}CD45.1^{+} live lymphocytes. Transferred donor (CD19^{+}CD45.1^{+}) cells were detected on day 7, but not on days 11 and 14, in the peritoneal fluid of CD19$^{-/-}$ CD45.2^{+} recipients. **(C)** Peritoneal fluid cells were analyzed for B220 and IgM on live lymphocytes. Note a reduced proportion of B cells in TMPD-injected reconstituted animals at all timepoints, more profoundly on day 14, compared to unmanipulated CD19$^{-/-}$ mice. Numbers on representative dot plots indicate percentage of cells. Data are representative of 3 independent experiments. Data are presented as mean±SEM. **P<0.01

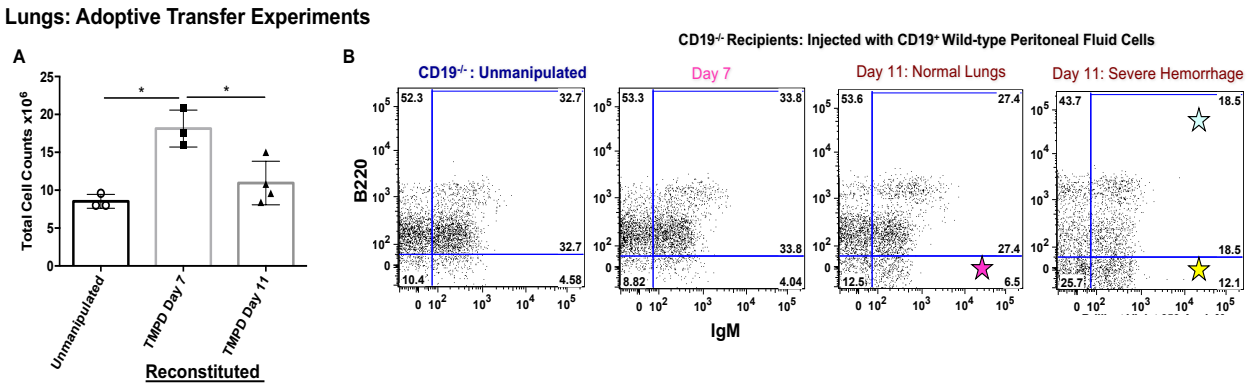

Fig 6.3 Flow cytometry analysis of Lung B cells in CD19$^{-/-}$ CD45.2^{+} B6 Recipients at Day 7 vs. Day 11, that were administered Donor CD45.1^{+}CD19^{+} B6 WT PF Cells and TMPD. Each naïve CD19$^{-/-}$ CD45.2^{+} recipient mouse was injected (ip) with 4 million peritoneal cells from unmanipulated Donor WT B6 mice (CD19^{+}CD45.1^{+}). Post 24 hours of transfer, all recipient mice were injected with TMPD (0.5 ml, ip), and mice were euthanized either on Day 7 or Day 11. Controls were unmanipulated CD19$^{-/-}$ CD45.2^{+} mice **(A)** Total cell counts in lungs were significantly increased in CD19$^{-/-}$ CD45.2^{+} recipients injected with Donor WT B6 cells on Day 7 vs. controls. Total cell counts in lungs were significantly decreased in Day 11 vs. Day 7 recipients. **(B)** Lung cells were gated on B220^{+}IgM^{+} live lymphocytes. The CD19$^{-/-}$ CD45.2^{+} recipients had higher proportions of B cells (B220^{+}IgM^{+}) than controls at all timepoints. Furthermore, at Day 11 the proportions of IgM^{+} cells were higher in a recipient that had severe lung hemorrhage (gross pathology) vs. controls. Numbers on a representative dot plot indicate percentage of cells. 1 X10^{6} cells were stained. Data are presented as mean±SEM. *P<0.05

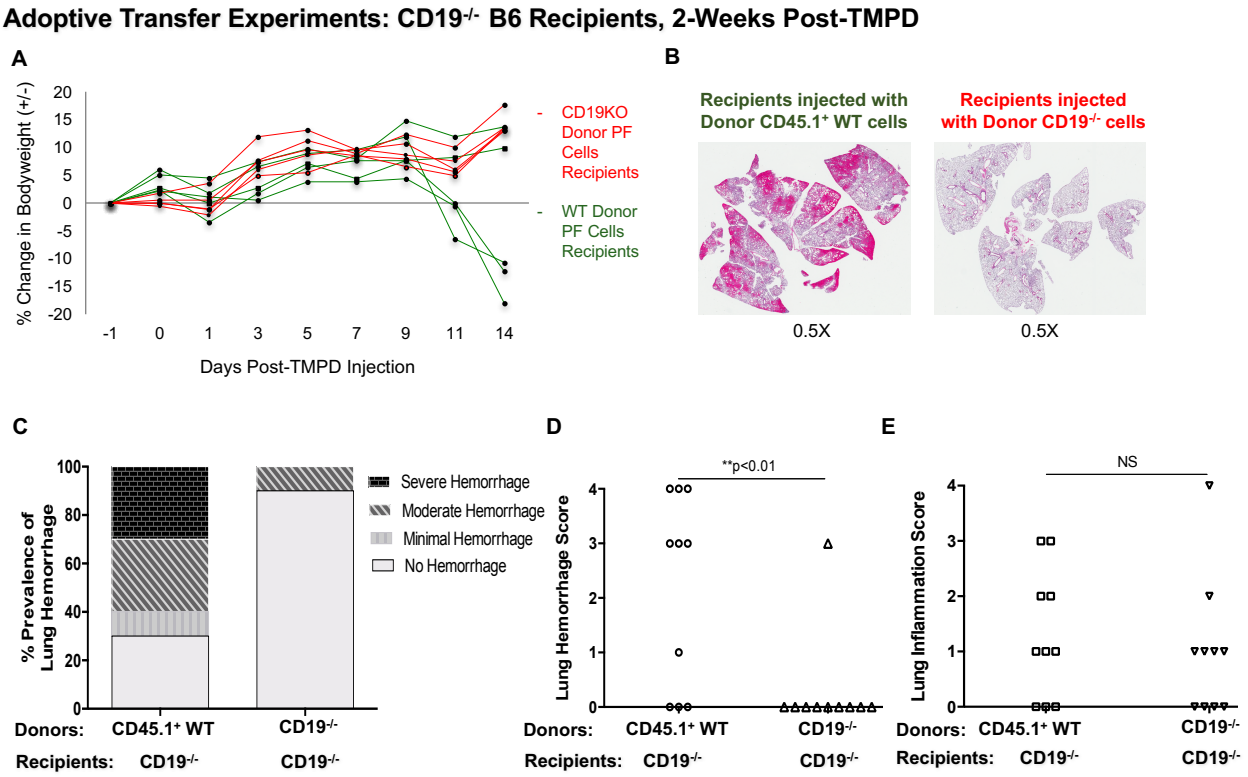

Fig 6.4 Effect of Adoptive Transfer of CD19$^+$ WT Peritoneal Fluid Cells on TMPD Induced Lung Inflammation and Hemorrhage in CD19$^{-/-}$ Mice. Each naïve CD19$^{-/-}$ CD45.2$^+$ recipient mouse (n=10/group) was injected (ip) with 4 million peritoneal cells from unmanipulated donor WT (CD19$^+$CD45.1$^+$) or donor CD19$^{-/-}$ CD45.2$^+$ B6 mice. Post 24-hours of transfer, all recipient mice were injected with TMPD (0.5 ml, ip), and were euthanized at 2-weeks. Females, 2 months old mice were used, and two independent experiments were performed. **(A)** Each mouse was weighed prior to donor PF cells administration (Day -1), and prior to TMPD injection (Day 0). Bodyweight was monitored at different timepoints for up to 2-weeks post exposure. 60% of the mice in the CD19$^+$CD45.1 WT cells recipients vs. 10% of the CD19$^-$CD45.2$^+$ cells recipients, lost 20% bodyweight within 2-weeks post TMPD-injection and correlated with lung hemorrhage. **(B)** and **(C)** Lung hemorrhage prevalence was greater 70% vs. 10%, respectively, in

$CD19^{+}CD45.1$ WT cells recipients vs. $CD19^{-}CD45.2^{+}$ cells recipients. Slides were digitized on a ScanScope AT (Leica Biosystems, Inc.), whole lung areas at 0.5X low magnification. **(D)** Lung hemorrhage scores in both groups, statistical analysis showed a significantly higher hemorrhage score in $CD19^{+}CD45.1$ WT cells recipients vs. $CD19^{-}CD45.2^{+}$ cells recipients. **(E)** Lung inflammation scores in both groups, although there was a trend of less inflammation in $CD19^{-}CD45.2^{+}$ cells recipients vs. $CD19^{+}CD45.1$ WT cells recipients, it was not statistically significant. **P<0.01

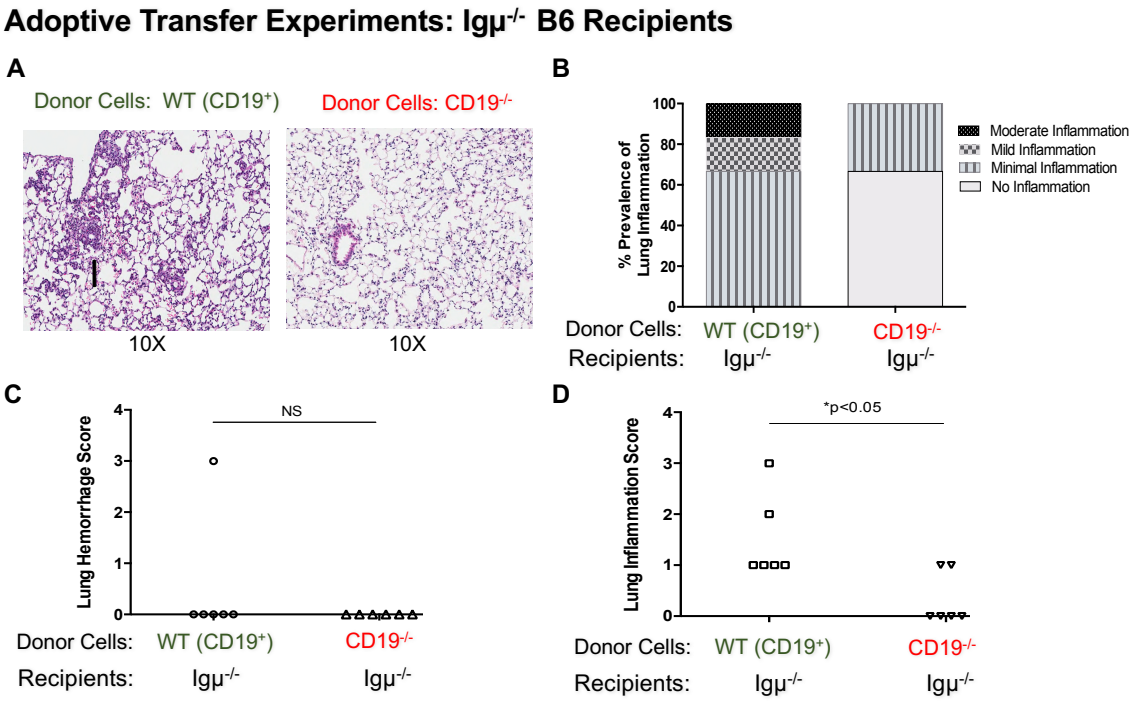

Fig 6.5 Effect of Adoptive Transfer of CD19^{+} WT Peritoneal Fluid Cells on TMPD Induced Lung Inflammation and Hemorrhage in B cell-Deficient (Igμ$^{-/-}$) Mice. Naïve Igμ$^{-/-}$ CD45.2^{+} mice were injected ip with 5 million peritoneal cells from unmanipulated WT (CD19^{+}CD45.1^{+}) or CD19$^{-/-}$ CD45.2^{+} mice (n = 6/group, 2-month-old males). After 24 hours of transfer, all recipient mice were injected with TMPD (0.5 ml, ip), monitored for general health, and euthanized at 3-weeks. **(A)**. Representative lung tissue sections showing more inflammation (I) in WT cell-recipients but not in CD19$^{-/-}$ cell recipients. Whole lung areas were digitized on a ScanScope AT (Leica Biosystems, Inc.) at 40X magnification, representative lung area at 10X. **(B)** Prevalence of lung inflammation. **(C, D)** Lung hemorrhage and inflammation scores. Results represent two independent experiments. *P<0.05

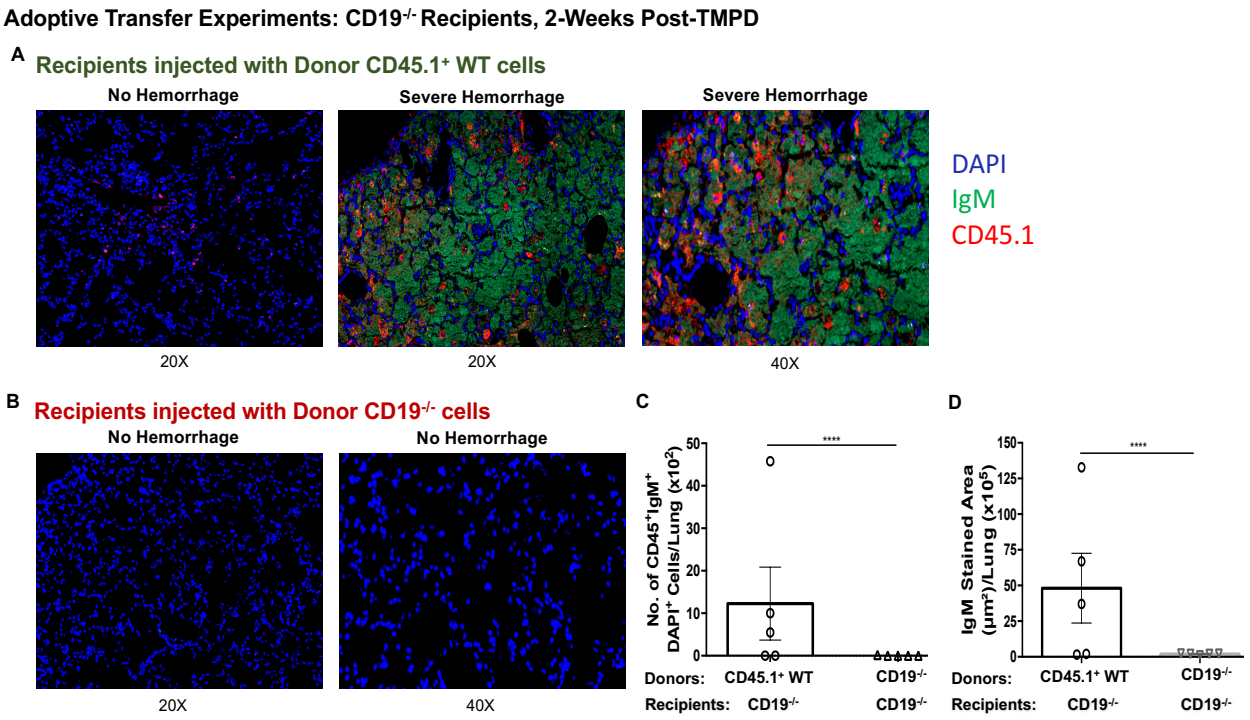

Fig 6.6 Migration of Donor WT CD45.1^{+}IgM^{+} Peritoneal Fluid Cells to the Lungs of CD19$^{-/-}$ CD45.2^{+} B6 Recipients. Naïve CD19$^{-/-}$ CD45.2^{+} recipient mice (n=5/group) were injected ip with 4 million peritoneal fluid cells from unmanipulated donor WT mice (CD19^{+}CD45.1^{+}) or donor CD19$^{-/-}$ CD45.2^{+} B6 mice, all 2-month-old females. After 24 hours of transfer, all recipient mice were injected with TMPD (0.5 ml, ip), and were euthanized at 2-weeks. Lung sections were stained for DAPI, IgM and CD45.1 to identify the donor cells expressing IgM in the recipient lungs. Representative fluorescence microscopy images are shown. Original magnification 40X. **(A)** CD19^{+}CD45.1^{+} WT cell-recipients: Normal lungs (no hemorrhage) had few CD45.1^{+}DAPI^{+} leukocytes. Lungs with hemorrhage had increased number of CD45.1^{+}IgM^{+}DAPI^{+} lymphocytes and increased IgM stained areas. The right panel is a magnified area of lung with hemorrhage highlighting the presence of CD45.1^{+}IgM^{+}DAPI^{+} lymphocytes. **(B)** CD19^{-} CD45.2^{+} cell-recipients: As expected, these lungs had no CD45.1^{+} leukocytes. Additionally, there were

few to no IgM^+DAPI^+ cells in these recipients. **(C, D)** The number of $CD45.1^+IgM^+DAPI^+$ cells in lungs and IgM^+ stained lung area were significantly higher in $CD19^+CD45.1^+$ WT cell-recipients than in $CD19^-CD45.2^+$ cell-recipients. ****P<0.0001

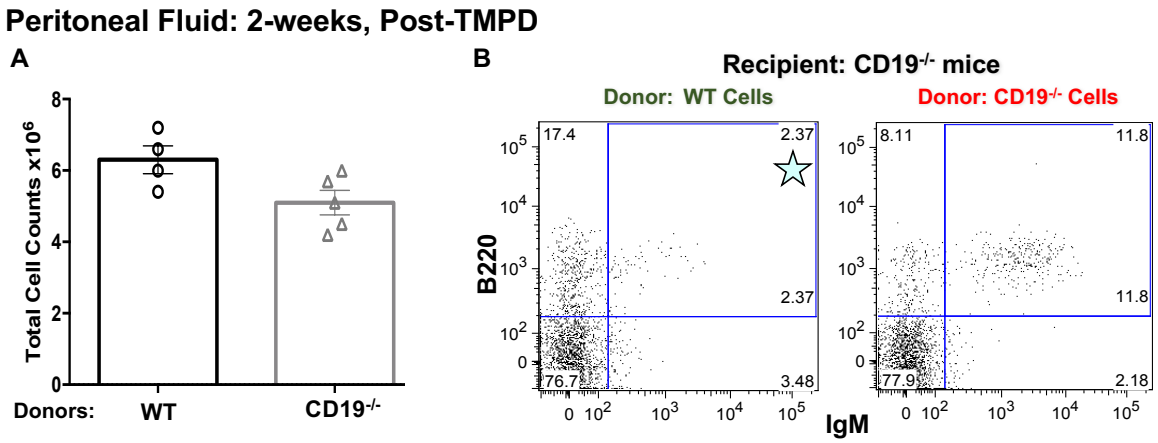

<u>Fig 6.7</u> Analysis of Peritoneal Fluid B cells in CD19$^{-/-}$ Recipients Reconstituted with WT or CD19$^{-/-}$ peritoneal fluid cells. Naïve CD19$^{-/-}$ B6 recipient mice were injected (ip) with 4 million peritoneal cells isolated from unmanipulated WT (CD19^{+}) or CD19$^{-/-}$ B6 mice (n=5/group, females). After 24 hours of transfer, all recipient mice were injected with TMPD (0.5 ml, ip), and euthanized at 2-weeks. **(A)** Total cell counts in peritoneal fluid were lower in recipients transferred with CD19$^{-/-}$ cells than with WT cells. Data are presented as individual animal values and as the mean±SEM. **(B)** Peritoneal fluid cells were analyzed for B cells on gated live lymphocytes. Numbers on representative dot plots indicate percentage of cells. The WT cell-recipients had lower percentage of B cells (B220^{+}IgM^{+}) compared to CD19$^{-/-}$ cell-recipients.

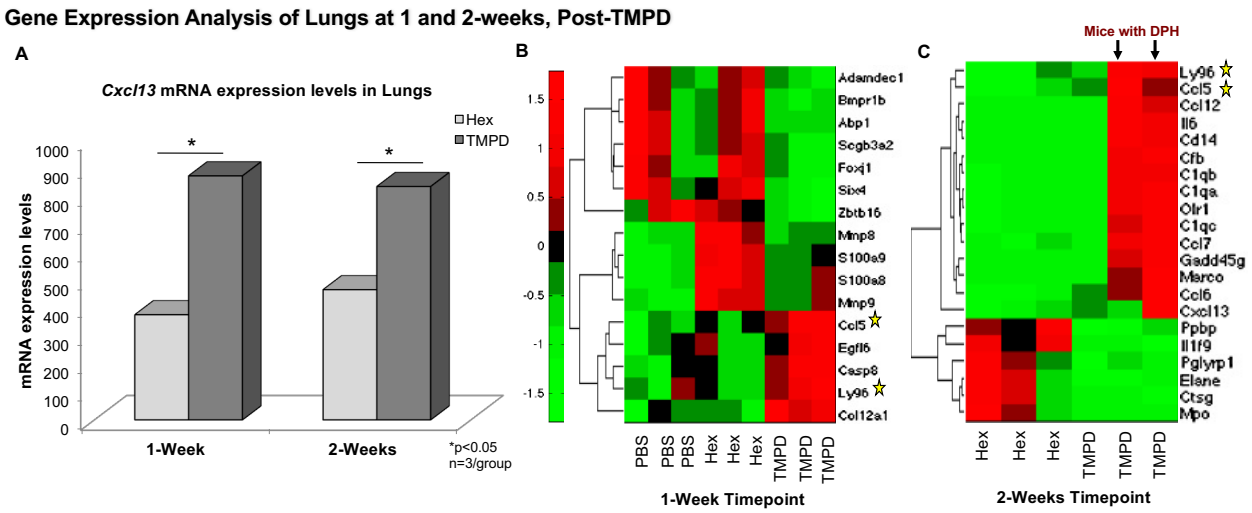

Fig 6.8 Gene Expression Analysis of Lungs at 1 and 2-weeks timepoints. WT B6 mice (males, 5 months old) were injected with a single dose of TMPD/Hex/PBS (0.5 ml, ip), and euthanized at either 1- or 2-weeks timepoints. **(A)** Microarray data analyses show that as compared to Hex controls, TMPD-injected WT B6 mice have an increased lung expression of chemokine *CXCL13* that is known to be required for the peritoneal/pleural homing as well as egress of B1 B cells. **(B)** Comparison between PBS, Hexadecane and TMPD at 1-week timepoint, by functional analysis revealed functional annotation clusters of genes involved in immune response/inflammation/chemotaxis/migration/defense response pathways. **(C)** Comparison between Hexadecane and TMPD at 2-weeks timepoint, functional analysis revealed a cluster of 21 immune response genes that included *Ccl5* and *Ly96*. N=3 mice/group; $p<0.05$ and fold change>1.5 as the cutoff. Statistical analysis performed with Empirical Bayes Moderated t-test. For functional analysis utilized DAVID Bioinformatics Resources 6.7, NIAID/NIH. Affymetrix Gene ST 2.0 mRNA microarray data.

CHAPTER 7

SUMMARY and DISCUSSION

In this study, we demonstrated that systemic (ip) administration of 500 µl of hydrocarbon oil TMPD induces weight loss, and pneumonitis, vasculitis and/or DPH within 2 weeks of exposure in B6 mice, whereas the same dose regimen of another hydrocarbon oil hexadecane induces ascites and mild lung infiltration but no weight loss or DPH up to 11 months post-exposure. Administration of lower doses of TMPD (250 µl or 125 µl, ip) elicits lung inflammation but minimal to no DPH. Direct lung exposure by oropharyngeal aspiration of low doses (4 µl) of TMPD also induces pneumonitis and DPH, whereas the same dose regimen of hexadecane only induces lung inflammation. Oropharyngeal aspiration of slightly higher doses (6 µl to 40 µl) of TMPD causes rapid morbidity and early mortality within days, along with lung inflammation, hyaline membrane formation in lungs, and increased serum creatinine kinase and aspartate aminotransferase.

At 2-weeks timepoint, all immune cells tested were abnormal in the diseased lungs of mice post-TMPD exposure (500 µl, ip). At earlier timepoints prior to histopathological changes, while both Hexadecane and TMPD caused myeloid cell abnormalities, only TMPD caused lung-infiltration with B cells that expressed markers of a subset of B cells, namely B1 B cells. Such B1 B cells were simultaneously reduced in their usual location (peritoneal cavity). A direct role of these cells in the pathogenesis of TMPD-induced DPH was shown using $CD19^{-/-}$ mice that have less B1 B cells. These mice developed less DPH and showed lower B cell infiltration in lungs after TMPD-injection (500 µl, ip) than WT B6 mice. The adoptive transfer of $CD45.1^{+}$ wild-type peritoneal-fluid cells into the peritoneum of naïve $CD45.2^{+}CD19^{-/-}$ recipients led to lung-infiltration with $CD45.1^{+}$ B-cells and more DPH/pneumonitis than $CD19^{-/-}$ recipients reconstituted with $CD19^{-}CD45.2^{+}$ B-cells. These observations provide a direct evidence that in response to TMPD, innate B1 B cells

traffic from the peritoneum into the lungs, where they contribute to the development of pneumonitis and DPH.

The consistent development of DPH within 10-30 days of administering TMPD (500 µl, ip) provides an excellent model to study the pathogenesis of autoimmune disease and of toxicity of hydrocarbon oils. Pneumonitis incidence was less, and disease development was slower at low doses of TMPD (125 and 250 µl, ip). This raises a question about the clinical significance of hydrocarbon oils as etiologic agents in autoimmune diseases, as humans are less likely to be acutely exposed to large doses of hydrocarbon oils, except in accidents. However, over time humans can be exposed to large doses of hydrocarbon oils via ingestion (foods, medications), inhalation (diesel exhaust, oil mists, aspiration of ingested mineral oil), and skin absorption (cosmetics, skin contact with oils or fuels) [8, 10, 11]. Nevertheless, studies are needed to assess the effect of chronic low dose exposure to hydrocarbon oils on the development of autoimmune and inflammatory diseases.

Hydrocarbons were implicated in almost 10 percent of all single substance fatalities in the pediatric population. Gasoline, chlorofluorocarbon propellants, motor oils, lighter fluid/naphtha, lamp oil, and mineral spirits, are the most commonly ingested substances [66]. In young children, the ingestion typically occurs due to exploratory behavior. Toxicity in adolescents often arises from inhalant abuse of hydrocarbon oils. Volatile hydrocarbons are highly lipid soluble and enter the circulation through the lungs and rapidly diffuse throughout the body and into the central nervous system (CNS). Neurons, which have a high lipid content, are particularly susceptible to the solvent properties. CNS manifestations also occur secondary to severe pulmonary injury and

hypoxia.

There are no published inhalation studies in animals. Studies of exposure via this route would be relevant to human exposure. We showed that oropharyngeal aspiration (OA) of a dose as low as 6 µl TMPD caused rapid morbidity/mortality by day 3, with increased serum creatinine kinase and aspartate aminotransferase, and pneumonitis. At a lower dose of 4 µl TMPD given via OA was less toxic; 75% animals survived up to day 17, and exhibited pneumonitis/DPH. It would be important to know whether repeated /chronic exposures to even lower doses of TMPD induces chronic autoimmune diseases.

In this study, we established clinical (20% weight loss), semi-quantitative (scoring criteria), and quantitative assessments (morphometric analysis to measure the area of eosin staining) of TMPD-DPH. Bodyweight loss as a method of predicting DPH in mice is a useful tool. This as well as scoring methods and quantitation of DPH area were helpful to evaluate the effects of various manipulations such as knockout and adoptive transfer studies in our experiments in a non-biased manner.

A recent study showed that Ig$\mu^{-/-}$ MT mice that have a complete deficiency of B cells were resistant to induction of DPH. Susceptibility to DPH was restored in Ig$\mu^{-/-}$ MT mice by infusing IgM [35]. Since activated B1 B cells produce large amounts of IgM, it is logical to posit a role of B1 B cells in the pathogenesis of TMPD-DPH. In fact, we demonstrate that CD19$^{-/-}$ mice that have less B1 B cells were protected from the development of TMPD. The knockout mice also had less IgM^{+} B cells and less IgM deposition in their lungs. Moreover, lungs were infiltrated with B1 B cells prior to the development of any histopathological changes after TMPD exposure, whereas another hydrocarbon oil hexadecane that does not induce DPH does not elicit B1 B cell infiltration

in the lungs.

We further demonstrated that these B1 B cells that are present in the lungs of TMPD-injected mice are recruited from their usual location, i.e., peritoneal cavity. The adoptive transfer of $CD45.1^{+}CD19^{+}$ peritoneal cells into the peritoneum of naïve $CD45.2^{+}$ $CD19^{-/-}$ recipients led to lung-infiltration with $CD45.1^{+}$ B cells and more DPH/pneumonitis as compared to $CD19^{-/-}$ recipients reconstituted with $CD19^{-/-}$ peritoneal cells. This finding directly demonstrates the trafficking of peritoneal B cells to the lungs. Consistent with this hypothesis, within hours of TMPD administration, we found a marked reduction in B1 B cells in the peritoneal cavity (data not shown). The administration of control hydrocarbon oil hexadecane also caused the reduction in peritoneal B1 B cells, however, B1 B cells were not detected in the lungs of hexadecane injected mice. The mechanism underlying this observation is not clear, however, we found a differential expression of a set of immune/inflammatory genes including chemokine *Cxcl13* that is known to drive B1 B cells' migration in lungs from TMPD-injected animals as compared to lungs from PBS or hexadecane injected mice. It remains to be determined whether the increased expression of *Cxcl13* or other chemokines/mechanisms drive the trafficking of B1 B cells from the peritoneum to the lungs.

How do B1 B cells promote the development of DPH? B1 B cells produce large amounts of IgM. A recent study showed that the development of DPH may involve opsonization of dead cells by natural IgM and complement followed by complement receptor-mediated lung inflammation [35]. Activated B1 B cells may also produce inflammatory cytokines and serve as strong antigen presenting cells to activate T cells.

Observations by us and another group showing the role of B cells in the

pathogenesis of DPH have important implications, as rituximab that depletes B cells is FDA-approved to treat patients with Wegeners granulomatosis that is known to manifest with DPH. Furthermore, a community comparison study that showed that people living near an oil field waste site in New Mexico with increased levels of TMPD in house dust had increased proportions of $CD19^+$ B cells in their peripheral blood and an increased prevalence of lupus and other immune disorders as compared to an unexposed population [12]. However, rituximab indiscriminately depletes all B cells and can cause adverse effects. Thus, our finding that implicates a specific subset of B cells and more so a specific mechanism driving the abnormal infiltration of a B cell subset has important translational implications with a potential to develop a highly targeted therapy for DPH that has no effective treatment currently.

The trafficking of B1 B cells to the lung may not be the only mechanism in all cases of DPH, as the development of pneumonitis/DPH was independent of $CD19^+$ B cells when the lungs were directly exposed to TMPD via OA route. In fact, a previous study reported that although the prevalence of DPH was lower in $Rag1^{-/-}$ B6 mice than in wild-type B6 mice, some $Rag1^{-/-}$ mice did develop DPH, suggesting that DPH can develop in the absence of T and B cells, although they may play a role in promoting DPH [4].

The results attained on immune mechanisms of DPH may have broad implications for DPH caused by exposure to toxic substances, such as isocyanates, trimellitic anhydrides, and certain pesticides, recreational drugs (crack cocaine), and medications (chemotherapeutic agents, propylthiouracil, and diphenylhydantoin). Furthermore, DPH is also known to occur after bone marrow or organ transplantation, and in many inflammatory diseases such as systemic vasculitides and lupus.

REFERENCES

1. Park, M.S., *Diffuse alveolar hemorrhage.* Tuberc Respir Dis (Seoul), 2013. 74: p. 151-62.

2. Aceves, E.P., Cristobal, M.P., Espinola Reyna, G.A., Andraca, R.A., Fridmann, D.X, Barile Fabris, L.A., *Chronic respiratory disfunction due to diffuse alveolar hemorrhage in patients with systemic lupus erythematosus and primary vasculitis.* Reumatol Clin 2013. 9(5): p. 263-8.

3. Chowdhary, V.R., Grande, J.P., Luthra, H.S. & David, C.S. , *Characterization of haemorrhagic pulmonary capillaritis: another manifestation of Pristane-induced lupus.* Rheumatology (Oxford), 2007. 46(9): p. 1405-1410.

4. Barker, T.T., Lee, P.Y., Kelly-Scumpia, K.M., Weinstein, J.S., Nacionales, D.C., Kumagai, Y., Akira, S., Croker, B.P., Sobel, E.S., Reeves, W.H. & Satoh, M. , *Pathogenic role of B cells in the development of diffuse alveolar hemorrhage induced by pristane.* Lab Invest., 2011. 91(10): p. 1540-1550.

5. Anderson, P.N., Potter,M., *Induction of plasma cell tumours in BALB-c mice with 2,6,10,14-tetramethylpentadecane (pristane).* Nature, 1969. 222(5197): p. 994-995.

6. Reeves, W.H., Lee, P.Y., Weinstein, J.S., Satoh, M. & Lu, L. , *Induction of autoimmunity by pristane and other naturally occurring hydrocarbons.* Trends in Immunology, 2009. 30(9): p. 455-464.

7. Grob, K., Huber, M., Boderius, U. & Bronz, M., *Mineral oil material in canned foods.* Food Addit Contam. , 1997. 14(1): p. 83-88.

8. Castle, L., Nichol, J. & Gilbert, J., *Migration of mineral hydrocarbons into foods. 4. Waxed paper for packaging dry goods including bread, confectionery and for domestic use including microwave cooking.* Food Addit Contam. , 1994. 11(1): p. 79-89.

9. Avigan, J., Blumer, M., *On the origin of pristane in marine organisms.* J. Lipid Res., 1968. 9(3): p. 350-352.

10. Chung, J.G., Garrett, L.R., Byers, P.E., Cuchens, M.A. , *A survey of the amount of pristane in common fruits and vegetables.* Journal of Food Composition and Analysis, 1989. 2(1): p. 22-27.

11. Heimbach, J.T., Bodor, A.R., Douglass, J.S., Barraj, L.M., Cohen, S.C., Biles, R.W. & Faust, H. R., *Dietary exposures to mineral hydrocarbons from food-use applications in the United States.* Food Chem Toxicol., 2002. 40(5): p. 555-571.

12. Dahlgren, J., Takhar, H., Anderson-Mahoney, P., Kotlerman, J., Tarr, J. & Warshaw, R. , *Cluster of systemic lupus erythematosus (SLE) associated with an oil field waste site: a cross sectional study.* Environmental Health, 2007. 6: p. 8-23.

13. Satoh, M., Reeves,W.H. , *Induction of lupus-associated autoantibodies in BALB/c mice by intraperitoneal injection of pristane.* J. Exp. Med., 1994. 180(6): p. 2341-2346.

14. Smith-Bouvier, D.L., et al., *A role for sex chromosome complement in the female bias in autoimmune disease.* J Exp Med, 2008. 205(5): p. 1099-108.

15. Smith, D.L., et al., *A female preponderance for chemically induced lupus in SJL/J mice.* Clin Immunol, 2007. 122(1): p. 101-7.

16. Singh, A.K., et al., *The natural killer T cell ligand alpha-galactosylceramide prevents or promotes pristane-induced lupus in mice.* Eur J Immunol, 2005. 35(4): p. 1143-54.

17. Yang, J.Q., et al., *Immunoregulatory role of CD1d in the hydrocarbon oil-induced model of lupus nephritis.* J Immunol, 2003. 171(4): p. 2142-53.

18. Yoshida, H., et al., *Effect of an exogenous trigger on the pathogenesis of lupus in (NZB x NZW)F1 mice.* Arthritis Rheum, 2002. 46(8): p. 2235-44.

19. Kuroda, Y., Ono, N., Akaogi, J., Nacionales, D.C., Yamasaki, Y., Barker, T.T., Reeves, W.H., Satoh, M., *Induction of lupus-related specific autoantibodies by non-specific inflammation caused by an intraperitoneal injection of n-hexadecane in BALB/c mice.* Toxicology, 2006. 218: p. 186–196.

20. Cruickshank, B., Thomas,M.J. , *Mineral oil (follicular) lipidosis: II. histologic studies of spleen, liver, lymph nodes, and bone marrow.* Hum. Pathol. , 1984. 15(8): p. 731–737.

21. Wanless, I.R., Geddie,W.R., *Mineral oil lipogranulomata in liver and spleen: a study of 465 autopsies.* Arch. Pathol. Lab. Med. , 1985. 109(3): p. 283–286.

22. Kuroda, Y., Akaogi, J., Nacionales, D.C., Wasdo, S.C., Szabo, N.J., Reeves, W.H. & Satoh, M. , *Distinctive patterns of autoimmune response induced by different types of mineral oil.* Toxicological Sciences, 2004. 78(2): p. 222-228.

23. Garrett, L. R., Bost, K.L., Buttke, T. M., Cuchens, M. A., *Changes in the DNA of lymphocytes from pristane treated rats.* Agents Actions., 1987. 20: p. 104-12.

24. Schurig, C, Miltner, A., Kaestner, M., *Hexadecane and pristane degradation potential at the level of the aquifer- evidence from sediment incubations compared to in situ microcosms.* Environ Sci Pollut Res Int., 2014. 21(15): p. 9081-94.

25. Le Bon, A.M., Cravedi, J.P., Tulliez, J.E., *Disposition and metabolism of pristane in rat.* Lipids, 1998. 23(5): p. 424-9.

26. Zhuang, H., et al., *Pathogenesis of Diffuse Alveolar Hemorrhage in Murine Lupus.* Arthritis Rheumatol., 2017. 69(6): p. 1280-1293.

27. Zhuang, H., Han, S., Xu, Y., Li, Y., Wang, H., Yang, L.J., Reeves, W.H., *Toll-like receptor 7-stimulated tumor necrosis factor α causes bone marrow damage in systemic lupus erythematosus.* Arthritis Rheumatol., 2014. 66(1): p. 140-51.

28. Le Bon, A.M., Cravedi, J.P., Tulliez, J., *Fate of the isoprenoid hydrocarbon, pristane, in rainbow trout.* Ecotoxicol Environ Saf., 1987 13(3): p. 274-81.

29. Garrett, L.R., Chung, J.G., Byers, P.E., Cuchens M.A., *Dietary effects of pristane on rat lymphoid tissues.* Agents and Actions, 1989. 28: p. 272.

30. Yang, J.Q., et al., *Repeated a-galactosylceramide administration results in expansion of NK T cells and alleviates inflammatory dermatitis in MRL-lpr/lpr mice.* J Immunol, 2003. 171(8): p. 4439-46.

31. Engel, P., Gomez-Puerta, J.A., Ramos-Casals, M., Lozano, F., and Bosch, X., *Therapeutic Targeting of B Cells for Rheumatic Autoimmune Diseases.* Pharmacological Reviews, 2011. 63: p. 127-56.

32. Malkiel, S., Kuhlow C.J., Mena, P., Benach, J.L., *The loss and gain of marginal zone and peritoneal B cells is different in response to relapsing fever and Lyme disease Borrelia.* J Immunol., 2009. 182(1): p. 498-506.

33. Yenson, V., Baumgarth, N., *Purification and immune phenotyping of B-1 cells from body cavities of mice.* Methods Mol Biol. , 2014. 1190: p. 17-34.

34. Shi, Y., Tsuboi, N., Furuhashi, K., Du, Q., Horinouchi, A., Maeda, K., Kosugi, T., Matsuo, S., Maruyama, S., *Pristane-induced granulocyte recruitment promotes phenotypic conversion of macrophages and protects against diffuse pulmonary hemorrhage in Mac-1 deficiency.* J Immunol., 2014. 193(10): p. 5129-39.

35. Zhuang, H., Han, S., Li, Y., Kienhöfer, D., Lee, P., Shumyak, S., Meyerholz, R., Rosadzinski, K., Rosner, D., Chan, A., Xu, Y., Segal, M., Sobel, E., Yang, L.J., Hoffmann, M.H., Reeves, W.H., *A Novel Mechanism for Generating the Interferon Signature in Lupus: Opsonization of Dead Cells by Complement and IgM.* Arthritis Rheumatol. , 2016. 68(12): p. 2917-2928.

36. Hamze, M., Desmetz, C., Guglielmi P., *B lymphocytes: a promising target to treat atherosclerosis?* Med Sci (Paris), 2014. 30(10): p. 874-81.

37. Wang, K., Wei, G., Liu, D., *CD19: a biomarker for B cell development, lymphoma diagnosis and therapy.* Exp Hematol Oncol., 2012. 1(1): p. 36.

38. Fairfax, K.A., Tsantikos, E., Figgett, W.A., Vincent, F.B., Quah, P.S., LePage, M., Hibbs, M.L., Mackay, F., *BAFF-driven autoimmunity requires CD19 expression.* J Autoimmun, 2015. 62: p. 1-10.

39. Xu, Y., Beavitt, S.J., Harder, K.W., Hibbs, M.L., Tarlinton, D.M., *CD19-dependent activation of Akt kinase in B-lymphocytes.* J Biol Chem, 2001. 276(2): p. 1474-8.

40. Engel, P., Zhou, L.J., Ord, D.C., Sato, S., Koller, B., Tedder, T.F., *Abnormal B lymphocyte development, activation, and differentiation in mice that lack or overexpress the CD19 signal transduction molecule.* Immunity, 1995. 3(1): p. 39-50.

41. Rickert, R.C., Roes, J., and Rajewsky, K., *B lymphocyte-specific, Cre-mediated mutagenesis in mice.* Nucleic Acids Res., 1997. 25(6): p. 1317–1318.

42. Sato, S., Ono, N., Steeber, D.A., Pisetsky, D.S., Tedder, T.F., *CD19 regulates B lymphocyte signaling thresholds critical for the development of B-1 lineage cells and autoimmunity.* J Immunol., 1996. 157(10): p. 4371-8.

43. Haas, K.M., Poe, J.C., Steeber, D.A., Tedder, T.F., *B-1a and B-1b cells exhibit distinct developmental requirements and have unique functional roles in innate and adaptive immunity to S. pneumoniae.* Immunity, 2005. 23(1): p. 7-18.

44. Yanaba, K., Kamata, M., Asano, Y., Tada, Y., Sugaya, M., Kadono, T., Tedder, T.F., Sato, S., *CD19 expression in B cells regulates atopic dermatitis in a mouse model.* Am J Pathol., 2013. 182(6): p. 2214-22.

45. Yoshizaki, A., Iwata, Y., Komura, K., Ogawa, F., Hara, T., Muroi, E., Takenaka, M., Shimizu, K., Hasegawa, M., Fujimoto, M., Tedder, T.F., Sato, S., *CD19 regulates skin and lung fibrosis via Toll-like receptor signaling in a model of bleomycin-induced scleroderma.* Am J Pathol., 2008. 172(6): p. 1650-63.

46. Zhou, S., Wang, Y., Meng, Y., Xiao, C., Liu, Z., Brohawn, P., Higgs, B.W., Jallal, B., Jia, Q., Qu, B., Huang, X., Tang, Y., Yao, Y., Harley, J.B., Shen, N., *In Vivo Therapeutic Success of MicroRNA-155 Antagomir in a Mouse Model of Lupus Alveolar Hemorrhage.* Arthritis Rheumatol., 2016. 68(4): p. 953-64.

47. Herman, S., Kny, A., Schorn, C., Pfatschbacher, J., Niederreiter, B., Herrmann, M., Holmdahl, R., Steiner, G., Hoffmann, M.H., *Cell death and cytokine production induced by autoimmunogenic hydrocarbon oils.* Autoimmunity, 2012. 45(8): p. 602-11.

48. Calvani, N., Caricchio, R., Tucci, M., Sobel, E.S., Silvestris, F., Tartaglia, P., Richards, H.B., *Induction of apoptosis by the hydrocarbon oil pristane: implications for pristane-induced lupus.* J Immunol., 2005. 175(7): p. 4777-4782.

49. Janz, S., Gawrisch, K., Lester, D.S., *Translocation and activation of protein kinase C by the plasma cell tumor-promoting alkane pristane.* Cancer Res.,1995. 55(3): p. 518-24.

50. Kimber, I., and Carrillo, J.C., *Oral exposure to mineral oils: Is there an association with immune perturbation and autoimmunity?* Toxicology, 2016. 344-346: p. 19-25.

51. Andreassen, M., Hjertholma, H., Cravedi, J., Grob, K., Alexander, J., Nygaard, U.C., *Effect of dietary pristane and other saturated mineral oils (MOSH) on autoimmune arthritis in rats.* Toxicology Reports, 2017. 4: p. 104-112.

52. Ho, F.C., and Fu, K.H., *A new model of AA-amyloidosis induced by oral pristane in BALB/c mice.* Br J Exp Pathol., 1987 68(3): p. 413-20.

53. De Vooght, V., Vanoirbeek, J.A., Haenen, S., Verbeken, E., Nemery, B., Hoet, P.H., *Oropharyngeal aspiration: an alternative route for challenging in a mouse model of chemical-induced asthma.* Toxicology, 2009. 259: p. 84-89.

54. Egger, C., Cannet, C., Gérard, C., Jarman, E., Jarai, G., Feige, A., Suply, T., Micard, A., Dunbar, A., Tigani, B., Beckmann, N., *Administration of bleomycin via the oropharyngeal aspiration route leads to sustained lung fibrosis in mice and rats as quantified by UTE-MRI and histology.* PLoS One, 2013; 8(5): e63432.

55. Loeb, W.F., and Quimby, F.W., *The Clinical Chemistry of Laboratory Animals.* Philadelphia, PA: Taylor & Francis, USA, 1999 (2nd ed.).

56. Tung, J.W., Parks, D.R., Moore, W.A., Herzenberg, L.A., Herzenberg, L.A., *Identification of B-cell subsets: an exposition of 11-color (Hi-D) FACS methods.* Methods Mol Biol., 2004. 271: p. 37-58.

57. Hastings, W.D., Gurdak, S.M., Tumang, J.R., Rothstein, T.L., *$CD5^{+}/Mac\text{-}1^{-}$ peritoneal B cells: a novel B cell subset that exhibits characteristics of B-1 cells.* Immunol. Lett., 2006. 105(1): p. 90-96.

58. Berland, R., and Wortis, H.H., *Origins and functions of B-1 cells with notes on the role of CD5.* Annu Rev Immunol., 2002. 20: p. 253-300.

59. Griffin, D.O., Holodick, N.E., Rothstein, T.L., *Human B1 cells in umbilical cord and adult peripheral blood express the novel phenotype $CD20^{+}$ $CD27^{+}$ $CD43^{+}$ $CD70^{-}$.* J Exp Med., 2011. 208(1): p. 67-80.

60. Griffin, D.O., and Rothstein, T.L., *Human "orchestrator" CD11b(+) B1 cells spontaneously secrete interleukin-10 and regulate T-cell activity.* Mol Med., 2012. 18: p. 1003-8.

61. Hamilton, K.J., Satoh, M., Swartz, J., Richards, H.B., Reeves, W.H., *Influence of microbial stimulation on hypergammaglobulinemia and autoantibody production in pristane-induced lupus.* Clin Immunol Immunopathol., 1998. 86(3): p. 271-9.

62. Huang, D.W., Sherman, B.T., Lempicki, R.A., *Systematic and integrative analysis of large gene lists using DAVID Bioinformatics Resources.* Nature Protoc., 2009. 4: p. 44-57.

63. Huang, D.W., Sherman, B.T., Lempicki, R.A., *Bioinformatics enrichment tools: paths toward the comprehensive functional analysis of large gene lists.* Nucleic Acids Res., 2009. 37: p. 1-13.

64. Ansel, K.M., Harris, R.B., Cyster, J.G., *CXCL13 is required for B1 cell homing, natural antibody production, and body cavity immunity.* Immunity, 2002. 16(1): p. 67-76.

65. Ha, S.A., Tsuji, M., Suzuki, K., Meek, B., Yasuda, N., Kaisho, T., Fagarasan, S., *Regulation of B1 cell migration by signals through Toll-like receptors.* J Exp Med., 2006. 203: p. 2541-50.

66. Bronstein, A.C., Spyker, D.A., Cantilena, L.R. Jr, Green, J.L., Rumack, B.H., Giffin, S.L., *2009 Annual Report of the American Association of Poison Control Centers' National Poison Data System (NPDS): 27th Annual Report.* Clin Toxicol. (Phila), 2010. 48: p. 979-1178.